MODELING OF WET GAS COMPRESSION IN TWIN-SCREW MULTIPHASE PUMP

A Dissertation

by

JIAN XU

Submitted to the Office of Graduate Studies of
Texas A&M University
in partial fulfillment of the requirements for the degree of

DOCTOR OF PHILOSOPHY

May 2008

Major Subject: Petroleum Engineering

MODELING OF WET GAS COMPRESSION IN TWIN-SCREW MULTIPHASE PUMP

A Dissertation

by

JIAN XU

Submitted to the Office of Graduate Studies of
Texas A&M University
in partial fulfillment of the requirements for the degree of

DOCTOR OF PHILOSOPHY

Approved by:

Chair of Committee,	Stuart L. Scott
Committee Members,	Maria A. Barrufet
	Gerald L. Morrison
	Robert A. Wattenbarger
Head of Department,	Steven A. Holditch

May 2008

Major Subject: Petroleum Engineering

ABSTRACT

Modeling of Wet Gas Compression in Twin-Screw Multiphase Pump.

(May 2008)

Jian Xu, B.S., Tianjin University, P. R. China;

M.S., Tianjin University, P. R. China

Chair of Advisory Committee: Dr. Stuart L. Scott

Twin-screw multiphase pumps experience a severe decrease in efficiency, even the breakdown of pumping function, when operating under wet gas conditions. Additionally, field operations have revealed significant vibration and thermal issues which can lead to damage of the pump internals and expensive repairs and maintenance. There are limited models simulating the performance of twin-screw pump under these conditions. This project develops a pump-user oriented simulator to model the performance of twin-screw pumps under wet gas conditions. Experimental testing is conducted to verify the simulation results. Based on the simulations, an innovative solution is presented to improve the efficiency and prevent the breakdown of pumping function.

A new model is developed based upon a previous Texas A&M twin-screw pump model. In this model, both the gas slip and liquid slip in the pump clearances are simulated. The mechanical model is coupled with a thermodynamic model to predict the pressure and temperature distribution along the screws. The comparison of experimental

data and the predictions of both isothermal and non-isothermal models show a better match than previous models with Gas Volume Fraction (GVF) 95% and 98%. Compatible with the previous Texas A&M twin-screw pump model, this model can be used to simulate the twin-screw pump performance with GVF from 0% to 99%.

Based on the effect of liquid viscosity, a novel solution is investigated with the newly developed model to improve the efficiency and reliability of twin-screw pump performance with GVF higher than 94%. The solution is to inject high viscosity liquid directly into the twin-screw pump. After the simulations of several different scenarios with various liquid injection rates and injection positions, we conclude that the volumetric efficiency increases with increasing liquid viscosity and injecting liquid in the suction is suggested.

DEDICATION

This work is dedicated to God, my shepherd, for loving me through good and bad times. Also, this work is dedicated to my beloved wife and my family for their unlimited support.

ACKNOWLEDGEMENTS

I would like to give my most sincere appreciation to my committee chair, Dr. Stuart L. Scott, for his valuable guidance, intellectual contributions and his patience in helping me complete this research. I would also like to thank my committee members, Dr. Barrufet, Dr. Morrison, and Dr. Wattenbarger, for their guidance and support throughout the course of this research.

Thanks also go to my friends and colleagues and the department faculty and staff for making my time at Texas A&M University a great experience. I also want to extend my gratitude to Evan Chan, Hemant Nikhar and all the people in the Multiphase Research Group for their unconditional support and friendship.

Thanks to MPUR Consortium and MPUR for providing the funding of this research project.

Last but not least, thanks go to my mother and father for their encouragement and to my wife for her patience and love.

TABLE OF CONTENTS

Page

LIST OF FIGURES

Page

Page

Page

Page

LIST OF TABLES

NOMENCLATURE

A	Area, ft^2
c	Clearance, in
c_c	Circumferential clearance, in
c_{eff}	Effective clearance, in
c_f	Flank clearance, in
c_r	Root clearance, in
c_p	Specific heat capacity, $BTU / lbm \cdot ^\circ R$
C_{eff}	Effective coefficient of clearance, dimensionless
d_h	Hydraulic diameter, in
D	Theoretical pump displacement, gal/rev
D_c	External diameter, in
D_r	Root diameter, in
f_c	Velocity correction factor, dimensionless
GVF	Gas volume fraction, dimensionless
h	Specific enthalpy, BTU/lbm
H	Enthalpy, BTU
l	Length, in
l_h	Circumferential gap width, in

l_s	Screw length, in
m	Mass, lb
$\dot{m}$	Mass flow rate, lb/min
n	Number of sealed chambers, dimensionless
n_t	Number of threads, dimensionless
N	Pump speed, rpm
p	Pressure, psia
Δp	Differential pressure, psi
q	Flow rate, gpm
q_G	Gas slip flow, gpm
q_L	Liquid slip flow, gpm
q_{rec}	Recirculation flow rate, gpm
q_{slip}	Slip flow, gpm
q_{TH}	Theoretical pump flow rate, gpm
Q	Heat, BTU
r	Roughness factor, dimensionless
Re	Reynolds number, dimensionless
s	Pitch, in/rev
t	Time, min
Δt	Period of time, min
T	Temperature, $^\circ R$

U	Internal energy, BTU
v	Velocity, ft/sec
V	Volume, gal
V_c	Volume of sealed chamber, gal
W	Work, BTU
X^2	Lockhart-Martinelli parameter, dimensionless
X'^2	Modified Lockhart-Martinelli parameter, dimensionless
z	Compressibility factor, dimensionless
α	Angle
ϕ_L^2	Two-phase friction multiplier
λ	Darcy-Weisbach friction factor, dimensionless
μ	Viscosity, cp
ρ	Density, lb/gal

Subscript

D	Discharge
G	Gas
i	Chamber index
L	Liquid
rec	Recirculation
S	Suction
TH	Theoretical

1. INTRODUCTION

Due to the pressure and temperature change from bottom hole to wellhead and the complex compositions of hydrocarbon mixture, almost all the wells in oil and gas industry produce a mixture of oil, water, and gas, and occasionally sand, natural gas hydrate, and waxes at the wellhead (Dal Porto and Larson, 1997). The transfer of these gas-liquid mixtures to the processing facility always requires pressure boosting facilities. In conventional production system, the liquid and gas in the mixture will be separated and boosted by traditional single phase pump and gas compressor, respectively. In many cases, to cut the expenditure and construction, gas has to be flared and only liquid could be retained for further processing (Corless, 2000). The emergence of multiphase pumping technology makes it possible to transfer the oil and gas production through a single flow line. The multiphase production system cut the capital expenditures, reduce infrastructure and gas flaring. The subsea application of multiphase boosting system decreases the wellhead pressure and makes the development of marginal field more economic.

This dissertation follows the style of *SPE Production and Operations.*

In the last two decades, the multiphase pumping technologies emerge from the simple adoption of traditional liquid pump. Now most of the multiphase pump is specially designed for multiphase fluid. Now, multiphase pumping is a proven technology for heavy oil production (Corless, 2000; Giuggioli et al., 1999; Gonzalez and Guevara, 1995), light oil (Putra, 2001; Putra and Uphold, 1999), wet gas compression (Muller-Link et al., 2002), and offshore production (Mobbs, 2002). Driven by the large demand and successful field cases， more and more new pumping technologies are applied to multiphase pumping.

After decades of field trials, several different types of pump stand out, including twin-screw, helicon-axial, counter-rotating axial flow, piston and progressive cavity pump. Among these pumps, both positive displacement twin-screw pump and multistage helicon-axial pump can handle high gas content in the fluid mixture. They are the most used two types of pump in multiphase production/boosting system. The comparison between the twin-screw and helical-axial pump can not determine which is better and it is still case by case. But due to the special design of fluid distribution, twin-screw pump are more insensitive to liquid slugs and large change in inlet gas density (Putra and Uphold, 1999). It is the most widely utilized multiphase pump (Scott et al., 2006).

The biggest physical challenge for the multiphase pump in oil and gas industry is the large variation of the GVF. In some cases, the GVF range from 0% to 100%. Field cases show that with recirculation system, twin-screw pump can handle GVF up to 99.5% (Muller-Link et al., 2002). With high gas content, the pump is acting as a “compressor”, the slip flow inside the twin-screw pump can not be pure liquid and the

gas slip can not be ignored. Furthermore, limited liquid in the pump can not carry out all the heat generated by gas compression. The gas compression procedure is no longer isothermal. The experimental data with GVF > 96% show tremendous temperature increase between the inlet and outlet of twin-screw pump (Singh, 2003). With the high demand of wet gas compression system, it is necessary to model the performance of twin-screw multiphase pump with wet gas conditions and provide solutions to increase both efficiency and reliability.

There are limited model available to predict the performance of twin-screw pump with wet gas conditions (GVF between 94% and 100%). Most pump manufacturer recommend to use twin-screw pump with GVF less than 95%. Also, most of them are developed by pump manufacturers for design optimization. These models need details about geometry of the pump which are not fully disclosed to pump users. This limits the application of these models and the application of twin-screw pump on wet gas compression.

To overcome the shortage of geometry information about the pump, a new model is developed based on previous Texas A&M twin-screw pump model by Martin and Scott (2003). The idea is to utilize the pump performance curve with water provided by the pump manufacturer to generate the basic parameters of the twin-screw pump. In this model, the gas slip in the pump is involved. The mechanic model is coupled with thermodynamic model to predict the pressure and temperature distribution along the screws. This model is more suitable to pump users who have limited information about the pump. This model is specially developed to predict the performance of twin-screw

multiphase pump with GVF from 0 to 99%. The extensive testing with field scale twin-screw pump shows a good match between the experimental data and the predictions.

A novel solution is investigated with the newly developed model to improve the efficiency and reliability of twin-screw pump performance with GVF higher than 94%.

Generally speaking, the objectives of this research are: 1) develop a new model to simulate twin-screw multiphase pump under wet gas condition. The simulations include pump performance, volumetric efficiency, pressure profile along the screw, temperature increase across the pump. 2) the model should be independent of the pump brand and require as little pump geometry data as possible. 3) based on the model, solution for wet gas compression is presented to improve the reliability and efficiency of the twin-screw multiphase pump.

1.1 Multiphase Production System

Traditionally, typical production system of oil field consists of separator, liquid pump, liquid meter, gas meter, gas compressor, and buffer tank as shown in **Fig. 1.1**. Produced fluid from the well, normally oil and gas mixture, is separated first， then boosted by liquid pump and gas compressor respectively and transferred through separate pipelines to the processing facility miles away. Sometime, Test separator is needed for well testing and flow rate measurement.

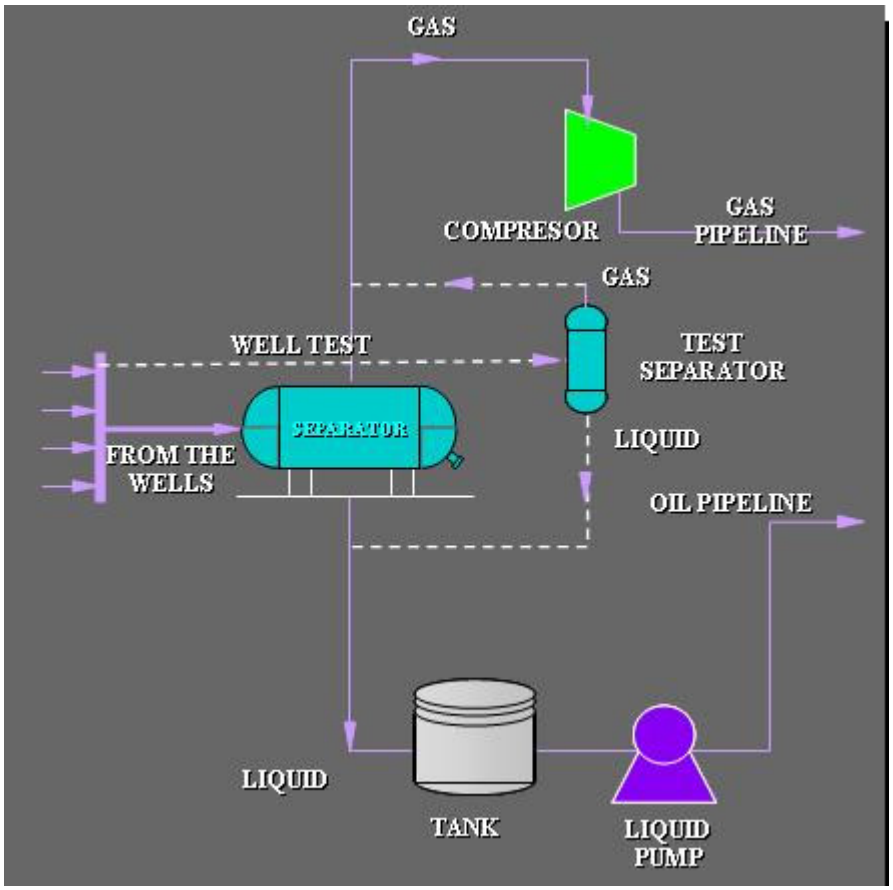

Fig. 1.1—Conventional production system (Uphold, 1999)

Different from conventional production system, multiphase production system eliminates the use of separator. The full well stream are boosted directly and transported through a single pipeline to the long-distance processing facility without separation. The layout of a typical multiphase production system is shown in **Fig. 1.2**. Multiphase pump replaces both single phase liquid pump and gas compressor. Test separator and manifold are replaced by multiphase meter and multiport valve. The production of each well can be selected by multiport valve through multiphase meter for well testing and measurement. By eliminating those equipments, multiphase production system can save

about 30% in investment for equal flow station capability (Gonzalez and Guevara, 1995) and significantly reduce the footprint of flow station, which is a big advantage for offshore/subsea application. In some cases, the application of multiphase production system can eliminate gas flaring and gives "zero" emission (Corless, 2001).

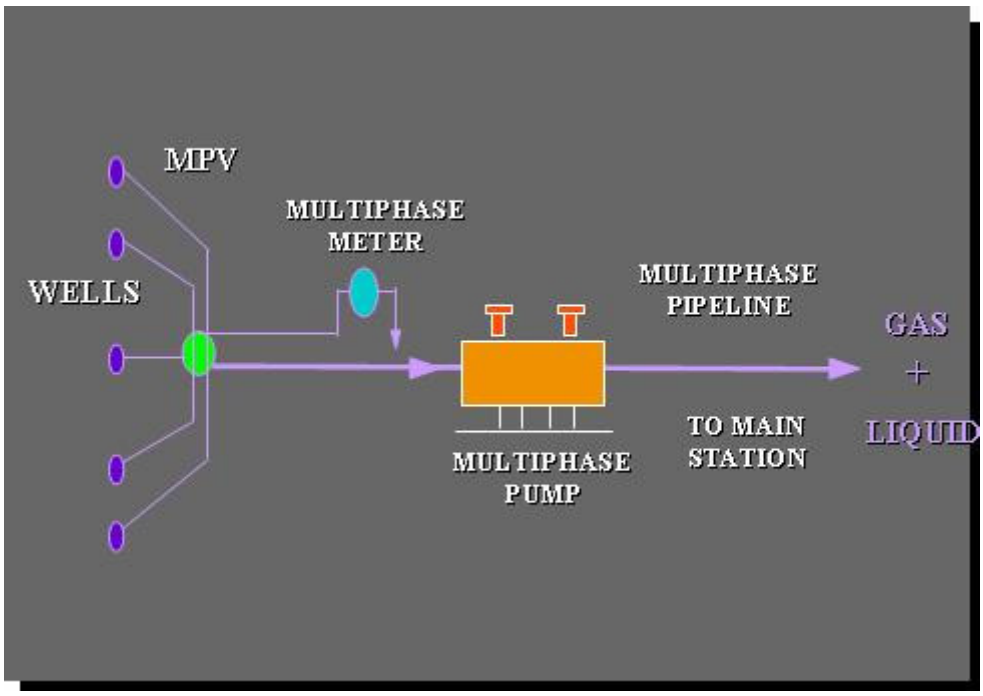

Fig. 1.2—Multiphase production system (Uphold, 1999)

Fig. 1.3 shows the comparison between existing Process Flow Diagram (PFD) and Multiphase Pump (MPP) PFD for Cold Lake project (Vena, 2003). Cold Lake, Canada is world's largest in-situ oil sand operation with annual production 35 million barrels of oil. Cyclic steam stimulation is used to heat and thin the bitumen which is too heavy and viscous to flow naturally to the surface. The existing PFD is shown in Fig. 1.3. It consisted of 3 pumps, 3 vessels, 3 heat exchangers and 2 compressors. With the

facility redesign, the conventional PFD was replaced by multiphase pumping system which consisted of only 1 multiphase pump, 1 vessel and 1 heat exchanger. Both the capital cost and footprint of the system are reduced.

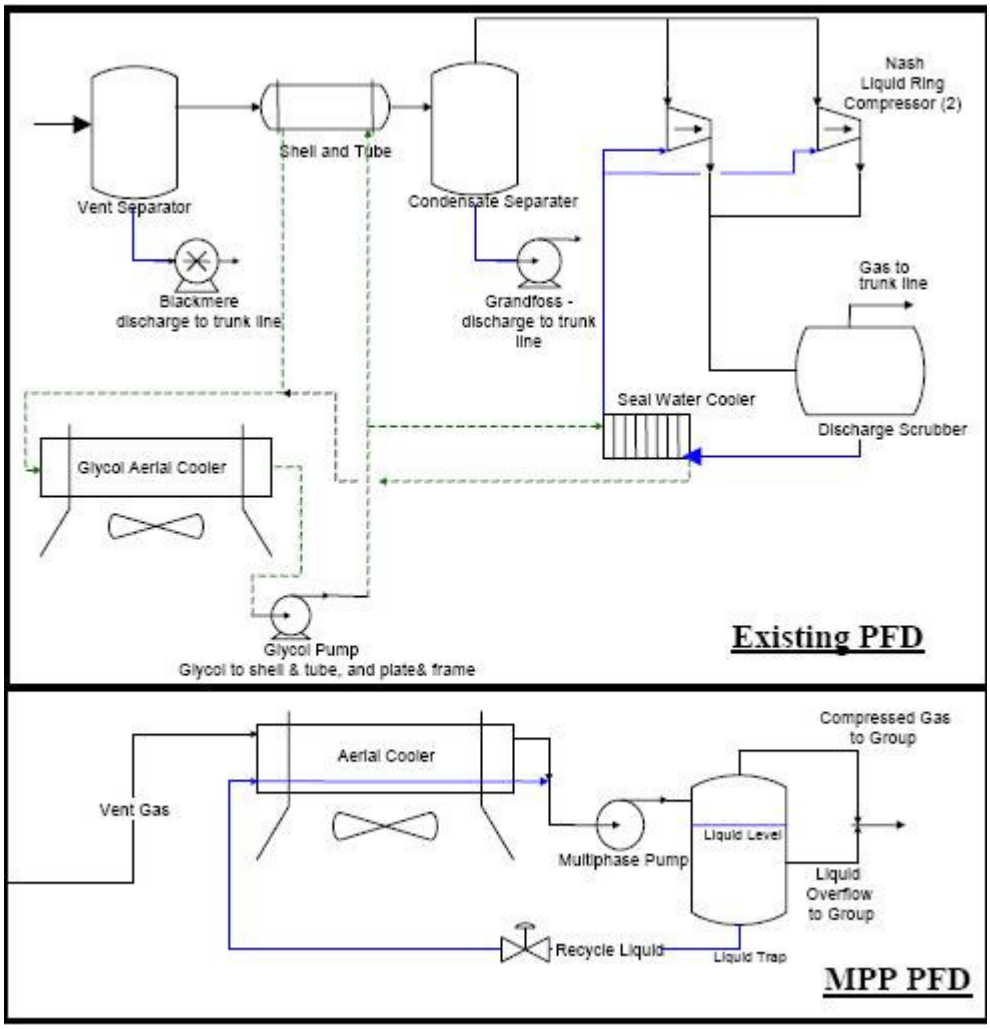

Fig 1.3—Comparison between existing Process Flow Diagram (PFD) and Multiphase Pump (MPP) PFD for Cold Lake project (Vena, 2003)

Multiphase production system also provides option for subsea production system. The dramatic reduction of development cost and small footprint are the biggest advantages driving the increasing use of subsea multiphase pumping system. Furthermore, multiphase pump can lower the subsea wellhead pressure and improve the hydrocarbon recovery. It also provides additional energy to boost the full well steam through long-distance pipeline, which make the development of remote marginal and deepwater fields more economical. With the multiphase pumping technologies being approved both onshore and on the topside of platform, subsea is the next big challenge. Reliability and operability are the top issues for subsea application. Table 1.1 lists the summary of ongoing or completed subsea projects worldwide. **Fig. 1.4** illustrates a subsea multiphase pumping system in Ceiba field, West Africa.

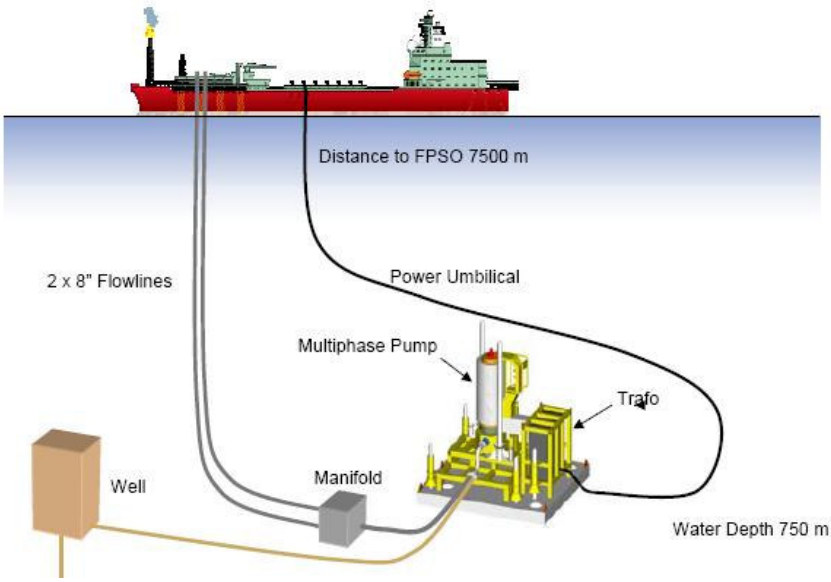

Fig 1.4—Subsea multiphase pumping system in Ceiba Field, West Africa (Pickard, 2003)

TABLE 1.1—SUMMARY OF SUBSEA MULTIPHASE PUMPING PROJECTS

(SCOTT ET AL., 2006)

Pump Technology	Subsea Integrator	Product Designation	Pump Manufacturer	Operator	Year	Field	Status
Helico-Axial	Framo	SMUBS	Framo	Shell	1994	Draugon	1 pump
	Framo	ELSMUBS	Framo	Staoil	1997	Lufeng	5 pumps
	Framo	ELSMUBS	Framo	ExxonMobil	1999	Topacio	2 pumps
	Framo	ELSMUBS	Framo	Hess	2002	Ceiba	2 pumps
	Framo	FDS	Framo	Hess	2003	Ceiba	5 pumps
	Framo	FSS	Framo	Santos	2004	Mutineer/Exeter	2 pumps
	Framo	FDS	Framo	BP	2006	W. of Shetland	4 pumps
	Framo	FDS	Framo	Oilexco	2006	Brenda	1 pump
	Technip	HYDRA/ELECTRA	Sulzer & IFP Sulzer	N/A Shell	2004 2005-2006	N/A N/A	conceptual prototype testing - increased pressure boost
Twin-Screw	Sonsub	DMBS	GE/Nuovo Pignone	Agip	1997	offshore Italy	N/A
	Curtiss Wright	SBMS-500	Leistritz	Petrobras	1996-present	Marlim	qualification tests completed at Atalaia; deployment 2006
	Aker/Kvaerner	SMPM	Bornemann	Demo 2000	2001-2002	K-Lab	tested w/ condensate & methane
	Aker/Kvaerner	SMPM	Bornemann	CNRL	2005-2006	Lyell (North Sea)	Installed Dec 2005
	Aker/Kvaerner	SMPM	Bornemann	BP	2006-2007	King (U.S. GOM)	2 pumps to be installed May 2007
	Bornemann	UW	Bornemann	Wintershall	2004	onshore sour gas field in Germany	onshore pressurized testing as part of German MPA program
	Subsea7 Subsea7	MPSP 1500 High-Boost, High-Power	Flowserve Flowserve	Total Shell	2000-2004 2005-2006	W. Africa N/A	conceptual prototype testing - increased pressure boost
		N/A	CAN-K	N/A	2004-2005	N/A	conceptual - adapting downhole high pressure technology
Piston	Hydril	N/A	Hydril	N/A	2004-2005	N/A	conceptual - adapting subsea mudlift technology

1.2 Wet Gas Compression

Another challenge for multiphase pumping technologies is wet gas compression. According to SPE glossary, “wet gas” is natural gas containing significant amounts of liquefiable hydrocarbons. But there is no standard of what percentage liquid phase should be in wet gas. Typically, GVF or gas quality is used to define the amount of

liquid in wet gas. Since most of the pump manufacturers recommend that the average GVF at the inlet of the pump should be limited to 95% to ensure the pump operability, for the purpose of research, GVF of 95% and above will be considered as wet gas compression (Singh, 2003).

Interests in the deployment of wet gas compressors is growing as companies seek for economical way to improve recovery of gas reservoirs both onshore and offshore. High gas price is also one of the forces driving the application of wet gas compression on stranded gas reservoir. **Table 1.2** summarizes the ongoing subsea wet gas compression projects.

TABLE 1.2—SUMMARY OF SUBSEA WET GAS COMPRESSION PROJECTS (SCOTT ET AL., 2006)

Compressor Type	Compressor Manufacturer	Product Designation	Subsea Integrator	Operator	Description/Status
Centrifugal	Seimens	Eco II	FMC	Shell and Statoil	Prototype-2003; Tested-2005
	Dresser-Rand		FMC	Statoil	2.8 MW version tested under wet-gas conditions
	Nuovo Pignone Kværner Eureka	Blue C Compressor Gas Booster	AkerKvaerner	Hydro	Tested in Demo 2000
Helico-Axial	Framo Engineering	WGC	Framo Engineering	Shell, Statoil and Hydro	contra rotating helico-axial design; 3.6 MW version tested in 2003
Twin-Screw	Bornemann	Digressive Screws	onshore and topside only	Wintershall, CNRL and others	onshore pressurized testing as part of German MPA program

Multiphase pumps, such as twin-screw pump and helicon-axial pump, face efficiency loss with increasing GVF. With GVF 100%, twin-screw pump can only last

less than 1 hour without any additional liquid. On the other hand, conventional dry gas compressor experience the same efficiency loss but with decreasing GVF from 100% to 97% (Brenne et al., 2005). With the amount of liquid increasing, severe damage could happen to the internal part of the compressor. To address the issues of wet gas compression, pump manufacturers are working to improve the efficiency and reliability of multiphase pump with GVF between 95% and 99% and compressor manufacturers are working to make the compressor tolerate 1-4% liquid (Scott et al., 2006).

1.3 Twin-Screw Multiphase Pumping Technology

Twin-screw pumping technology is one of the most used multiphase pumping technologies in the oil and gas industry. It was adopted from the widely used intermeshing counter-rotating twin-screw extruder. Before its application in multiphase boosting system, it is an important part of processing technology especially for polymer processing. It was originally developed to process difficult viscous industrial fluids such as coal-oil masses, ceramic masses and rubber compounds in early 20^{th} century (White, 1991). Now it is still used to pump highly viscous fluids in food and chemical industry.

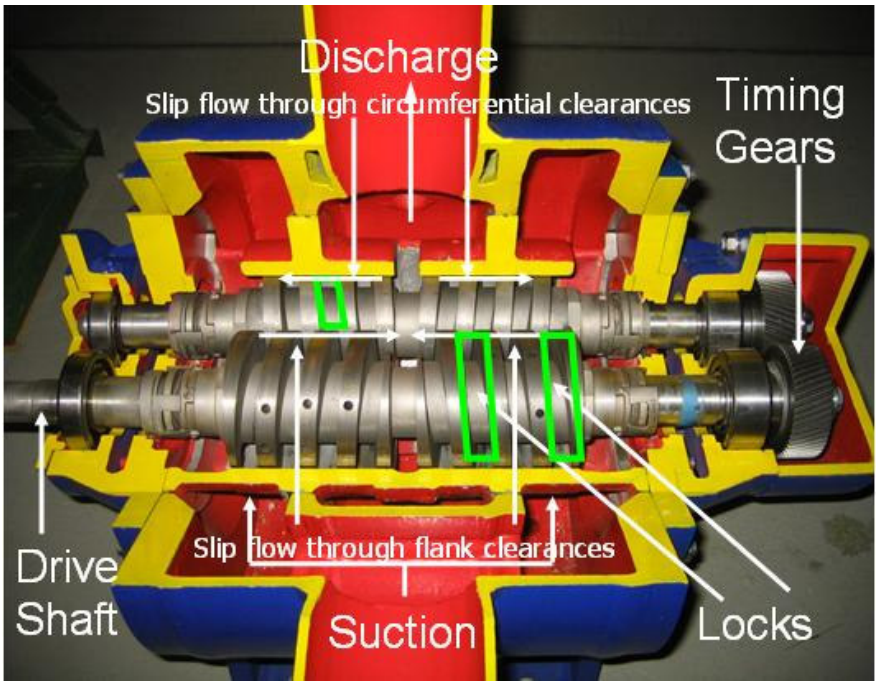

Fig. 1.5—Twin-screw pump cutaway

As shown in **Fig. 1.5**, twin-screw pumps are rotary, self-priming positive displacement pump. Typical twin-screw multiphase pumps used in oil and gas industry are categorized as intermeshing counter-rotating twin-screw pump. As its name indicated, it consists of two intermeshing screws. One screw is connected with motor through the drive shaft and transfers the drive force to the other screw by timing gears. The timing gears ensure there is no contact between the screws. Due to the special design of fluid path, the incoming fluid is divided to both ends of the pump. As the two screws counter-rotating, they generate a series of C-shaped sealed chambers (as shown in **Fig 1.6**) and push the fluid inside the chambers from both ends of the screws (suction) to the center of the pump (discharge). This inboard-to-outboard double-flow feature provides an axially balanced rotor set and minimize the bearing thrust load (Putra and Uphold, 1999). When

liquid slug hit the pump, it is split and hit both end of the screw at the same time. The net resultant force is zero. This makes twin-screw multiphase pump an ideal candidate for offshore or subsea multiphase boosting system. The “no contact” design between screws, screw and liner enables the pump to tolerate some amount of sand or solids in the fluid. But the clearances between screws, screw and liners also provide path for the fluid flowing “back” from discharge to suction which decreases the volumetric efficiency of the twin-screw pump. So the clearances are critical parameters for twin-screw pump design.

Furthermore, the unique axial flow pattern and low internal velocities of twin-screw pump make it a strong candidate to handle heavy oil production where liquid agitation or churning can cause severe emulsion problem.

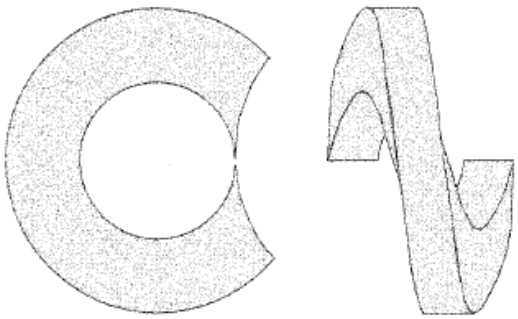

Fig 1.6—Shape of chambers created by the screw meshing

1.4 Speed Control of Twin-Screw Multiphase Pump

For twin-screw pump in subsea application, one of the challenges is speed control (Scott et al., 2006). While traditionally the industry has relied on variable

frequency drives (VFD's), the large size of the subsea multiphase pumps has generated interest in the use of torque converters for speed control. These devices become cost effective for large applications and may offer some advantages for subsea operations. The ability to place the speed control equipment on the seafloor rather than on a floating platform may provide cost savings. Also the cold deepwater temperatures will be able to dissipate any heat generated by the torque converter.

Multiphase pumps must handle a changing and unpredictable mixture of liquids, gas and even solids. Their operation requires speed control torque and speed over a wide range of operating conditions. The hydrodynamic variable speed drive is an alternative, which offers significant benefits compared to a variable frequency drive (VFD). The conventionally used driver is an oversized electric motor, controlled by a variable frequency drive with a limited torque transmission capability and reliability.

The hydrodynamic torque converter with its proven reliability is an interesting option to the variable frequency controlled motors. It can easily handle the different speed and power requirements of the twin-screw and rotodynamic pumps can transmit a constant or even rising torque and offers a number of other benefits such as savings on space/weight, longer mean time to failure than variable frequency drives (VFD's), and the ability to start the motor under an unloaded condition. For subsea operations the torque converter can also multiply the motor torque by a factor of 10 to provide greater ability to start up the pump even when filled with cold, viscous fluids. As will be discuss later, the torque converter has the ability to adsorb the normal excursion in motor speed that a multiphase pump experiences during slug flow, providing protection to the motor.

Torque converters are hydrodynamic transmission units, that continuously control the torque and speed between their input and output shaft. The heart of the hydrodynamic torque converter is the hydraulic circuit; consisting of pump, turbine and guide wheel with adjustable guide vanes (**Fig. 1.7**). The mechanical energy of the motor is converted into hydraulic energy through the torque converter pump wheel. In the turbine wheel, the same hydraulic energy is converted back into mechanical energy and transmitted to the output shaft (**Fig. 1.8**). The adjustable vanes of the guide wheel regulate the mass flow in the circuit. At closed guide vanes (small mass flow) the power transmission is minimal, while at completely open guide vanes (large mass flow) the power transmission is at its maximum. The power is transmitted by the kinetic energy of the oil, without any mechanical connection between driver and driven machine. This protects the motor if sudden load changes occur (like slugs in the pipeline) and provides an excellent shock and vibration damping over the entire speed range.

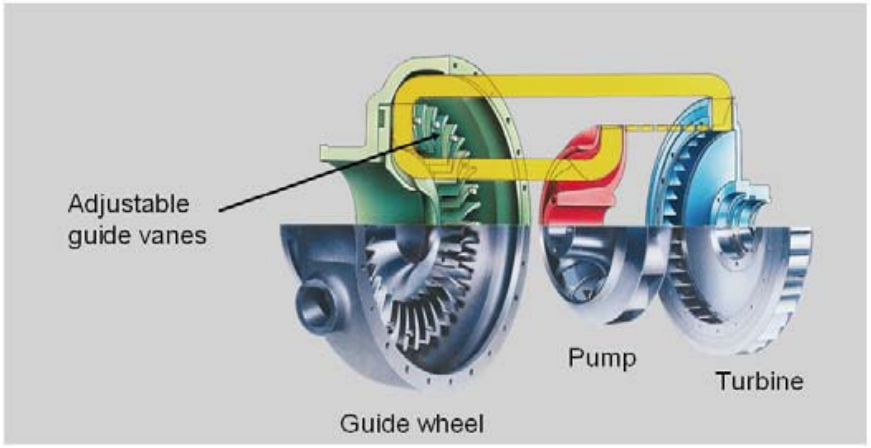

Fig. 1.7—Hydrodynamic torque converter

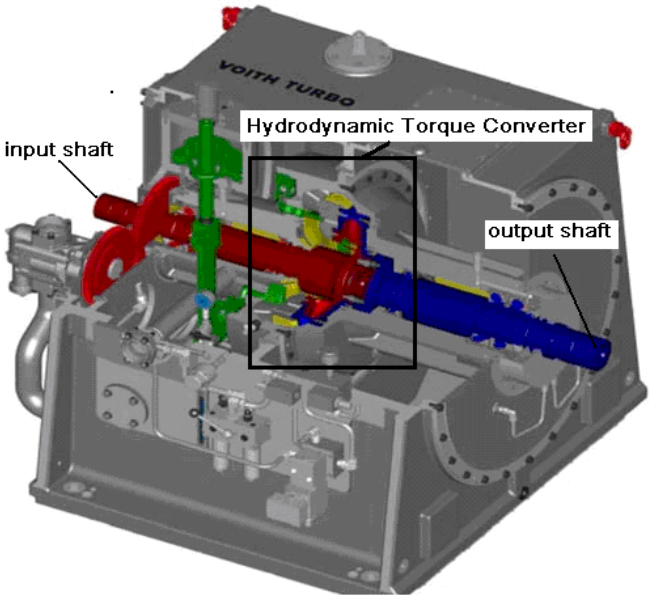

Fig. 1.8—Hydrodynamic variable speed drive

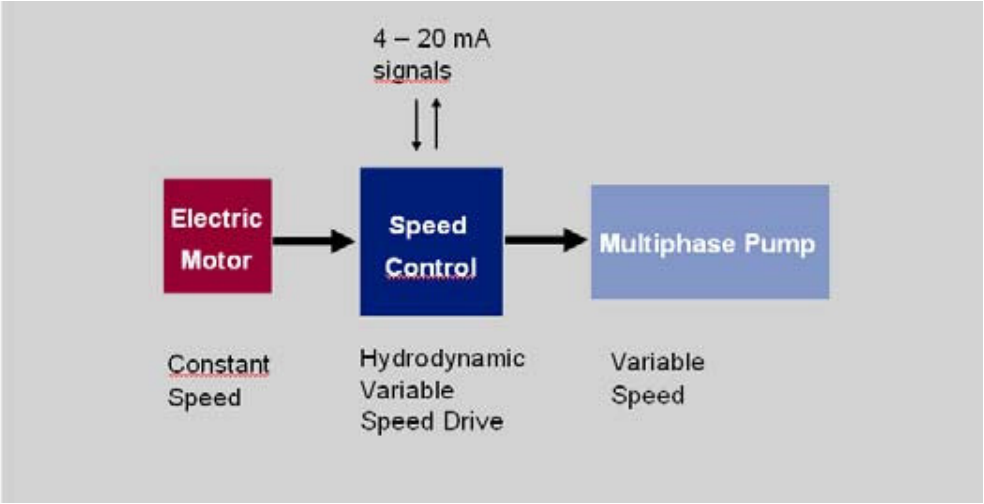

Fig. 1.9—Operation principles and controls

The torque converter is arranged between a fixed speed motor and the multiphase pump (**Fig. 1.9**). The arrangement can either be vertical or horizontal. The torque converter output speed is controlled by applying a 4 to 20 mA signal from the master control system to the guide vane actuator. This actuator moves the guide vanes and

provides a fast and precise speed control over the entire speed range to the multiphase pump. The electric / hydraulic guide vane actuator is designed and manufactured by Voith and was originally developed to control steam and gas turbines. The master control system typically uses pressure or flow as an input to compute the 4 to 20 mA signal to increase or decrease the multiphase pump speed via the torque converter. The multiphase pump train with the torque converter can easily be incorporated in a closed control loop.

The unique characteristic of a torque converter is the reason, why torque converters are used in so many applications worldwide. It can control, reduce or increase the speed, protect the driver from sudden load changes, increase the transmitted torque during start-up and enables gas or diesel engines to start with no load. The adjustable guide vanes allow a step less speed control of the multiphase pump.

Fig. 1.10 illustrates how the torque converter allows starting the motor and the multiphase pump separately. The guide vane positions of the torque converter can be closed and allow the motor a no load start up. Once the motor is up to full speed, the torque converter guide vanes can be opened to accelerate the multiphase pump smoothly. The torque difference between motor torque and load is available for acceleration

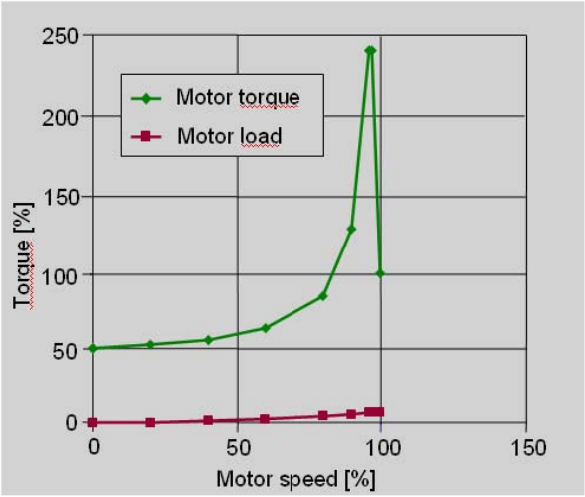

Fig. 1.10—Unloaded motor start

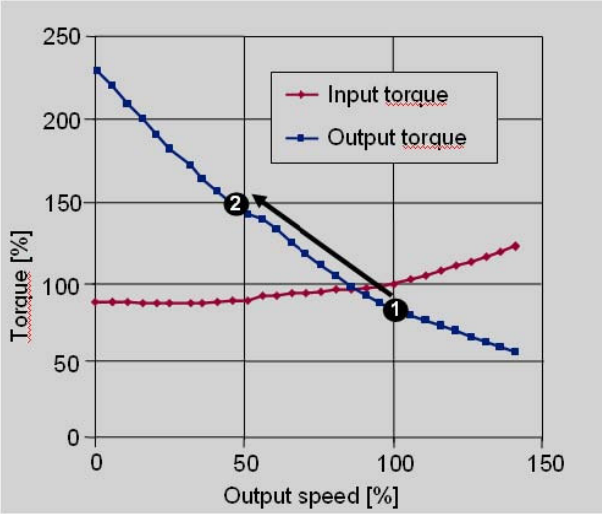

Fig. 1.11—Overload protection of motor

One of the most interesting features is handling of slug flow. **Fig. 1.11** shows the input and output torque for one guide vane position. The torque converter output torque will always follow the blue line, if the guide vane position is not changed. I.e. if a slug occurs and the torque of the multiphase pump increases, the torque converter will automatically reduce the speed and increase the torque. At the same time, the input

torque does hardly change, even if the output speed is reduced significantly. After the slug has passed the multiphase pump, the torque and speed will return to their normal value.

From Sep.1, 2004 to May.20, 2005, test of torque converter for speed control of twin-screw multiphase pump have been conducted at the Texas A&M University Multiphase Field Laboratory as shown in **Fig. 1.12**.

Fig. 1.12—Voith torque converter EL 6 installed at Texas A&M University

A series of tests include testing with fixed Guide Vane Position (**GVP**), testing with fixed MPP speed, testing with fixed suction pressure and overspeed testing. Overall, the experiments with Voith Torque Converter have demonstrated the ability of a torque converter to control speed of twin-screw multiphase pump. The following recommendations are made based on the data acquired during these experiments. For wet gas application, with small motor, torque converter can provide high torque to pump liquid slugs and high pump speed at high GVF (Scott et al., 2006).

2. TWIN-SCREW MULTIPHASE PUMP MODEL UNDER WET GAS CONDITION

2.1 Literature Review

While twin-screw pump is widely used for decades, limited modeling work has been found on the single phase liquid. Most of the models are for the intermeshing counter-rotating twin-screw extrusion (White, 1991). The main reason probably is because the pump is mainly used in high viscous fluid. The fluid is limited to laminar flow.

Vetter and Wincek (1993; 2000) presented the first twin-screw pump model for two phase gas/liquid flow. They simplified the geometry of the twin-screw pump to a series of parallel disks as shown in **Fig. 2.1**. The volumes between the disks represent the sealed chambers. The slip flow through the circumferential, flank and radial clearances are considered as the exchange of fluid between the chambers.

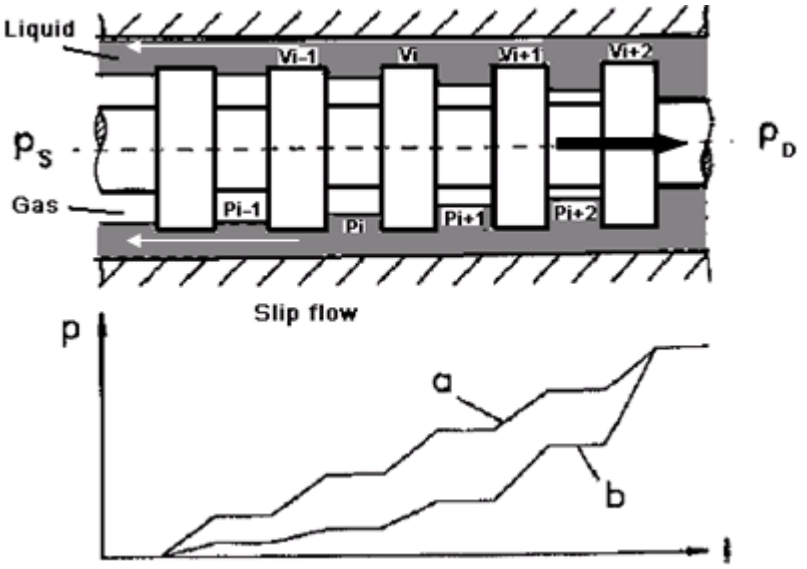

Fig. 2.1—Simplified pump model and theoretical pressure distribution (a: single-phase; b: two-phase) (Vetter and Wincek, 1993)

By modeling the slip flow through those clearances, the real flow rate will be predicted for single phase liquid flow. For two-phase flow, the main assumptions are: 1) all clearance is sealed by liquid, there is no gas slip flow; 2) gas compression is achieved by the liquid slip flow to the relevant chambers only; 3) gas phase is considered as ideal gas; 4) The gas compression is isothermal. Later experimental work of Vetter (2000) and Prang (2002) proved that these assumptions are valid with GVF up to 85%. Vetter and Wincek calculated the clearance slip flow by the addiction of two effects: pressure losses in clearances and rotational component. By dividing the relevant chamber movement into differential time segments, the flow balance and the chamber pressure can be calculated. With iteration, the total leakage flow will be computed. The actual two-phase

flow rate of the pump would be the difference between the theoretical volumetric flow rate and total leakage flow rate.

$$\Delta p = \lambda \frac{l}{d_h} \frac{\rho_L}{2} v^2 \tag{2.1}$$

$$\mathrm{Re} = \frac{d_h v}{\nu} \tag{2.2}$$

For laminar flow,

$$\lambda = \frac{96}{\mathrm{Re}} \tag{2.3}$$

For turbulent flow, with smooth clearance,

$$\lambda = 0.3322\,\mathrm{Re}^{-0.25} \tag{2.4}$$

With rough clearance,

$$\frac{1}{\sqrt{\lambda}} = 2\lg\frac{2s}{K} + 0.97 \tag{2.5}$$

Egashira et al. (1998) presented a new model by an empirical equation of pressure distribution along the screw. They model the relationship between pressure losses and leakage flow rate by the following equation.

$$\Delta p = \frac{\rho v^2}{2}\left(\frac{\lambda l}{4c} + 1.5\right) \tag{2.6}$$

1.5 in the equation is the empirical factor to account for the entry loss.

For laminar flow,

$$\lambda = \frac{64}{\mathrm{Re}} \tag{2.7}$$

For turbulent flow, Blasius equation is suggested (Egashira et al., 1998).

Different from Vetter's model, Egashira gave an empirical equation for the pressure distribution along the screw.

$$\frac{p_i - p_S}{p_D - p_S} = \left(\frac{i}{n_t + 1} \right)^r \tag{2.8}$$

where r is a parameter indicating the compressibility of the fluids. For single phase flow, r=1. For two-phase flow, r increase with higher fluid compressibility.

Prang and Cooper (2002; 2004) verified the assumptions of Vetter's model and introduced an empirical factor f_t to modify the leakage flow through the circumferential clearance. For turbulent flow, the factor is 0.8, which indicate about 80% of total leakage flow pass through the circumferential clearance.

$$\Delta p = \frac{\rho_L \left(f_t \frac{Q_{s,i}}{A_{s,i}} \right)^2}{2} \left(k_e + f \frac{l}{d_h} \right) \tag{2.9}$$

where k_e is the loss coefficient for entry of the flow into the clearance.

Assuming the gas compression process is isothermal, then

$$Q_{g,i+1} = Q_{g,i} \frac{p_i}{p_{i+1}} \tag{2.10}$$

Base on Vetter and Wincek's model, Nakashima (2002) considered the thermodynamic process inside the pump. They assume the compression is adiabatic and there is heat exchange only between phases of the multiphase fluid. Following Vetter and Wincek's assumption, there is only liquid flows back through the clearance. The effects of shaft deflection are neglected. In this model, the process inside the chamber is

simulated by the combination of 4 different processes: separator, compressor, pump and mixer. With process simulator, the process in the pump can be simulated.

Martin and Scott (2003) developed a new model based on the assumption of liquid-only backflow and isothermal compression. Different from other available models, Martin's model is pump-user oriented. An effective clearance is generated by regression of pump performance with pure water. All the leakage flow is assumed to go through the circumferential gap with the effective clearance number. The entry loss and viscosity effect are considered.

For laminar flow,

$$q_{slip} = C\Delta p \tag{2.11}$$

For turbulent flow,

$$q_{slip} = C\Delta p^{0.57} \tag{2.12}$$

C can be obtained by linear regression of water pump performance curve.

With isothermal compression, the mass balance equations for each chamber at certain time can be converted as following:

$$
\begin{aligned}
&V_S\left(\frac{p_S Z_1}{p_1 Z_S}-1\right)+(q_1-q_0)\Delta t=0\\
&V_1\left(\frac{p_1 Z_2}{p_2 Z_1}-1\right)+(q_2-q_1)\Delta t=0\\
&\qquad\vdots\\
&V_{i-1}\left(\frac{p_{i-1} Z_i}{p_i Z_{i-1}}-1\right)+(q_i-q_{i-1})\Delta t=0\\
&\qquad\vdots\\
&V_{n-1}\left(\frac{p_{n-1} Z_D}{p_D Z_{n-1}}-1\right)+(q_n-q_{n-1})\Delta t=0
\end{aligned}
\tag{2.13}
$$

Rausch et al (2004) presented a new model in a different way. They did not model the back flow rate and differential pressure; instead, they used energy and mass balances of each chamber with the assumption that the chamber is adiabatic. The kinetic energy of gap streams and wall friction are neglected. The leakage flow is assumed to be pure liquid.

Rabiger et al (2006) developed a thermodynamic model to describe the performance of twin-screw pump at very high gas volume fraction. He assumes not only the gas compression process inside the chamber is adiabatic, but also the leakage flow. He used the conservation equations of mass, momentum and energy. To match the transition of pure liquid leakage flow with GVF<85% to pure gas leakage flow at 100%, a new correlation is used but the detail is not released. The differential equations are solved by a fourth-order Runge-Kutta scheme.

Current models for twin-screw pump are listed in **Table 2.1**.

TABLE 2.1—SUMMARY OF CURRENT MODELS FOR TWIN-SCREW PUMP

Leakage flow in Clearance	Gas Compression	
	Isothermal	**Adiabatic**
Liquid only	**Vetter and Wincek (1993)** **Prang and Cooper (2002)** **Martin and Scott (2003)**	**Nakashima (2002)** **Rausch et al (2004)**
Gas/liquid flow	**Vetter et al (2000)**	**Rabiger et al (2006)**

2.2 Slip Flow Model Development

To model the performance of twin-screw multiphase pump, it is necessary to define the key geometric parameters of the screw. To be compatible with Texas A&M Twin-Screw Multiphase Pump Model, this research follow the terms and definitions in Martin's paper (Martin, 2003). The following are the brief review of the definitions and dimensions to describe twin-screw pump.

As shown in **Fig. 2.2**, the distance from a point on a screw thread to a corresponding point on the next thread measured parallel to the axis is called pitch (s). Pitch is also the axial distance of one full turn of the screw. The length of one set of screw in twin-screw pump is called screw length (l_s). Other dimensions include the root diameter D_r, external diameter D_c and the thread number n_t. Fig. 2.2 shows the single-

threaded (single flight) screw. For single-thread screw, $n_t = 1$; for double-thread (two flight as shown in **Fig. 2.3**) screw, $n_t = 2$; for triple-thread (three flight as shown in **Fig. 2.4**), $n_t = 3$. Most the design of twin-screw pumps are either single- threaded or double-threaded. In the research, all the models are developed based on single-threaded twin-screw pump. The thread number is considered in some equations.

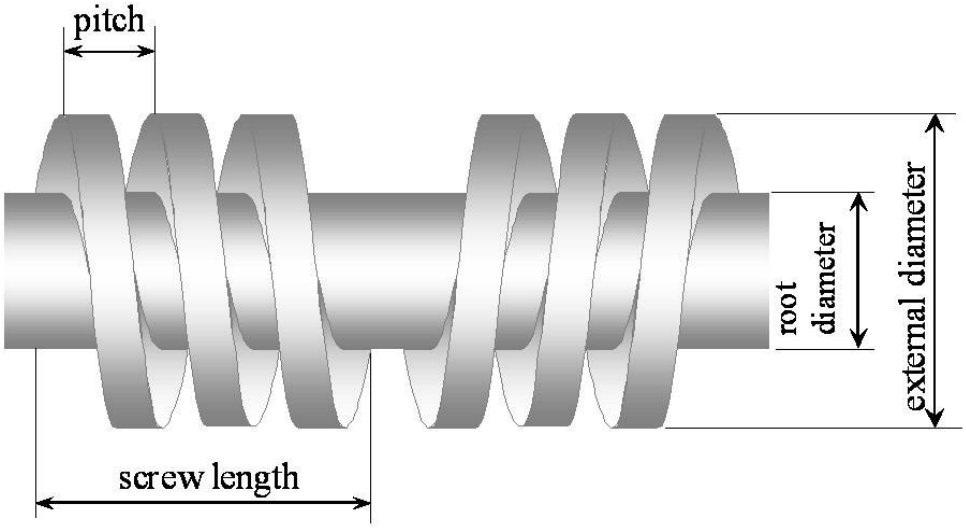

Fig. 2.2—Main dimensions of single-thread twin-screw pump rotor (Martin, 2003)

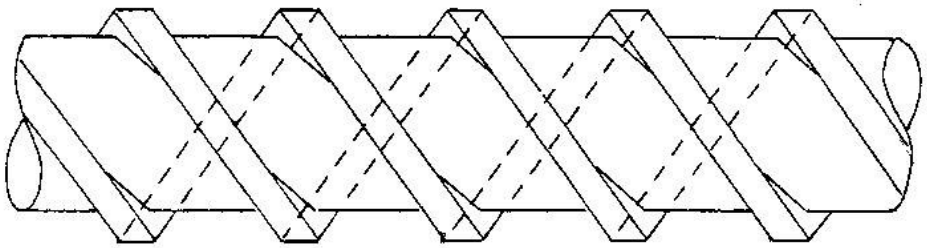

Fig. 2.3—Double-thread twin-screw pump rotor (White, 1991)

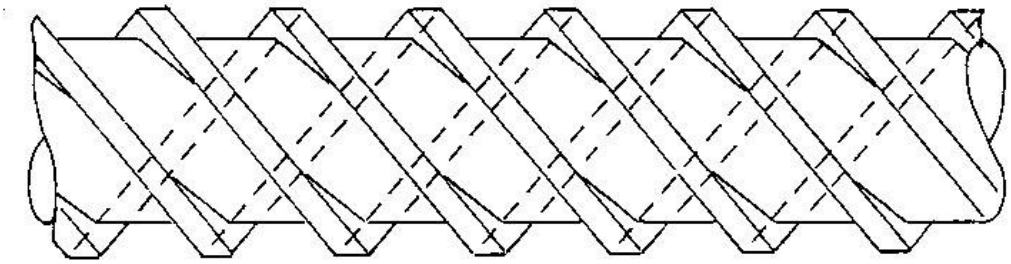

Fig. 2.4—Triple-thread twin-screw pump rotor (White, 1991)

The intermeshing of two screws generates a series of sealed chambers. With every revolution of the screws, the pump will deliver a certain amount of fluid trapped inside the chambers. The amount of fluid is defined as displacement volume D, which is the theoretical volume delivered per revolution.

$$D = n_t V_c \tag{2.14}$$

V_c is the volume of the C-shaped chamber as shown in Fig. 1.6. The calculation of V_c depends on the pump geometry (Vetter and Wincek, 1993; White, 1991).

The theoretical flow rate q_{TH} is another measurement of pump delivery, which is the theoretical pump throughput with no internal clearances. It is dependent on both the geometry of the pump and the speed N, which is:

$$q_{TH} = DN \tag{2.15}$$

However, to minimize the abrasion between screws, screws and liners, timing gear is used to keep the two screws from touching each other under working conditions. There are internal clearances between screws and liner. **Fig. 2.5** and **Fig. 2.6** illustrate the three distinct clearances in the twin-screw pump, which are Circumferential

Clearance (CC) c_c between the screws and the liner, Root Clearance (RC) c_r between the external and root diameter of the two screws, and Flank Clearance (FC) c_f between two flanks of two screws. Through these clearances, fluid flows back from discharge to suction driven by the pressure gradient across the pump, which is called slip flow or leakage flow q_{slip}. So the actual flow rate or the throughput of twin-screw pump q is the theoretical flow rate minus the slip flow. That is

$$q = q_{TH} - q_{Slip} \tag{2.16}$$

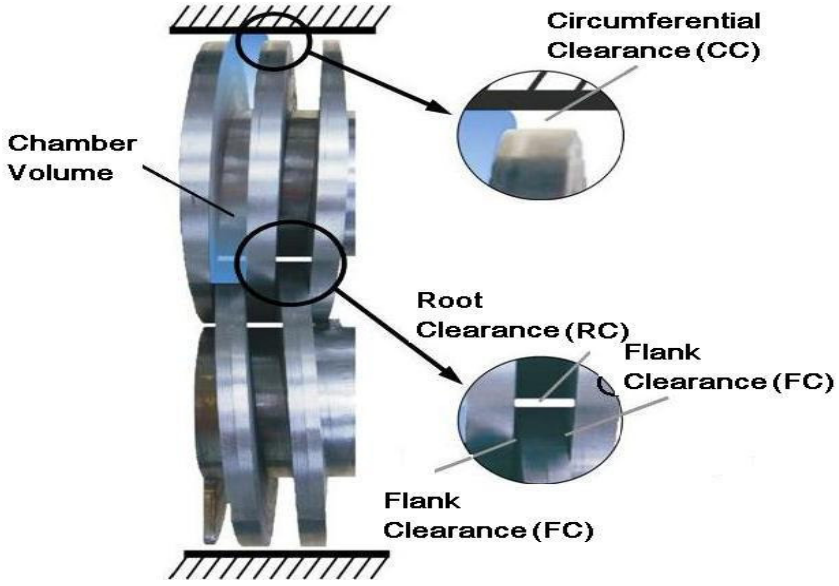

Fig. 2.5—Three main clearances inside the twin-screw pump

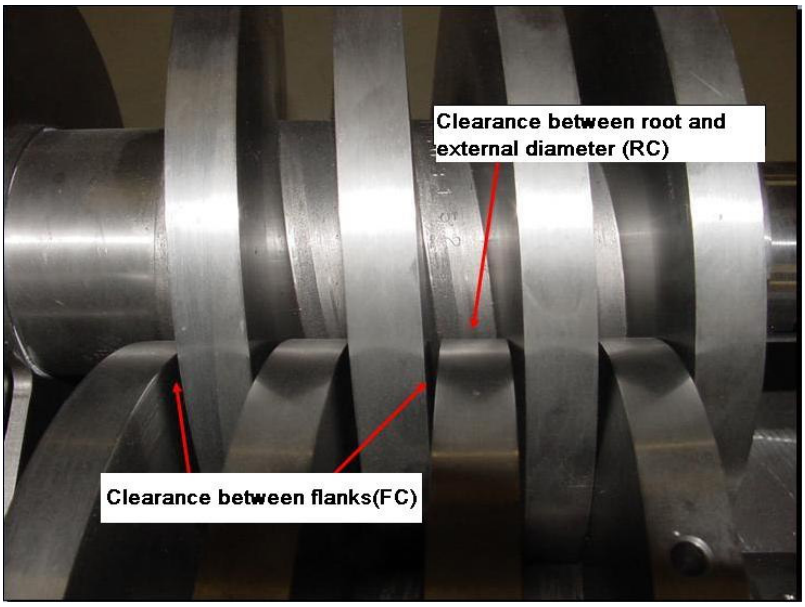

Fig. 2.6—Flank Clearance and Root Clearance

Another important parameter to model twin-screw pump is the number of sealed chambers, n, which is the number of effectively sealed chamber by the intermeshing of two screws. For single thread twin-screw pump,

$$n = 4 \times INT\left(\frac{l_s - 0.5s}{s}\right) \tag{2.17}$$

If $\left(\frac{l_s - 0.5s}{s}\right)$ is not an integer, then the real number of sealed chamber from the suction to the discharge is either n or $n+1$, which depends on the angle of rotation. The index of the chambers is shown as **Fig. 2.7**.

By simplification, the pump geometry can be described by a series of discs moving axially inside a cylindrical liner (Vetter and Wincek, 1993). Then the multiphase pumping process in the twin-screw pump with screw sets shown in Fig. 2.7 can be

simplified as **Fig. 2.8**. Due to the centrifugal force and large density difference between liquid and gas, the liquid is distributed mostly around the external side of the chamber which provides seals for the clearances and traps most of the gas inside the chamber.

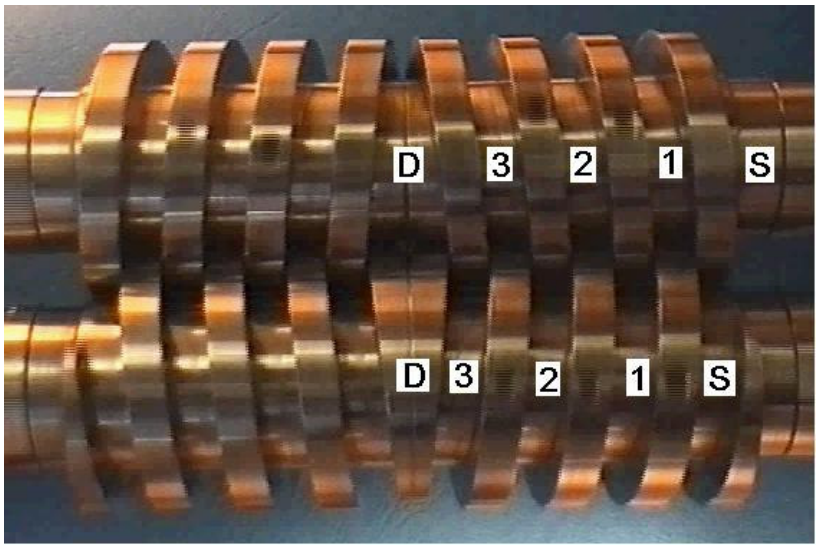

Fig. 2.7—The index of real sealed chambers inside twin-screw pump

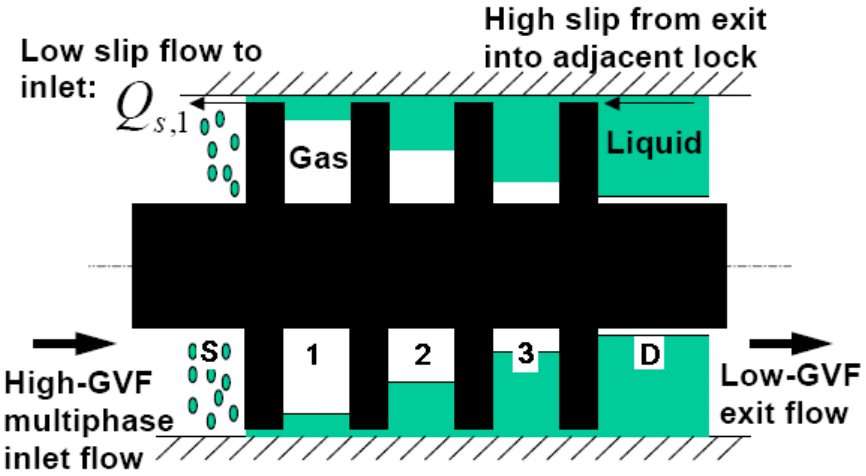

Fig. 2.8—Simplification of multiphase flow process in twin-screw pump

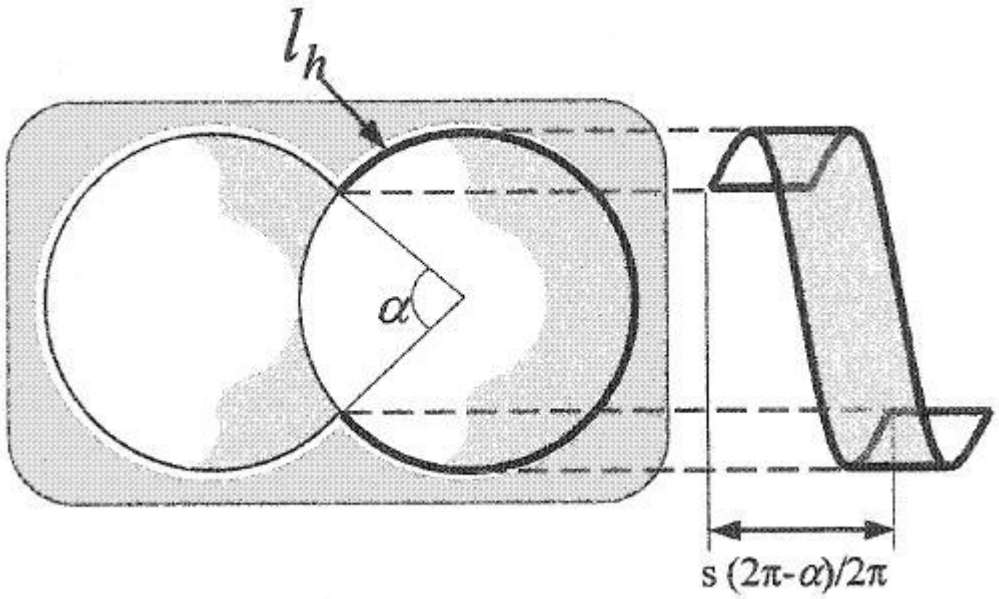

Fig. 2.9—Geometry of circumferential slip flow path

Fig. 2.9 illustrates the complicated geometry of the circumferential slip flow path. To simplify the model, it is flattened as two parallel plates as shown in **Fig. 2.10**. The distance between two plates is the circumferential clearance. The length along the flow direction is the thickness of the screw L.

For most of the screws, $L = \frac{s}{2}$

The width is l_h, Martin calculated l_h with a simple trigonometric approach (Martin, 2003).

$$l_h = (2\pi - \alpha)\sqrt{\left(\frac{s}{2\pi}\right)^2 + R_c^2} \tag{2.18}$$

where α is the portion of the circumferential channel interrupted by the screw meshing.

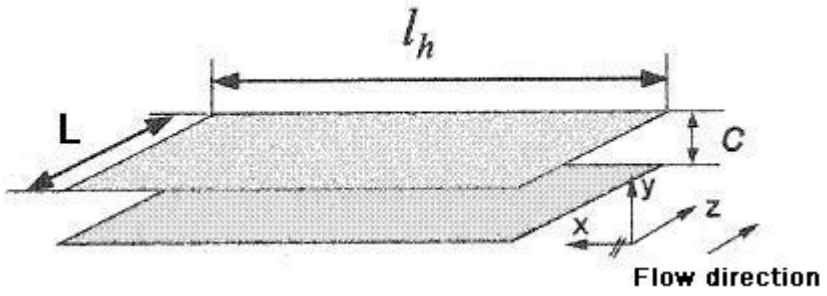

Fig. 2.10—Simplification of circumferential slip flow path

Similar with circumferential clearance, the flank slip flow path can also be approximated by simulation of two parallel plates as shown in **Fig. 2.11**.

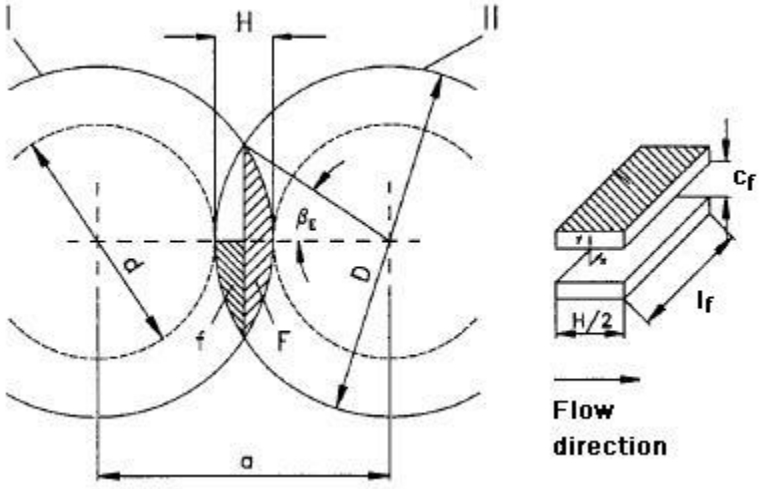

Fig. 2.11—Simplification of flank slip flow path (Vetter et al., 2000)

Martin used effective clearance to simulate the total liquid slip flow in twin-screw pump (Martin, 2003). For turbulent flow in circumferential clearance, $\mathrm{Re} > 2300$,

using the Fanning friction factor for smooth pipe by Hirs in bulk-flow turbulent model (Hirs, 1973),

$$\lambda = \frac{0.066}{\mathrm{Re}^{0.25}} \tag{2.19}$$

With

$$\mathrm{Re} = \frac{\rho \cdot c_c \cdot v}{\mu} \tag{2.20}$$

then

$$\Delta p = 4 \cdot \lambda \cdot \left(\frac{L}{2c_c} \right) \frac{\rho \cdot v^2}{2} \tag{2.21}$$

$$q_{slip,circumferencial} = l_h \cdot \left(\frac{c_c^3}{0.033 \cdot \rho^{0.75} \cdot \mu^{0.25} \cdot s} \right)^{0.57} \Delta p^{0.57} \tag{2.22}$$

For turbulent flow in flank clearance,

$$q_{slip,flank} = l_f \cdot \left(\frac{c_f^3}{0.033 \cdot \rho^{0.75} \cdot \mu^{0.25} \cdot H} \right)^{0.57} \Delta p^{0.57} \tag{2.23}$$

$$q_{slip} = q_{slip,circumferential} + q_{slip,flank} + q_{slip,root} \tag{2.24}$$

According to Vetter and Wincek (1993), for double-thread pump, the circumferential clearances contributed about 80% of the total slip flow and 5% through the flank clearances. The rest 15% is through root clearances. For single-thread pump, the combination of circumferential and flank clearances contributed more than 85% of the total slip flow. Neglect the root clearances and for the four sets of screws, then

$$q_{slip} = 4\left[l_h \cdot \left(\frac{c_c^3}{0.033 \cdot \rho^{0.75} \cdot \mu^{0.25} \cdot s} \right)^{0.57} + l_f \cdot \left(\frac{c_f^3}{0.033 \cdot \rho^{0.75} \cdot \mu^{0.25} \cdot H} \right)^{0.57} \right] \Delta p^{0.57} \tag{2.25}$$

Assume

$$q_{slip} = 4 \cdot l_h \cdot \left(\frac{c^3}{0.033 \cdot \rho^{0.75} \cdot \mu^{0.25} \cdot s} \right)^{0.57} \Delta p^{0.57} \tag{2.26}$$

then c is called the effective clearance.

Let

$$C_{eff} = 4 \cdot l_h \cdot \left(\frac{c^3}{0.033 \cdot \rho^{0.75} \cdot \mu^{0.25} \cdot s} \right)^{0.57} \tag{2.27}$$

Then the actual flow rate can be expressed as

$$q = q_{TH} - C_{eff} \cdot \Delta p^{0.57} \tag{2.28}$$

By least-squares linear regression, C_{eff} can be calculated with the data from water pump performance curve provided by the pump manufacturers. Then the effective clearance can be obtained.

For laminar flow, Martin used a correction factor to adjust the slip rate with the effective clearance obtained from turbulent flow regime.

$$q_{slip} = f_c \cdot l_h \cdot \frac{c^3}{6\mu \cdot s} \Delta p \tag{2.29}$$

After the comparison of all available single-phase liquid twin-screw pump data with 3 different manufacturers in both laminar and turbulent flow regimes, Martin suggested

$$f_c = 5$$

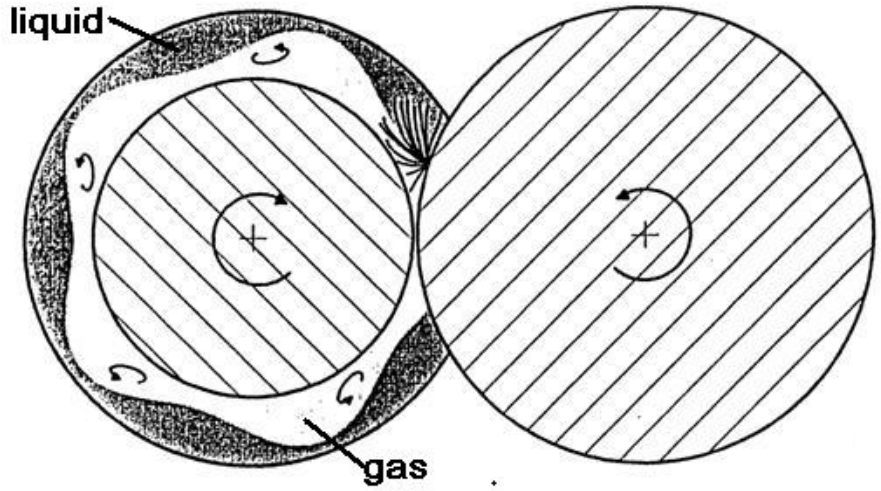

Fig. 2.12—Disturbances of gas liquid mixture in twin-screw pump (Vetter et al., 2000)

Due to the centrifugal force, liquid phase is pushed against the liner. But the rotation and forward movement of the screws do not separate liquid and gas phases perfectly. The intermeshing with the other screws also cause disturbance at the boundary area as shown in **Fig. 2.12**. With higher gas content, the liquid can not seal the slip flow path completely. Gas slip will flow back through the path. But the circumferential leakage is still playing a key role in the total slip flow. To simulate the slip flow with high gas content, liquid and gas two-phase flow must be considered in the circumferential clearances.

Since $l_h >> c$, the simulation of two-phase flow pressure drop in complex circumferential clearances become the simulation of two-phase flow pressure drop in narrow channels between two flat parallel plates.

To simulate friction pressure drop of two-phase flow, Lockhart-Martinelli parameter, X^2 is used. Lockhart-Martinelli parameter, X^2 is defined as the ratio of the single-phase friction pressure drop of liquid when liquid phase flow alone in the clearances, $\Delta p_{F,SPL}$, to that of gas when gas flow alone in the clearances, $\Delta p_{F,SPG}$ (Lockhart and Martinelli, 1949).

$$X^2 = \left(\frac{\Delta p}{\Delta z}\right)_{F,SPL} \Big/ \left(\frac{\Delta p}{\Delta z}\right)_{F,SPG} \tag{2.30}$$

With two phase flow, if $\mathrm{Re}_L < 2300$ and $\mathrm{Re}_G < 2300$, then the two-phase flow is laminar flow. When single-phase liquid with flow rate q_L goes through the clearances alone, the friction pressure drop

$$\Delta p_{F,SPL} = \frac{6 \cdot \mu_L \cdot s}{f_c \cdot l_h \cdot c^3} \cdot q_L \tag{2.31}$$

When single-phase gas with flow rate q_G goes through the clearances alone, the friction pressure drop

$$\Delta p_{F,SPG} = \frac{6 \cdot \mu_G \cdot s}{f_c \cdot l_h \cdot c^3} \cdot q_G \tag{2.32}$$

Recall the definition of Lockhart-Martinelli parameter,

$$X = \sqrt{\left(\frac{\Delta p}{\Delta z}\right)_{F,SPL} \Big/ \left(\frac{\Delta p}{\Delta z}\right)_{F,SPG}} \tag{2.33}$$

then

$$X = \left(\frac{\mu_L}{\mu_G}\right)^{0.5} \left(\frac{q_L}{q_G}\right)^{0.5} \tag{2.34}$$

Since the model should be applicable with liquid where $GVF = 0$ and theoretically, twin-screw pumps are not able to work properly with dry gas where $GVF = 100\%$, the main focus of this research is GVF from 0 to 99%. Then when there is no gas in the twin-screw pump, $\Delta p_{F,SPG} = 0$. Lockhart-Martinelli parameter, X^2 is not applicable. For the compatibility with single-phase liquid flow, the reciprocal of Lockhart-Martinelli parameter is used.

Let

$$X'^2 = \left(\frac{\Delta p}{\Delta z}\right)_{F,SPG} \Big/ \left(\frac{\Delta p}{\Delta z}\right)_{F,SPL} \tag{2.35}$$

then

$$X'_{lam} = \left(\frac{\mu_G}{\mu_L}\right)^{0.5} \left(\frac{q_G}{q_L}\right)^{0.5} \tag{2.36}$$

If $\mathrm{Re}_L > 2300$ or $\mathrm{Re}_G > 2300$, the two-phase flow is described as turbulent flow. When single-phase liquid with flow rate q_L goes through the clearances alone, the friction pressure drop

$$\Delta p_{F,SPL} = \frac{0.033 \cdot \rho_L^{0.75} \mu_L^{0.25} \cdot s}{l_h^{1.75} \cdot c^3} \cdot q_L^{1.75} \tag{2.37}$$

Since the length of flow path along the flow direction L is relatively short, the density change of gas phase is neglected. When single-phase gas with flow rate q_G goes through the clearances alone, the friction pressure drop

$$\Delta p_{F,SPG} = \frac{0.033 \cdot \rho_G^{0.75} \mu_G^{0.25} \cdot s}{l_h^{1.75} \cdot c^3} \cdot q_G^{1.75} \tag{2.38}$$

The modified Lockhart-Martinelli parameter

$$X'_{turb} = \left(\frac{\rho_G}{\rho_L}\right)^{0.375} \left(\frac{\mu_G}{\mu_L}\right)^{0.125} \left(\frac{q_G}{q_L}\right)^{0.875} \tag{2.39}$$

Assuming the accelerational pressure drop to be negligible, the two-phase flow frictional pressure drop can be estimated by two-phase friction multiplier ϕ_L^2, which is defined as the ratio of the two-phase friction pressure drop $\Delta p_{F,TP}$, to the single-phase liquid friction pressure drop $\Delta p_{F,SPL}$ (Ali et al., 1993). That is

$$\phi_L^2 = \left(\frac{\Delta p}{\Delta z}\right)_{F,TP} \Big/ \left(\frac{\Delta p}{\Delta z}\right)_{F,SPL} \tag{2.40}$$

To obtain the value of ϕ_L^2, the Lockhart-Martinelli type correlation for smooth tubes is presented (Chisholm and Laird, 1958), which is

$$\phi_L^2 = 1 + \frac{C}{X} + \frac{1}{X^2} \tag{2.41}$$

In term of modified Lockhart-Martinelli parameter X'

$$\phi_L^2 = 1 + CX' + (X')^2 \tag{2.42}$$

After examining all available experimental data with two-phase flow through narrow channels between flat plates, Ali suggested C value of 20 with mass flow rate larger than $400\,kg/m^2 s$

2.3 Isothermal Compression Model

The slip flow model established the relationship between the gas and liquid slip flows and the pressure gradient across clearances. But to simulate the performance of twin-screw pump with the only known parameters p_S p_D and GVF_S, gas slip flow q_{G0} and liquid slip flow q_{L0} have to be obtained, then the equations modeling the pressure distribution in each chamber must be found.

Since twin-screw pump is positive placement pump and each sealed chamber has the same volume. As the screw rotating, the total gas and liquid volume in the chamber must be constant. **Fig. 2.13** illustrates the pressure distribution in sealed chambers along the screws in static state at time t assuming the pressure and temperature in each chamber are homogenous.

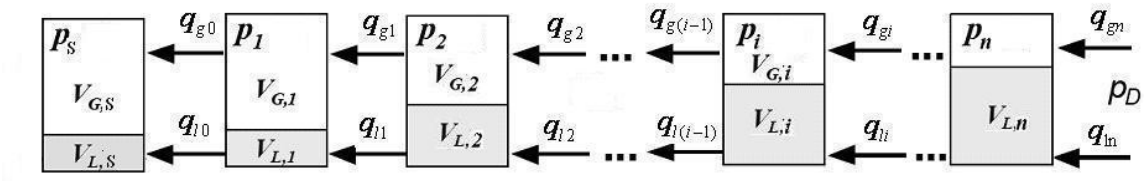

Fig. 2.13—Simplified isothermal compression model (pressure distribution from suction to discharge at time t)

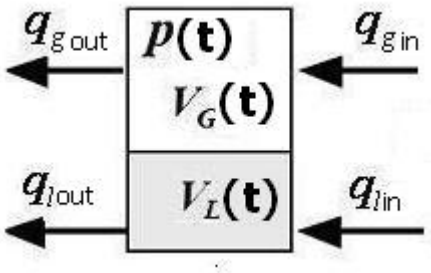

Fig. 2.14—Control volume around sealed chamber (Martin, 2003)

We define a control volume around the mixture of gas and liquid in a sealed chamber at suction as shown in **Fig. 2.14**. Then the control volume is the volume of a sealed chamber, V_c. From the suction, with each revolution, the control volume move forward one chamber, that is, from chamber (i-1) to chamber i. **Fig. 2.15** illustrates the movement of control volume from suction to discharge starting at time t.

$$\Delta t = \frac{1}{N} \tag{2.43}$$

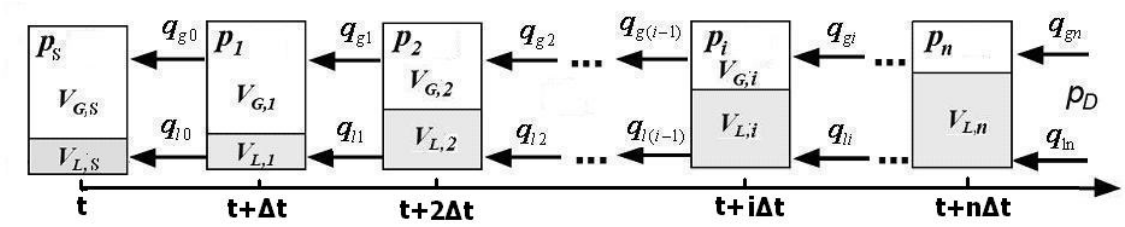

Fig. 2.15—Simplified isothermal compression model (movement of control volume from suction to discharge)

Assume that the gas slip flow rate in each chamber q_{Gi} is at suction pressure and suction temperature. At time t, the control volume is at the suction. GVF_S is the GVF of inlet fluid, then the total composition of control volume is the inlet fluid plus the gas and liquid slip flow $q_{G0} \cdot \Delta t$ and $q_{L0} \cdot \Delta t$. It can be expressed as

$$\begin{aligned} V_c = &\left(V_c - q_{L0} \cdot \Delta t - q_{G0} \cdot \Delta t\right) \cdot GVF_S + q_{L0} \cdot \Delta t + q_{G0} \cdot \Delta t \\ &+ \left(V_c - q_{L0} \cdot \Delta t - q_{G0} \cdot \Delta t\right) \cdot \left(1 - GVF_S\right) \end{aligned} \tag{2.44}$$

Then the total gas volume in the control volume is

$$V_{GS} = \left(V_c - q_{L0} \cdot \Delta t - q_{G0} \cdot \Delta t\right) \cdot GVF_S + q_{G0} \cdot \Delta t \tag{2.45}$$

The total liquid volume in the control volume is

$$V_{LS} = \left(V_c - q_{L0} \cdot \Delta t - q_{G0} \cdot \Delta t\right) \cdot (1 - GVF_S) + q_{L0} \cdot \Delta t \tag{2.46}$$

The total volume is

$$V_c = V_{GS} + V_{LS} \tag{2.47}$$

Assume the compression is isothermal. After one full revolution, at time $t + \Delta t$, the control volume moves from suction to chamber 1, the pressure of the control volume is p_1. The total composition of control volume is fluid from previous chamber plus the gas and liquid inlet slip flow $q_{G1} \cdot \Delta t$ and $q_{L1} \cdot \Delta t$ minus the gas and liquid outlet slip flow $q_{G0} \cdot \Delta t$ and $q_{L0} \cdot \Delta t$. It can be expressed as

$$V_c = V_{GS} \frac{p_S z_1}{p_1 z_S} - q_{G0} \cdot \Delta t \frac{p_S z_1}{p_1 z_S} + q_{G1} \cdot \Delta t \frac{p_S z_1}{p_1 z_S} + V_{LS} + q_{L1} \cdot \Delta t - q_{L0} \cdot \Delta t \tag{2.48}$$

Then the total gas volume in the control volume is

$$V_{G1} = \left(V_{GS} - q_{G0} \cdot \Delta t + q_{G1} \cdot \Delta t\right) \frac{p_S z_1}{p_1 z_S} \tag{2.49}$$

Then the total liquid volume in the control volume is

$$V_{L1} = \left(V_c - q_{L0} \cdot \Delta t - q_{G0} \cdot \Delta t\right) \cdot (1 - GVF_S) + q_{L1} \cdot \Delta t \tag{2.50}$$

Follow the same rule at time $t + 2\Delta t$,

$$V_c = V_{G1} \frac{p_1 z_2}{p_2 z_1} + (q_{G2} - q_{G1}) \Delta t \frac{p_S z_1}{p_1 z_S} + V_{L1} + q_{L2} \cdot \Delta t - q_{L1} \cdot \Delta t \tag{2.51}$$

$$V_{G2} = V_{G1} \frac{p_1 z_2}{p_2 z_1} + \left(q_{G2} - q_{G1}\right) \Delta t \frac{p_S z_2}{p_2 z_S} \tag{2.52}$$

$$V_{L2} = \left(V_c - q_{L0} \cdot \Delta t - q_{G0} \cdot \Delta t\right) \cdot (1 - GVF_S) + q_{L2} \cdot \Delta t \tag{2.53}$$

In the same manner, at time $t + i\Delta t$, the control volume moves to chamber i. The total composition of control volume is fluid from chamber $i - 1$ plus the gas and liquid inlet slip flow $q_{Gi} \cdot \Delta t$ and $q_{Li} \cdot \Delta t$ minus the gas and liquid outlet slip flow $q_{G(i-1)} \cdot \Delta t$ and $q_{L(i-1)} \cdot \Delta t$. It can be expressed as

$$V_c = V_{G(i-1)} \frac{p_{(i-1)} z_i}{p_i z_{(i-1)}} + (q_{Gi} - q_{G(i-1)}) \Delta t \frac{p_S z_i}{p_i z_S} + V_{L(i-1)} + q_{Li} \cdot \Delta t - q_{L(i-1)} \cdot \Delta t \tag{2.54}$$

The total gas volume in the control volume is

$$V_{Gi} = V_{G(i-1)} \frac{p_{(i-1)} z_i}{p_i z_{(i-1)}} + (q_{Gi} - q_{G(i-1)}) \Delta t \frac{p_S z_i}{p_i z_S} \tag{2.55}$$

The total liquid volume in the control volume is

$$V_{Li} = \left(V_c - q_{L0} \cdot \Delta t - q_{G0} \cdot \Delta t\right) \cdot (1 - GVF_S) + q_{Li} \cdot \Delta t \tag{2.56}$$

Then Eq. (2.48) minus Eq. (2.47) and so on, a group of equations can be obtained as following,

$$\begin{gathered}
V_{GS}\left(\frac{p_S z_1}{p_1 z_S}-1\right)+\left(q_{G1}-q_{G0}\right)\Delta t\frac{p_S z_1}{p_1 z_S}+\left(q_{L1}-q_{L0}\right)\Delta t=0 \\
V_{G1}\left(\frac{p_1 z_2}{p_2 z_1}-1\right)+\left(q_{G2}-q_{G1}\right)\Delta t\frac{p_S z_2}{p_2 z_S}+\left(q_{L2}-q_{L1}\right)\Delta t=0 \\
\vdots \\
V_{G(i-1)}\left(\frac{p_{(i-1)} z_i}{p_i z_{(i-1)}}-1\right)+\left(q_{Gi}-q_{G(i-1)}\right)\Delta t\frac{p_S z_i}{p_i z_S}+\left(q_{Li}-q_{L(i-1)}\right)\Delta t=0 \\
\vdots \\
V_{G(n-1)}\left(\frac{p_{(n-1)} z_i}{p_n z_{(n-1)}}-1\right)+\left(q_{Gn}-q_{G(n-1)}\right)\Delta t\frac{p_S z_n}{p_n z_S}+\left(q_{Ln}-q_{L(n-1)}\right)\Delta t=0
\end{gathered} \tag{2.57}$$

In Eq. (2.57), $p_1, p_2, \ldots, p_n$, $q_{L0}, q_{L1}, \ldots, q_{Ln}$ and $q_{G0}, q_{G1}, \ldots, q_{Gn}$ are unknown. The total number of unknown variables is $3n+2$. Recalling the function of the pressure drop through all the clearances, there are totally $2n+1$ equations. There are still $n+1$ equations needed to calculate all the unknown variables.

Normally, the twin-screw pump is running at lower speed than centrifugal pump, the centrifugal force is not dominant. As shown in Fig. 2.12, the turbulence by the intermeshing of two screws mitigates the separation effect. Assume the slip flow in the clearance has the same GVF with the chamber of which it flows out. Recall q_{Gi} is the gas slip flow rate at suction pressure, then

$$\frac{q_{Li}}{q_{Gi}\dfrac{p_S z_{(i+1)}}{p_{(i+1)} z_S}}=\frac{1-GVF_{(i+1)}}{GVF_{(i+1)}} \tag{2.58}$$

Assume

$$\frac{q_{Ln}}{q_{Gn}\dfrac{p_S z_D}{p_D z_S}} = \frac{1-GVF_D}{GVF_D} \tag{2.59}$$

Assume there is no phase transfer, according to energy balance

$$\frac{m_{L,in}}{m_{G,in}} = \frac{m_{L,out}}{m_{G,out}} \tag{2.60}$$

that is

$$\frac{1-GVF_S}{GVF_S}\cdot\frac{\rho_L}{\rho_{GS}} = \frac{1-GVF_D}{GVF_D}\cdot\frac{\rho_L}{\rho_{GD}} \tag{2.61}$$

$$GVF_D = \frac{1}{\dfrac{p_D z_S}{p_S z_D}\cdot\dfrac{1-GVF_S}{GVF_S}+1} \tag{2.62}$$

The GVF in each chamber can be calculated as

$$GVF_i = 1-\frac{V_{Li}}{V_c} \tag{2.63}$$

Put Eq. (2.56) into Eq. (2.63),

$$GVF_i = 1-\frac{\left(V_c - q_{L0}\cdot\Delta t - q_{G0}\cdot\Delta t\right)\cdot(1-GVF_S)+q_{Li}\cdot\Delta t}{V_c} \tag{2.64}$$

Then GVF_i is function of $q_{G0}\cdot\Delta t$ and $q_{L0}\cdot\Delta t$, which makes Eq. (2.64) difficult to solve. To involve the effect of radial gas/liquid separation, the GVF of slip flow in the clearances GVF_i' should be lower than that in the chamber. But due to the complex geometry of twin-screw pump and flow pattern of multiphase flow, the actual GVF is difficult to be calculated. To simplify the calculation of GVF of slip flow, an approximation is made. $q_{G0}\cdot\Delta t$ and $q_{L0}\cdot\Delta t$ are neglected.

Assume

$$GVF_i' = 1 - \frac{V_c \cdot (1 - GVF_S) + q_{Li} \cdot \Delta t}{V_c} \tag{2.65}$$

then

$$GVF_i = GVF_S - \frac{q_{Li} \cdot \Delta t}{V_c} \tag{2.66}$$

Due to the complication of functions, $p_1, p_2, \ldots, p_n$ can not be calculated explicitly. Let

$$f_i = V_{G(i-1)} \left(\frac{p_{(i-1)} z_i}{p_i z_{(i-1)}} - 1 \right) + \left(q_{Gi} - q_{G(i-1)} \right) \Delta t \frac{p_S z_i}{p_i z_S} + \left(q_{Li} - q_{L(i-1)} \right) \tag{2.67}$$

$$F = \sqrt{\sum_{i=1}^{n} f_i^2} \tag{2.68}$$

then the solution of Eq. (2.68) become finding $p_1, p_2, \ldots, p_n$ which make the value of F minimum. It can only be estimated by iteration.

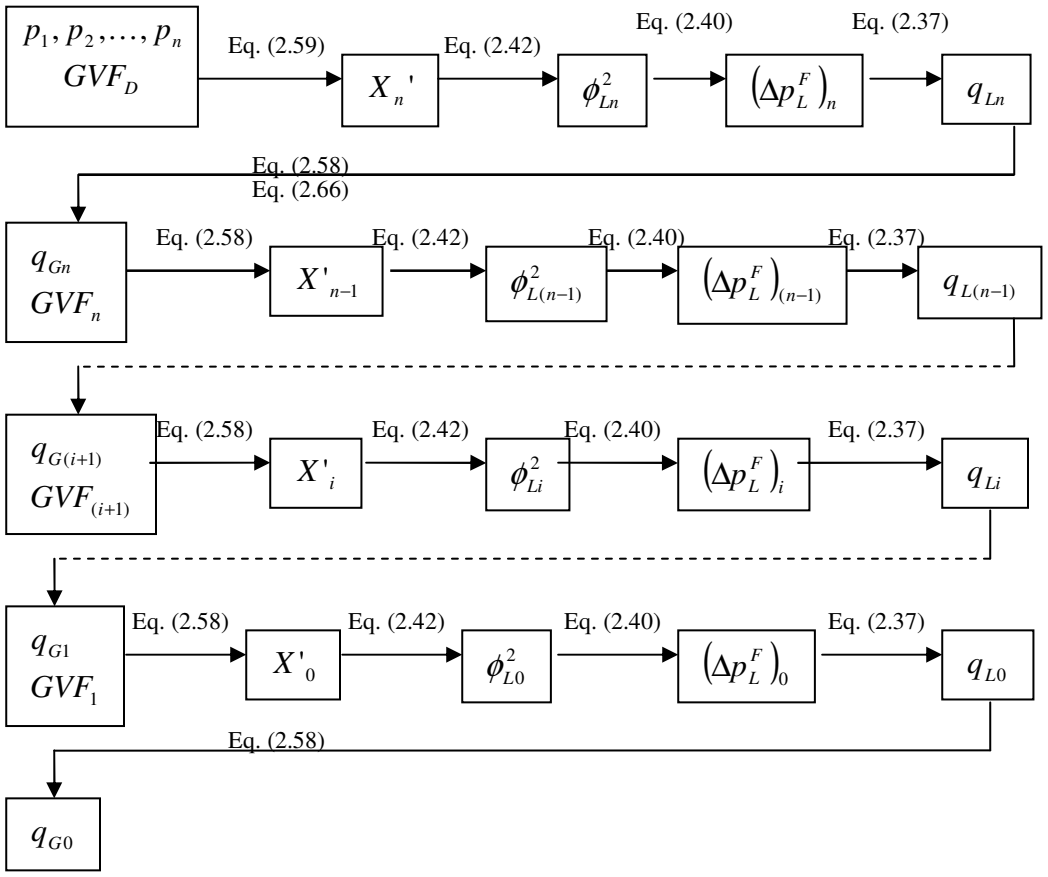

Fig. 2.16—Procedure of calculating variables in simplified isothermal compression model

Fig. 2.16 indicates the procedure of calculating, $q_{L0}, q_{L1,} \ldots, q_{Ln}$ and $q_{G0}, q_{G1,} \ldots, q_{Gn}$, given. $p_1, p_2, \ldots, p_n$. Assume gas is ideal gas, $z_i = 1$. Put all the variables into Eq. (2.64) and the minimum value of F and corresponding $p_1, p_2, \ldots, p_n$, $q_{L0}, q_{L1,} \ldots, q_{Ln}$, and $q_{G0}, q_{G1,} \ldots, q_{Gn}$ are estimated by Powell algorithm.

2.4 Non-isothermal Compression Model

Normally, liquid has much larger density and heat capacity than gas. For example, the density of water is 10 to 100 times as the density of gas depending on the pressure and temperature. And the heat capacity of water is more than four times as gas. When twin-screw pump boost gas and liquid mixture with low GVF, the heat generated by gas compression can only make the liquid temperature increase a little if it is all absorbed by liquid. The compression process is isothermal. But when there is very high gas content in the twin-screw pump, the limited liquid in the pump can not absorb all the heat and keep the temperature constant. Vetter (1993) suggested the isothermal process is only available with GVF less than 96%. The thermodynamic process deviates from isothermal process toward adiabatic with increasing compression ratio and GVF. Furthermore, the slip flow returns back from discharge to suction through clearances and makes an extra increment in fluid temperature (Nakashima et al., 2006).

To simulate the thermal process in the twin-screw pump, the mechanical model shown has to be coupled with thermal model. **Fig. 2.17** illustrates the mechanical model with different temperature distribution.

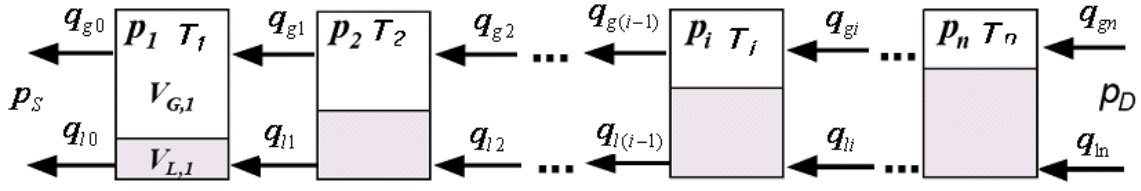

Fig. 2.17—Simplified mechanical model of twin-screw pump with temperature distribution

Assume the gas is ideal gas, and then the mechanical model is modified from isothermal model as following.

The GVF at the discharge is

$$GVF_D = \frac{1}{\frac{p_D T_S}{p_S T_D} \cdot \frac{1-GVF_S}{GVF_S} + 1} \tag{2.69}$$

$$\frac{q_{Li}}{q_{Gi}\frac{p_S T_{(i+1)}}{p_{(i+1)} T_S}} = \frac{1-GVF_{(i+1)}}{GVF_{(i+1)}} \tag{2.70}$$

In chamber i,

$$V_{Gi} = V_{G(i-1)}\frac{p_{(i-1)}T_i}{p_i T_{(i-1)}} + (q_{Gi} - q_{G(i-1)})\Delta t \frac{p_S T_i}{p_i T_S} \tag{2.71}$$

$$V_{Li} = \left(V_c - q_{L0}\cdot\Delta t - q_{G0}\cdot\Delta t\right)\cdot(1-GVF_S) + q_{Li}\cdot\Delta t \tag{2.72}$$

$$\begin{aligned}
V_{GS}\left(\frac{p_S T_1}{p_1 T_S} - 1\right) + \left(q_{G1} - q_{G0}\right)\Delta t \frac{p_S T_1}{p_1 T_S} + \left(q_{L1} - q_{L0}\right)\Delta t = 0 \\
V_{G1}\left(\frac{p_1 T_2}{p_2 T_1} - 1\right) + \left(q_{G2} - q_{G1}\right)\Delta t \frac{p_S T_2}{p_2 T_S} + \left(q_{L2} - q_{L1}\right)\Delta t = 0 \\
\vdots \\
V_{G(i-1)}\left(\frac{p_{(i-1)}T_i}{p_i T_{(i-1)}} - 1\right) + \left(q_{Gi} - q_{G(i-1)}\right)\Delta t \frac{p_S T_i}{p_i T_S} + \left(q_{Li} - q_{L(i-1)}\right)\Delta t = 0 \\
\vdots \\
V_{G(n-1)}\left(\frac{p_{(n-1)}T_i}{p_n T_{(n-1)}} - 1\right) + \left(q_{Gn} - q_{G(n-1)}\right)\Delta t \frac{p_S T_n}{p_n T_S} + \left(q_{Ln} - q_{L(n-1)}\right)\Delta t = 0
\end{aligned} \tag{2.73}$$

Let

$$f_{i,non-isotheraml} = V_{G(i-1)}\left(\frac{p_{(i-1)}T_i}{p_i T_{(i-1)}} - 1\right) + \left(q_{Gi} - q_{G(i-1)}\right)\Delta t \frac{p_S T_i}{p_i T_S} + \left(q_{Li} - q_{L(i-1)}\right) \tag{2.74}$$

The mass and energy balance for each chamber i in the pump is shown in **Fig. 2.18**.

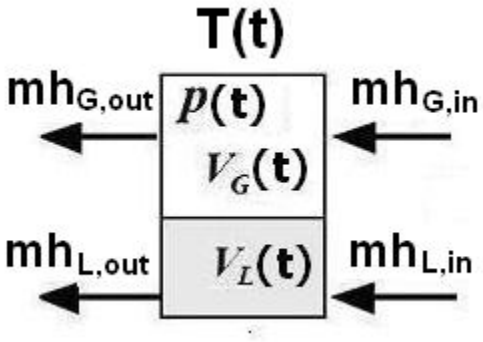

Fig. 2.18—Mass and energy balance for control volume around sealed chamber

Energy balance around the control volume

$$\frac{dU}{dt} = \dot{Q} - \dot{W} + \dot{m}_{in} h_{in} - \dot{m}_{out} h_{out} - q_{Gi} \cdot \frac{p_S T_i}{p_{i+1} T_S} \cdot \frac{p_{i+1} + p_i}{2} + q_{G(i-1)} \cdot \frac{p_S T_i}{p_i T_S} \cdot \frac{p_{i-1} + p_i}{2} \tag{2.75}$$

After a short period Δt

$$dU = Q - W + \dot{m}_{in} \cdot \Delta t \cdot h_{in} - \dot{m}_{out} \cdot \Delta t \cdot h_{out} - q_{Gi} \cdot \Delta t \cdot \frac{p_S T_i}{p_{i+1} T_S} \cdot \frac{p_{i+1} + p_i}{2} + q_{G(i-1)} \cdot \Delta t \cdot \frac{p_S T_i}{p_i T_S} \cdot \frac{p_{i-1} + p_i}{2} \tag{2.76}$$

Recalling the definition of enthalpy,

$$U = H - pV \tag{2.77}$$

and

$$\Delta H = H_i - H_{i-1} = m_i c_p \left(T_i - T_{i-1}\right) \tag{2.78}$$

$$\Delta U = U_i - U_{i-1} \tag{2.79}$$

$$\begin{aligned} \Delta U = {} & V_{Gi} \cdot \rho_{GS} \cdot \frac{p_i T_S}{p_S T_i} \cdot c_{pG} \cdot T_i + V_{Li} \cdot \rho_L \cdot c_{pL} \cdot T_i - p_i \cdot V_c \\ & - V_{G(i-1)} \cdot \rho_{GS} \cdot \frac{p_{i-1} T_S}{p_S T_{i-1}} \cdot c_{pG} \cdot T_{i-1} - V_{L(i-1)} \cdot \rho_L \cdot c_{pL} \cdot T_{i-1} + p_{i-1} \cdot V_c \end{aligned} \tag{2.80}$$

According to the definition of work W

$$W = \int_{i-1}^{i} p dV \tag{2.81}$$

Because the time period Δt is short, the pressure change Δt is replaced by the average pressure between the initial pressure and end pressure. That is

$$\overline{p} = \frac{p_{i-1} + p_i}{2} \tag{2.82}$$

then after short period Δt ,

$$W = \overline{p}_{i-1} \cdot \Delta V_{G(i-1)} + \overline{p}_i \cdot \Delta V_{G,in} \tag{2.83}$$

$$W = \frac{p_{i-1} + p_i}{2} V_{G(i-1)} \left(\frac{p_{i-1} T_i}{p_i T_{i-1}} - 1 \right) + q_{Gi} \Delta t \left(\frac{p_S T_{i+1}}{p_{i+1} T_S} - \frac{p_S T_i}{p_i T_S} \right) \frac{p_i + p_{i+1}}{2} \tag{2.84}$$

Assume the chamber is adiabatic, that is, there is no heat transfer between the fluid and the surrounding liner and screws. The kinetic energy and wall friction are neglected. And there is no heat loss. Then

$$Q = 0 \tag{2.85}$$

With

$$\begin{aligned} m_{in} h_{in} - m_{out} h_{out} = {} & q_{Gi} \cdot \Delta t \cdot \rho_{GS} \cdot c_{pG} \cdot T_{i+1} + q_{Li} \cdot \Delta t \cdot \rho_L \cdot c_{pL} \cdot T_{i+1} \\ & - q_{G(i-1)} \cdot \Delta t \cdot \rho_{GS} \cdot c_{pG} \cdot T_i - q_{L(i-1)} \cdot \Delta t \cdot \rho_L \cdot c_{pL} \cdot T_i \end{aligned} \tag{2.86}$$

Put Eq. (2.78), (2.80) and (2.84) into (2.76),

$$\begin{aligned}
&V_{Gi}\cdot\rho_{GS}\cdot\frac{p_iT_S}{p_ST_i}\cdot c_{pG}\cdot T_i+V_{Li}\cdot\rho_L\cdot c_{pL}\cdot T_i-p_i\cdot V_c-V_{G(i-1)}\cdot\rho_{GS}\cdot\frac{p_{i-1}T_S}{p_ST_{i-1}}\cdot c_{pG}\cdot T_{i-1}\\
&-V_{L(i-1)}\cdot\rho_L\cdot c_{pL}\cdot T_{i-1}+p_{i-1}\cdot V_c\\
&+\frac{p_{i-1}+p_i}{2}V_{G(i-1)}\left(\frac{p_{i-1}T_i}{p_iT_{i-1}}-1\right)+q_{Gi}\Delta t\left(\frac{p_ST_{i+1}}{p_{i+1}T_S}-\frac{p_ST_i}{p_iT_S}\right)\frac{p_{i+1}+p_i}{2}\\
&+q_{G(i-1)}\cdot\Delta t\cdot\rho_{GS}\cdot c_{pG}\cdot T_i+q_{L(i-1)}\cdot\Delta t\cdot\rho_L\cdot c_{pL}\cdot T_i-q_{Gi}\cdot\Delta t\cdot\rho_{GS}\cdot c_{pG}\cdot T_{i+1}\\
&-q_{Li}\cdot\Delta t\cdot\rho_L\cdot c_{pL}\cdot T_{i+1}+q_{Gi}\cdot\Delta t\cdot\frac{p_ST_i}{p_{i+1}T_S}\cdot\frac{p_{i+1}+p_i}{2}-q_{G(i-1)}\cdot\Delta t\cdot\frac{p_ST_i}{p_iT_S}\cdot\frac{p_{i-1}+p_i}{2}=0
\end{aligned}\tag{2.87}$$

For the discharge,

$$\begin{aligned}
&V_{GD}\cdot\rho_{GS}\cdot\frac{p_DT_S}{p_ST_D}\cdot c_{pG}\cdot T_D+V_{LD}\cdot\rho_L\cdot c_{pL}\cdot T_D-p_D\cdot V_c-V_{Gn}\cdot\rho_{GS}\cdot\frac{p_nT_S}{p_ST_n}\cdot c_{pG}\cdot T_n\\
&-V_{Ln}\cdot\rho_L\cdot c_{pL}\cdot T_n+p_n\cdot V+\frac{p_n+p_D}{2}V_{Gn}\left(\frac{p_{i-1}T_i}{p_iT_{i-1}}-1\right)\\
&+q_{Gn}\cdot\Delta t\cdot\rho_{GS}\cdot c_{pG}\cdot T_D+q_{Ln}\cdot\Delta t\cdot\rho_L\cdot c_{pL}\cdot T_D=0
\end{aligned}\tag{2.88}$$

Let

$$\begin{aligned}
f_{i,thermal}=&V_{Gi}\cdot\rho_{GS}\cdot\frac{p_iT_S}{p_ST_i}\cdot c_{pG}\cdot T_i+V_{Li}\cdot\rho_L\cdot c_{pL}\cdot T_i-p_i\cdot V_c\\
&-V_{G(i-1)}\cdot\rho_{GS}\cdot\frac{p_{i-1}T_S}{p_ST_{i-1}}\cdot c_{pG}\cdot T_{i-1}-V_{L(i-1)}\cdot\rho_L\cdot c_{pL}\cdot T_{i-1}+p_{i-1}\cdot V_c\\
&+\frac{p_{i-1}+p_i}{2}V_{G(i-1)}\left(\frac{p_{i-1}T_i}{p_iT_{i-1}}-1\right)+q_{Gi}\Delta t\left(\frac{p_ST_{i+1}}{p_{i+1}T_S}-\frac{p_ST_i}{p_iT_S}\right)\frac{p_{i+1}+p_i}{2}\\
&+q_{G(i-1)}\cdot\Delta t\cdot\rho_{GS}\cdot c_{pG}\cdot T_i+q_{L(i-1)}\cdot\Delta t\cdot\rho_L\cdot c_{pL}\cdot T_i-q_{Gi}\cdot\Delta t\cdot\rho_{GS}\cdot c_{pG}\cdot T_{i+1}\\
&-q_{Li}\cdot\Delta t\cdot\rho_L\cdot c_{pL}\cdot T_{i+1}+q_{Gi}\cdot\Delta t\cdot\frac{p_ST_i}{p_{i+1}T_S}\cdot\frac{p_{i+1}+p_i}{2}-q_{G(i-1)}\cdot\Delta t\cdot\frac{p_ST_i}{p_iT_S}\cdot\frac{p_{i-1}+p_i}{2}
\end{aligned}\tag{2.89}$$

Given p_S , p_D and T_S , $p_1, p_2, \ldots, p_n$ and $T_1, T_2, \ldots, T_n, T_D$ should satisfy Eq. (2.69)-(2.88). Let

$$F = \sqrt{\sum_{i=1}^{n} \left(f_{i,non-isothermal}^2 + f_{i,thermal}^2 \right)} \tag{2.90}$$

To solve the equation group, the procedure of calculating, $q_{L0}, q_{L1,} \ldots, q_{Ln}$ and $q_{G0}, q_{G1,} \ldots, q_{Gn}$, given. $p_1, p_2, \ldots, p_n$ will be following as shown in Fig. 2.16. Put all the variables into Eq. (2.90) and the minimum value of F and corresponding $p_1, p_2, \ldots, p_n$, $q_{L0}, q_{L1,} \ldots, q_{Ln}$, and $q_{G0}, q_{G1,} \ldots, q_{Gn}$ are estimated by Powell algorithm.

3. TWIN-SCREW PUMP MODEL VALIDATION

3.1 Experimental Facility

The experiments were carried out at the Multiphase Field Laboratory, located at the Texas A&M University Riverside Campus. This facility is outfitted with field scale equipments including two full-size twin-screw multiphase pumps. The layout of Multiphase Field Laboratory facility is illustrated in **Fig. 3.1**.

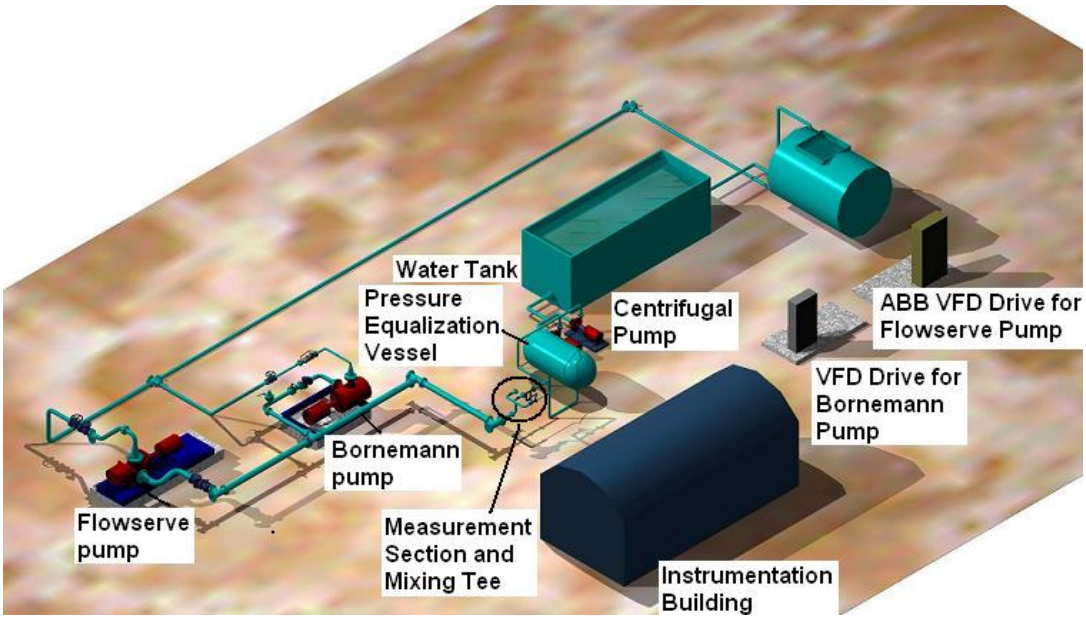

Fig. 3.1—The layout of Multiphase Field Laboratory facility

The twin-screw multiphase pump used for wet gas compression is Bornemann MW-6.5zk-37 which has a 37 mm pitch and 50hp electric motor. This pump has a capacity of 10,000 bbl/day with a maximum differential pressure of 250 psi and maximum pump speed of 1800 rpm. The pump speed is controlled by a Variable

Frequency Drive (VFD) using a Kimo MotorMaster frequency inverter. **Fig. 3.2** shows a side view of this Bornemann pump with motor. The discharge section of the pump is upwards and the outlet diameter is much larger than the pipeline, which helps retain liquid inside the pump.

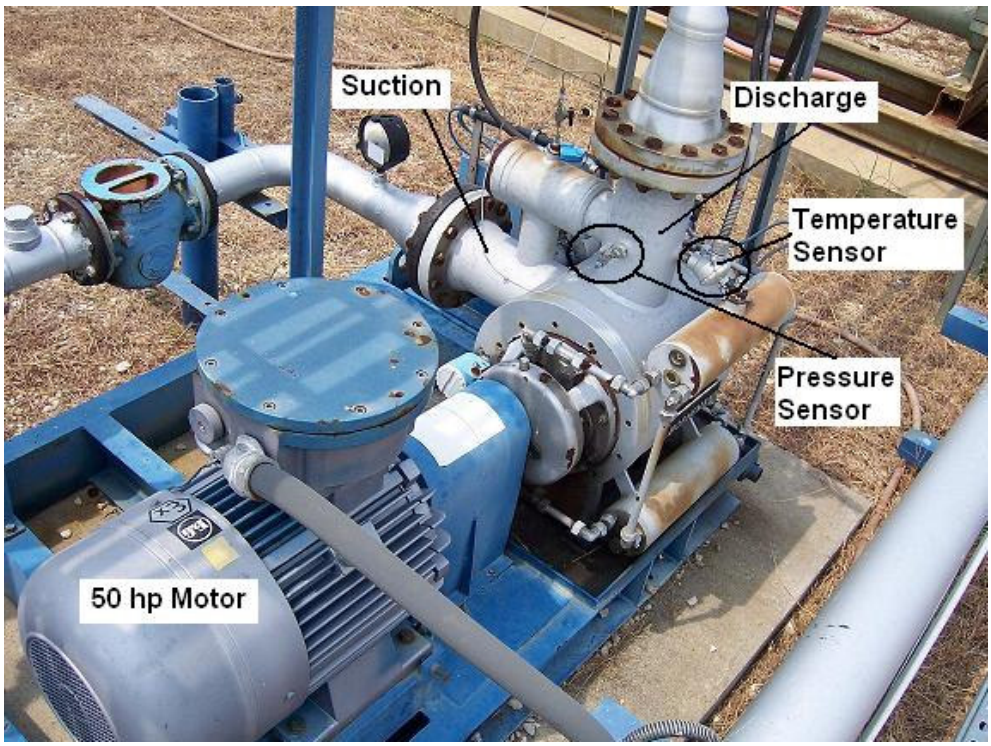

Fig. 3.2—Bornemann MW-6.5zk-37 twin-screw multiphase pump with motor

Fig. 1.12 shows Flowserve LSIJS twin-screw pump and 200hp motor with the Voith torque converter EL6. The Flowserve pump has a capacity of 17,000 bbl/day and maximum speed of 2000 rpm and the maximum pressure boost of 500psi. It can handle GVF up to 85%, so it is used for the torque converter test instead of wet gas compression.

Fig. 3.3 shows the flow diagram of the flow loop at this test facility. water is boosted from a water tank by two 15 hp centrifugal pumps as charging pump shown in **Fig. 3.4**. The configuration of pipeline connecting the suctions and discharges of both centrifugal pumps enable them to run either in parallel or in series, which gives flexibility to control the suction pressure of the twin-screw pump.

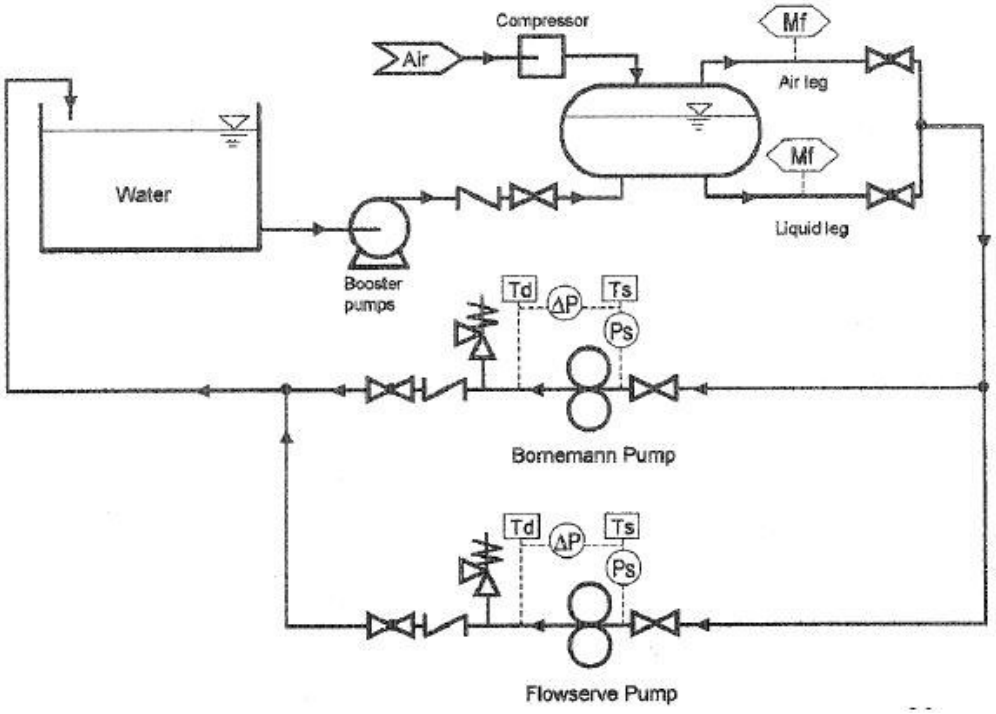

Fig. 3.3—Flow diagram of test facility (Martin, 2003)

Fig. 3.4—Configuration of pipelines and two 15 hp centrifugal pumps

Air is injected into a pressure equalization vessel using a 49hp, 185 CFM air compressor. Water is also pumped into this vessel. The inlet and outlet of air are on top of the vessel and the inlet and outlet of liquid are on the bottom as shown in **Fig. 3.5.** The vessel helps equalize the pressure of each phase and damps any pulsation that could be generated by the compressor and phase mixing.

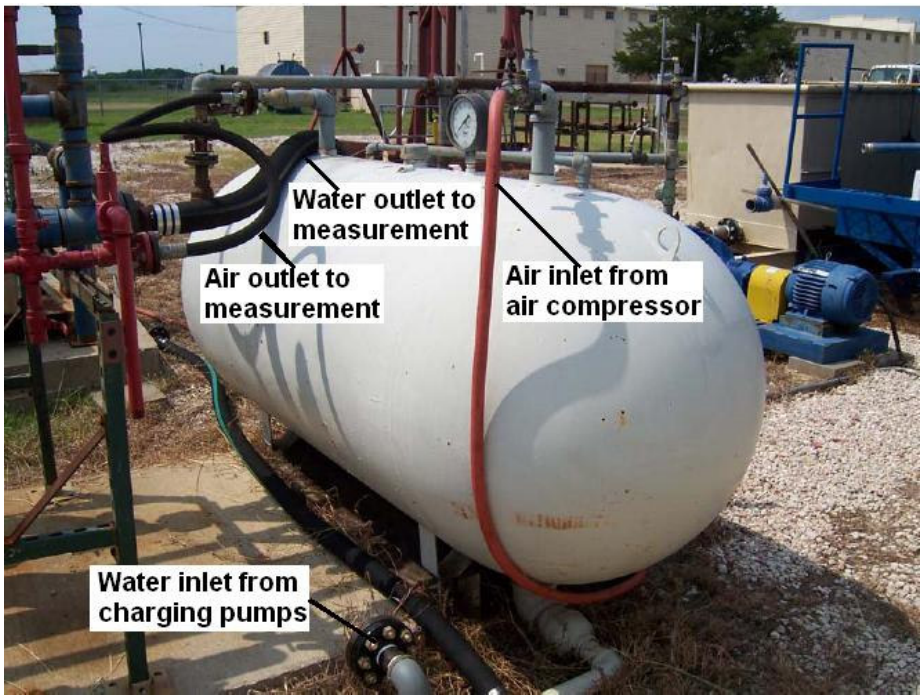

Fig. 3.5—Configuration of pressure equalization vessel

Air is then taken from the top of the vessel to the air measurement leg where a 1-inch MicroMotion gas coriolis mass-flow meter measures the air mass rate. Water from the bottom of the vessel is pushed by the pressure in the vessel to the liquid measurement leg and the flow is measured by a 3-inch MicroMotion liquid coriolis mass-flow meter. These types of meters are highly accurate with errors of ± 0.10% for liquid flow rates and ± 0.50% for gas flow rates. A ball valve in the liquid measurement leg and a needle valve in the air measurement leg regulate the flowrates of liquid and air, respectively, controlling the gas-volume fraction at the suction of the twin-screw pump. The air and liquid are mixed in a mixing tee, and from there the mixture flows to the

twin-screw pump. The coriolis meters of both gas and liquid, together with the mixing tee are shown in **Fig. 3.6**.

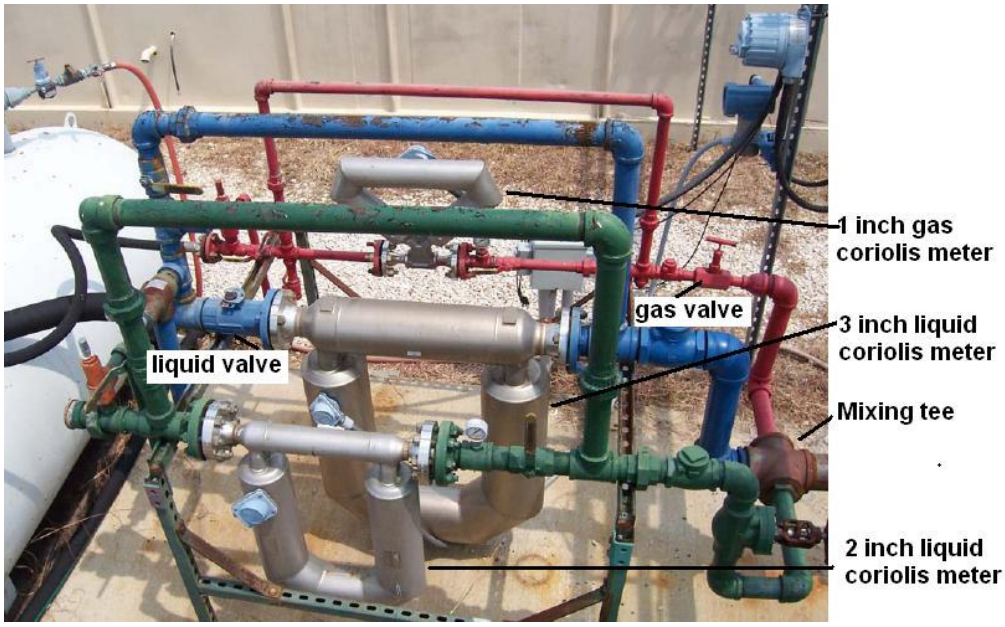

Fig. 3.6—Gas and liquid coriolis meters and mixing tee

Temperature and pressure transducers measure the suction temperature and pressure, and ΔP across the twin-screw pump. A valve is used at the discharge of the pump to adjust the backpressure of the pump. **Table 3.1** listed all types of meters and transducers used in this experiment.

Signals from the flow meters, temperature and pressure transducers were captured using a PC with a National Instruments PCI data acquisition card. LabVIEW 8 was used to record data. The GVF at the suction of the twin-screw pump is calculated by the liquid and gas volumetric flow rates. The gas flow rate is calculated by the mass flow

rate of gas, the pressure and temperature at the suction of twin-screw pump. Due to the slug and instability of multiphase flow, data was recorded for an extended period of time (2 minutes) and then averaged.

TABLE 3.1—METERS INVOLVED IN THE EXPERIMENTS

Measurement	Type	Manufacturer	Model	Calibrated Range	Accuracy
Liquid mass flow rate	Coriolis	Micro Motion - Elite Series	CMF300M355NUR	0-2500 lb/min	±0.1%
Gas mass flow rate	Coriolis	Micro Motion - Elite Series	CMF100M329NU	0-20 lb/min	±0.5%
Differential pressure across the twin-screw pump	Pressure transducer	Rosemount	1151DP7E22M1B2	0-300psi	±0.075%
Suction pressure of the twin-screw pump	Pressure transducer	Rosemount	1151AP6E12M1B1	0-100psia	±0.075%
Temperatures of suction and discharge of the twin-screw pump	Temperature transducer	Weed Instruments	17A00A1	0-300deg F	

3.2 Results and Discussion

Same as Martin's model, this simulator used the main parameters of twin-screw pump and single-phase water performance curves to generate the effective clearance data. **Table 3.2** lists the parameters of Bornemann MW-6.5zk-37 twin-screw pump as input data to the similar. Single phase water performance curve is generated with pump speed

1350rpm. The data matrix with Bornemann twin-screw multiphase pump is listed in **Table 3.3**.

TABLE 3.2—MAIN PARAMETERS OF BORNEMANN PUMP

Model	D (gal/rev)	s (in/rev)	l_s (in)	D_c (in)	D_r (in)	n_t
MW 6.5zk-37	0.17	1.46	5.90	5.24	2.79	1

TABLE 3.3—DATA MATRIX IN WET GAS COMPRESSION EXPERIMENT

Viscosity (cp)	GVF (%)	Pump Speed (rpm)
1 (water)	0	1350
5 (glycerin-water mixture)	95	1700
	98	

To simulate the effect of liquid viscosity to twin-screw pump performance, glycerin-water mixture is used. The viscosity with weight concentration and temperature is listed in **Table 3.4**. The glycerin weight concentration is 50%. The measured density of mixture is 9.395 lb/gal and the viscosity is 5cp. Because the mixture is Newtonian fluid, the viscosity is only the function of glycerin concentration and temperature, not the shear rate. It is ideal to evaluate the effect of liquid viscosity without the influence of pump speed.

TABLE 3.4—VISCOSITY OF AQUEOUS GLYCERIN SOLUTIONS IN CENTIPOISES

Glycerine percent weight	Temperatur e (°C)										
	0	10	20	30	40	50	60	70	80	90	100
0 [1]	1.792	1.308	1.005	0.8007	0.6560	0.5494	0.4688	0.4061	0.3565	0.3165	0.2838
10	2.44	1.74	1.31	1.03	0.826	0.680	0.575	0.500	–	–	–
20	3.44	2.41	1.76	1.35	1.07	0.879	0.731	0.635	–	–	–
30	5.14	3.49	2.50	1.87	1.46	1.16	0.956	0.816	0.690	–	–
40	8.25	5.37	3.72	2.72	2.07	1.62	1.30	1.09	0.918	0.763	0.668
50	14.6	9.01	6.00	4.21	3.10	2.37	1.86	1.53	1.25	1.05	0.910
60	29.9	17.4	10.8	7.19	5.08	3.76	2.85	2.29	1.84	1.52	1.28
65	45.7	25.3	15.2	9.85	6.80	4.89	3.66	2.91	2.28	1.86	1.55
67	55.5	29.9	17.7	11.3	7.73	5.50	4.09	3.23	2.50	2.03	1.68
70	76	38.8	22.5	14.1	9.40	6.61	4.86	3.78	2.90	2.34	1.93
75	132	65.2	35.5	21.2	13.6	9.25	6.61	5.01	3.80	3.00	2.43
80	255	116	60.1	33.9	20.8	13.6	9.42	6.94	5.13	4.03	3.18
85	540	223	109	58	33.5	21.2	14.2	10.0	7.28	5.52	4.24
90	1310	498	219	109	60.0	35.5	22.5	15.5	11.0	7.93	6.00
91	1590	592	259	127	68.1	39.8	25.1	17.1	11.9	8.62	6.40
92	1950	729	310	147	78.3	44.8	28.0	19.0	13.1	9.46	6.82
93	2400	860	367	172	89	51.5	31.6	21.2	14.4	10.3	7.54
94	2930	1040	437	202	105	58.4	35.4	23.6	15.8	11.2	8.19
95	3690	1270	523	237	121	67.0	39.9	26.4	17.5	12.4	9.08
96	4600	1580	624	281	142	77.8	45.4	29.7	19.6	13.6	10.1
97	5770	1950	765	340	166	88.9	51.9	33.6	21.9	15.1	10.9
98	7370	2460	939	409	196	104	59.8	38.5	24.8	17.0	12.2
99	9420	3090	1150	500	235	122	69.1	43.6	27.8	19.0	13.3
100	12070	3900	1410	612	284	142	81.3	50.6	31.9	21.3	14.8

[1] Viscosity of water taken from "Properties of Ordinary Water-Substance." N.E. Dorsey, p. 184. New York (1940)

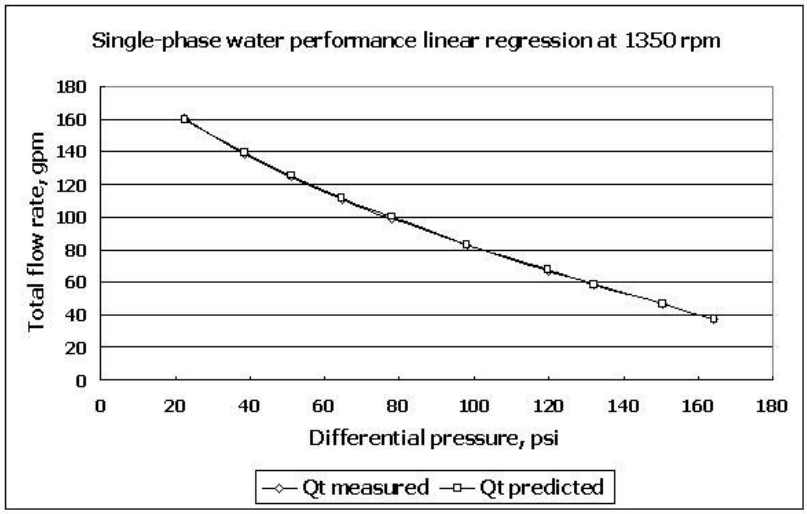

Fig. 3.7—Linear regressions with single-phase water performance curve at 1350 rpm (water)

Fig. 3.7 shows the linear regression with single-phase water performance curve at 1350 rpm. The effective clearance is generated. And this effective clearance is used for the following simulation of Bornemann pump at different GVF, viscosity and pump speed.

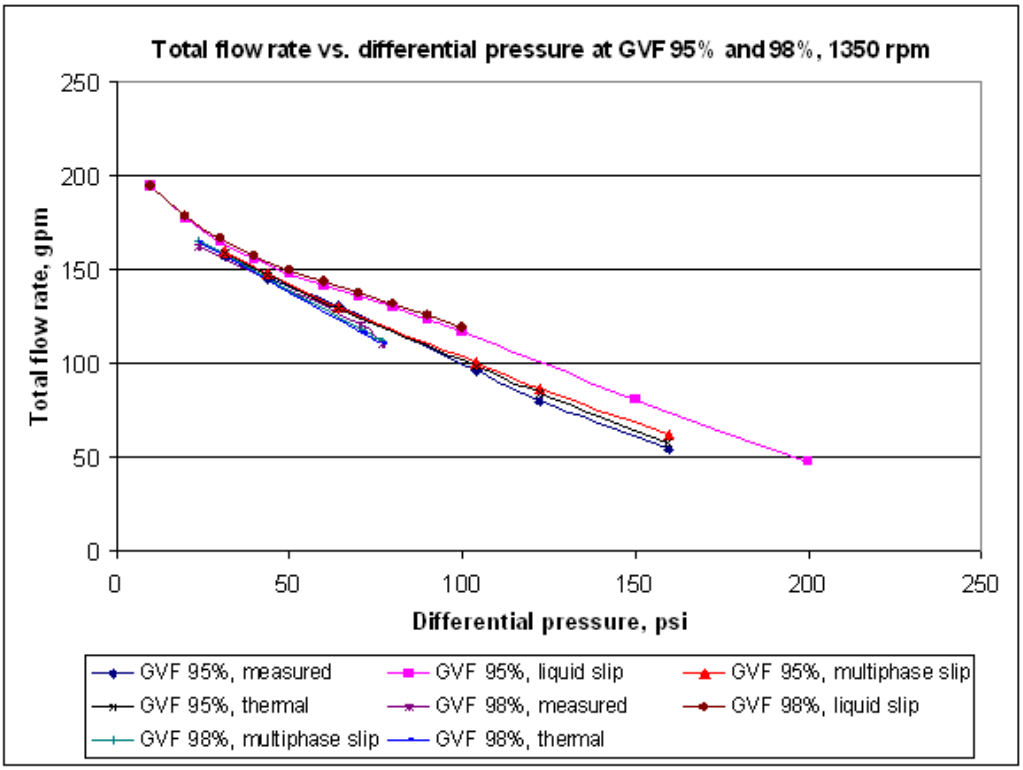

Fig. 3.8—Total flow rate vs. differential pressure with GVF 95% and 98% at 1350 rpm (water)

By changing the differential pressure across the pump, pump performance data are collected. **Fig. 3.8** shows the comparison of collected data and predictions of several models. "Liquid slip" model assumes that the slip flow is only liquid and the

compression is isothermal. “Multiphase slip” model is based on the assumption that at high GVF, the slip flow is gas and liquid multiphase flow and the compression is isothermal. “Thermal” model combines both the mechanical model and thermal model and assumes the slip flow is gas and liquid multiphase flow and the compression is not isothermal.

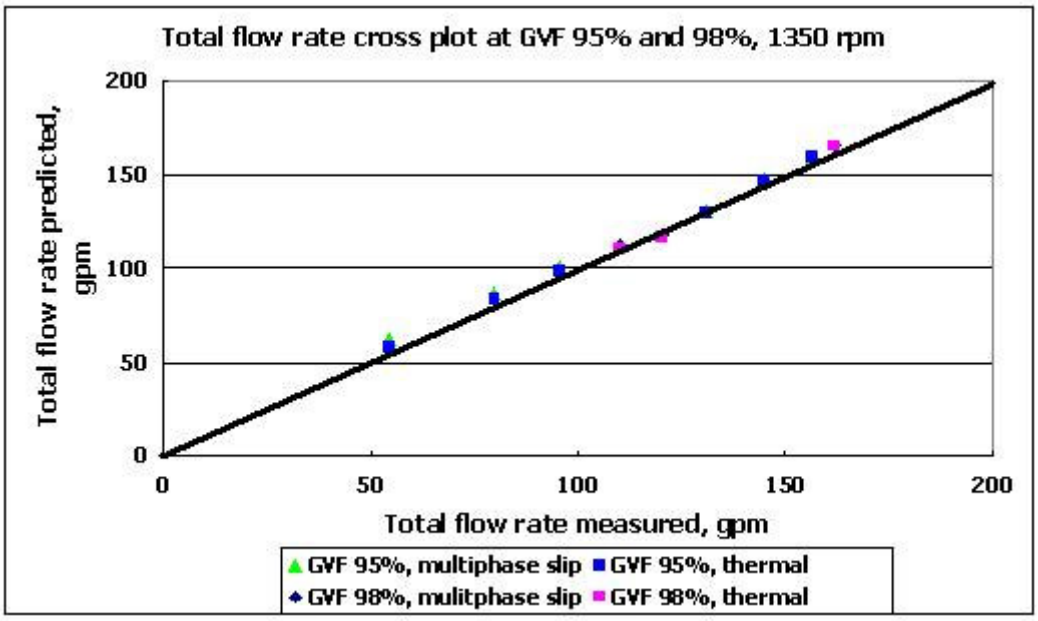

Fig. 3.9—Total flow rate cross plot with GVF 95% and 98% at 1350 rpm (water)

From Fig. 3.8, at 1350 rpm with both 95% and 98% GVF, the “liquid slip” model over predict the total flow because of the gas slip. From the experimental data, the total flow rate with GVF 98% is slightly lower than GVF 95%, which approves the existence of gas slip at high GVF. The data and the comparison between “multiphase slip” model and “thermal” model also show the temperature increase inside the twin-screw pump has

limited effect on the throughput of the pump. **Fig. 3.9** shows the cross plot comparing isothermal and non-isothermal model with the measured data. Both models predicted total flow rate very well.

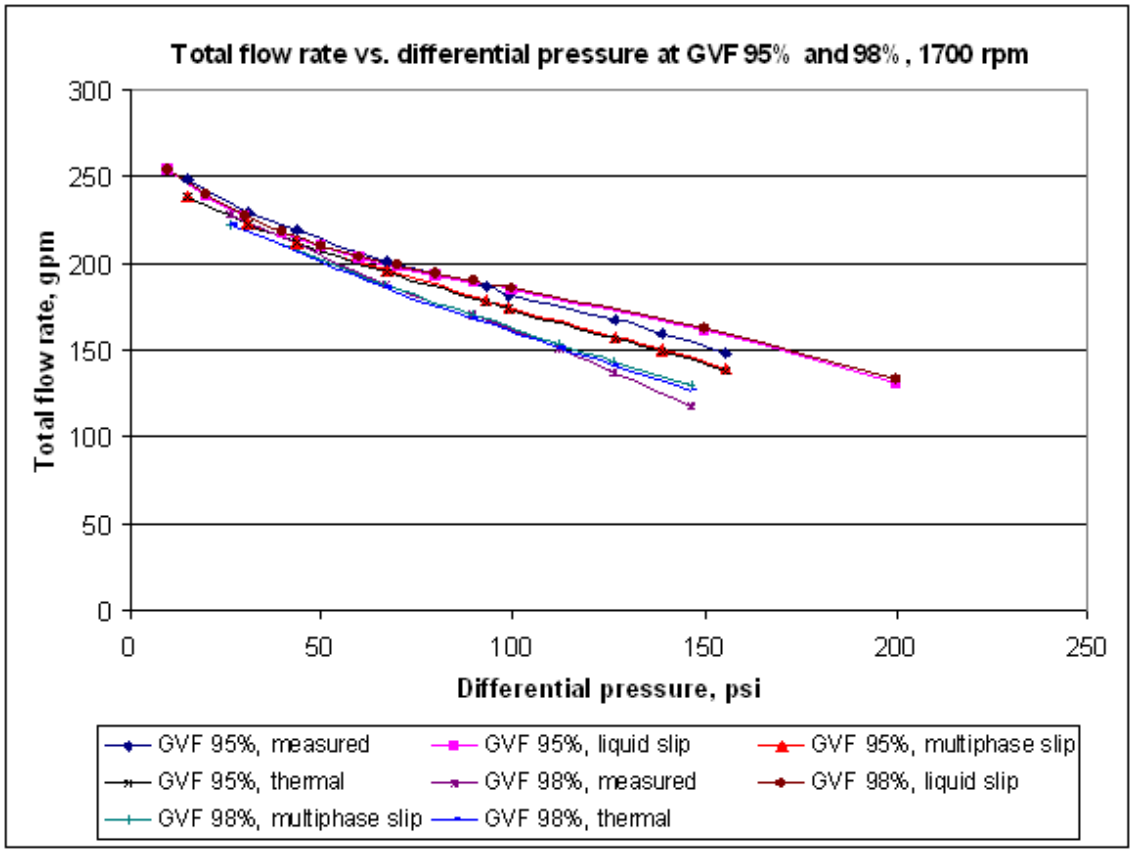

Fig. 3.10—Total flow rate vs. differential pressure with GVF 95% and 98% at 1700 rpm (water)

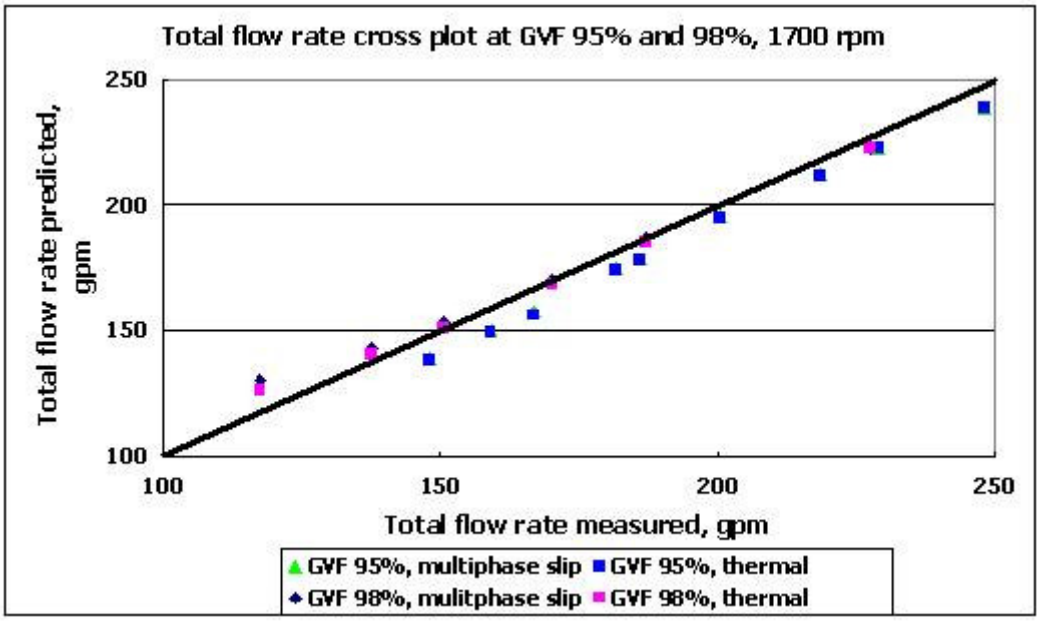

Fig. 3.11—Total flow rate cross plot with GVF 95% and 98% at 1700 rpm (water)

At 1700 rpm, we observe the similar results as 1350 rpm. From **Fig. 3.10** and **Fig. 3.11**, the models under predicted the total flow rate but still in line with the measure results. That is because at higher pump speed, the centrifugal force pushes more liquid against the liner, and then there is more liquid flowing through the circumferential clearances. The GVF inside the clearances is higher than the average GVF in the chamber.

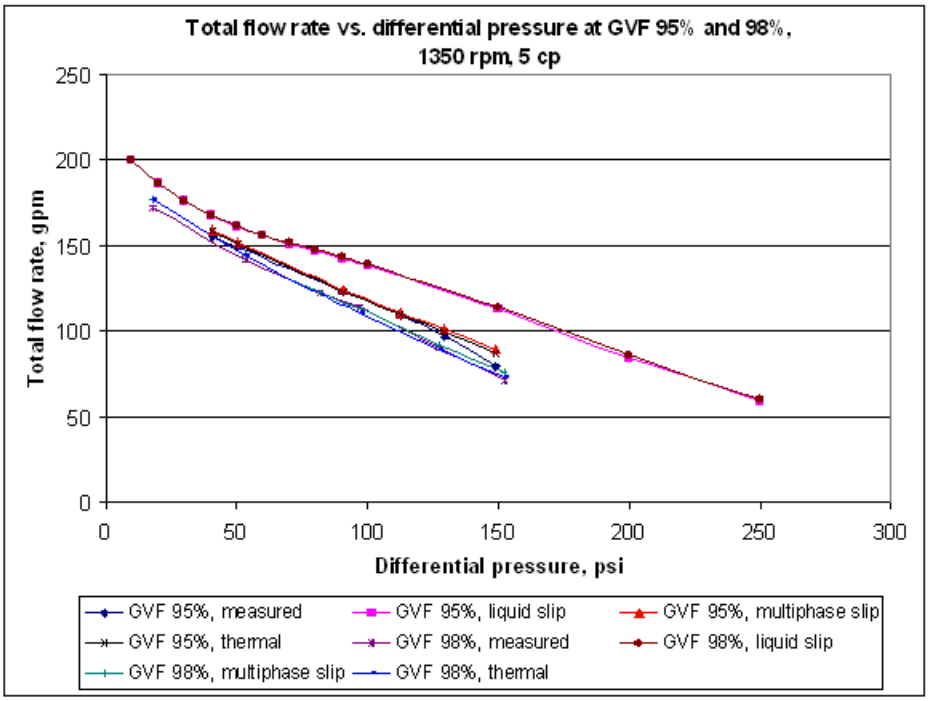

Fig. 3.12—Total flow rate vs. differential pressure with GVF 95% and 98% at 1350 rpm using glycerin-water mixture with viscosity 5 cp

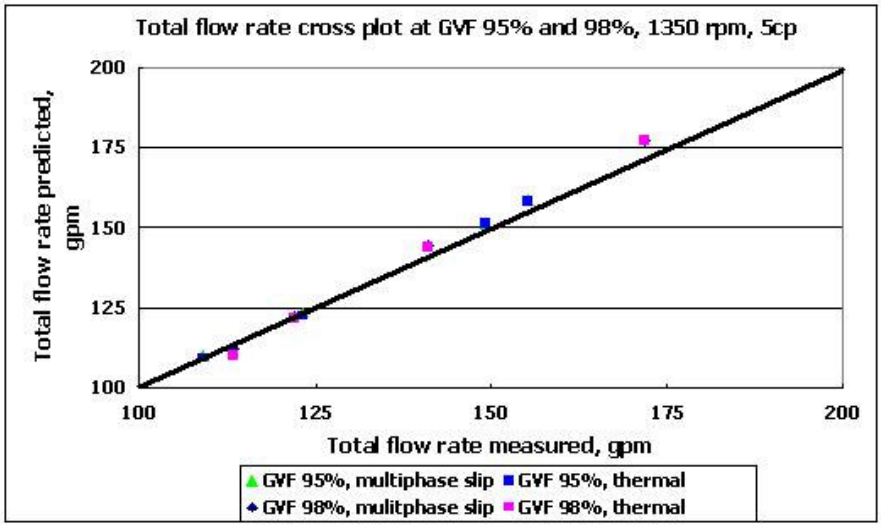

Fig. 3.13—Total flow rate cross plot with GVF 95% and 98% at 1350 rpm using glycerin-water mixture with viscosity 5 cp

Fig. 3.12 shows the data using glycerin-water solution as liquid phase. The viscosity is 5 cp according to the sample measured by viscometer. Basically, the comparison of three models shows the same trend as water. The cross plot shown in **Fig. 3.13** has the similar range of error with water, which indicates the ability of the model to predict the pump performance not only with higher GVF but also with liquid having higher viscosity than water.

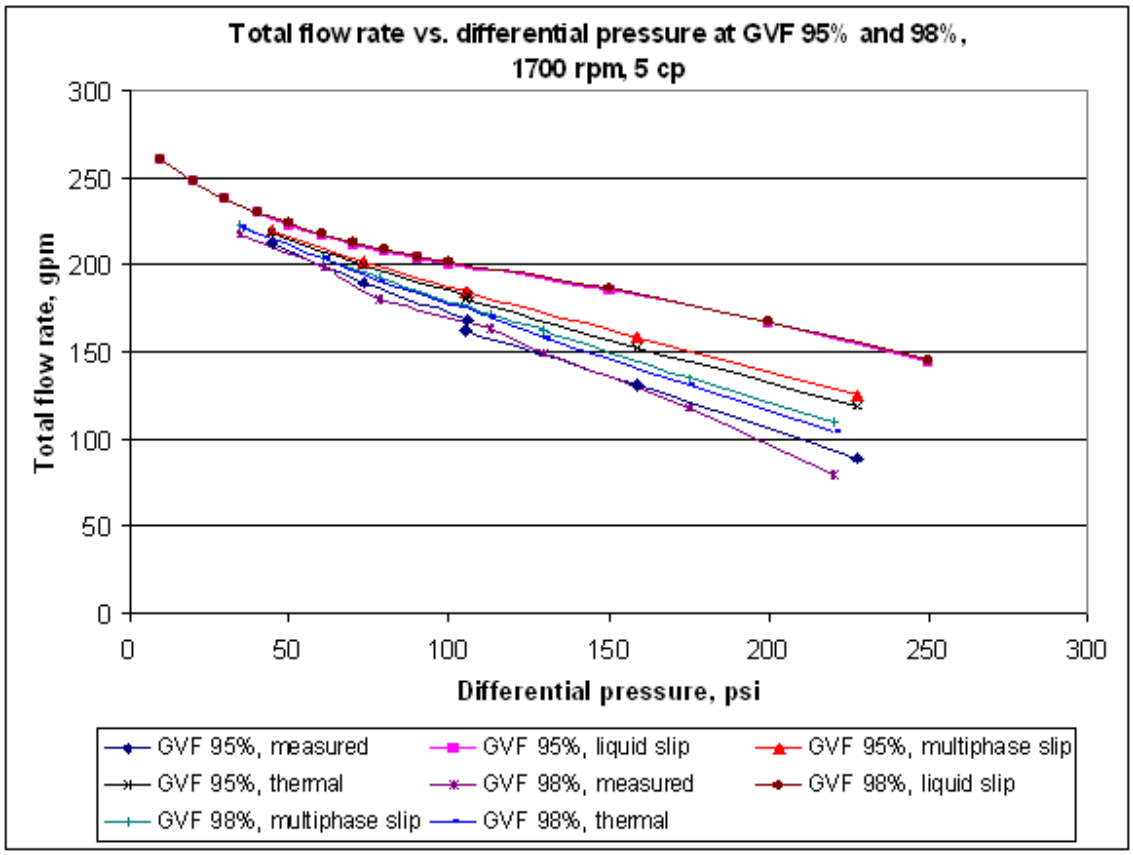

Fig. 3.14—Total flow rate vs. differential pressure with GVF 95% and 98% at 1700 rpm using glycerin-water mixture with viscosity 5 cp

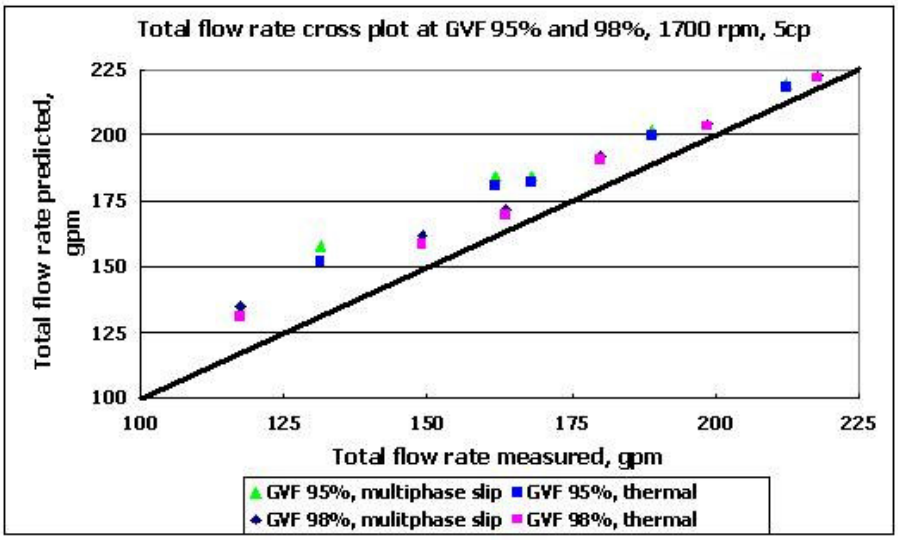

Fig. 3.15—Total flow rate cross plot with GVF 95% and 98% at 1700 rpm using glycerin-water mixture with viscosity 5 cp

As shown in **Fig. 3.14** and **Fig. 3.15**, the trend is the same at 1700 rpm, which is that the models with gas slip simulations predict better results than the model with only liquid slip simulations. With larger temperature gradient inside the pump, the difference between isothermal model and non-isothermal model is clearer. But the range of error is bigger and all the models seem to generally under predict the slip flow. This can be explained by the change of glycerin viscosity with temperature. As shown in Table 3.4, glycerin solution is sensitive to the temperature change. With pump speed at 1700 rpm and GVF 98%, the temperature rise dramatically, which lead to the decrease of liquid viscosity. For example, with discharge temperature 175 $^{\circ}F$ (80 $^{\circ}C$), the viscosity of glycerin solution is 1.25 cp which is just a little bit higher than water. The lower

viscosity of liquid phase encourages higher slip flow rate and decrease the throughput of the twin-screw pump.

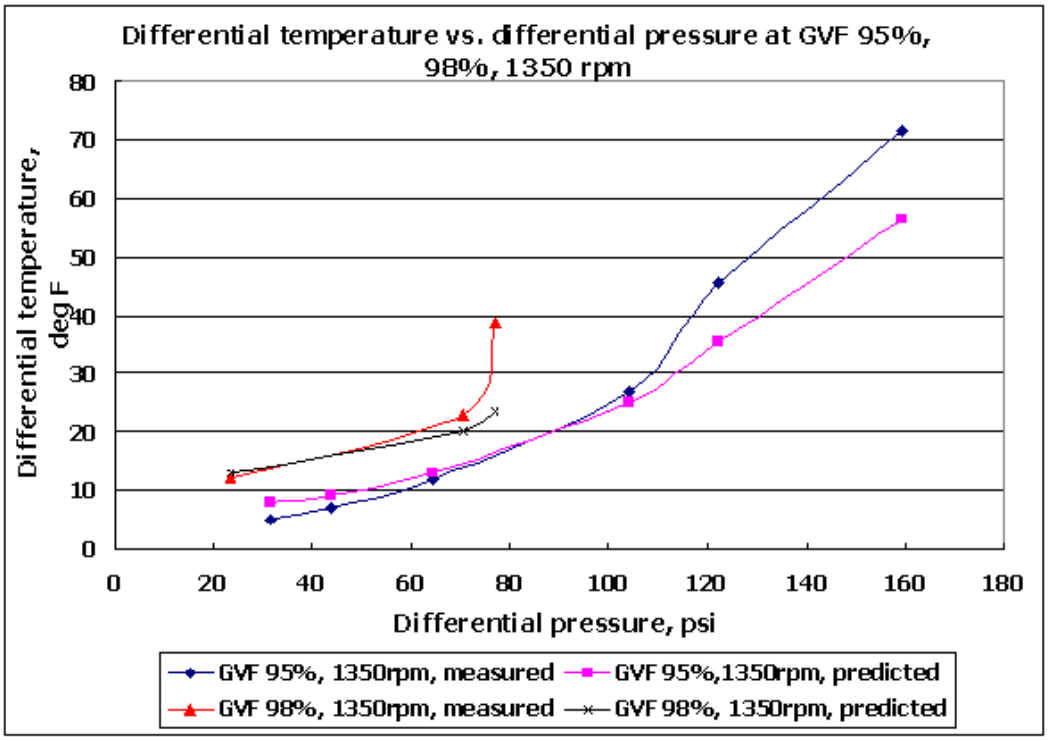

Fig. 3.16—Differential temperature vs. differential pressure with GVF 95% and 98% at 1350 rpm (water)

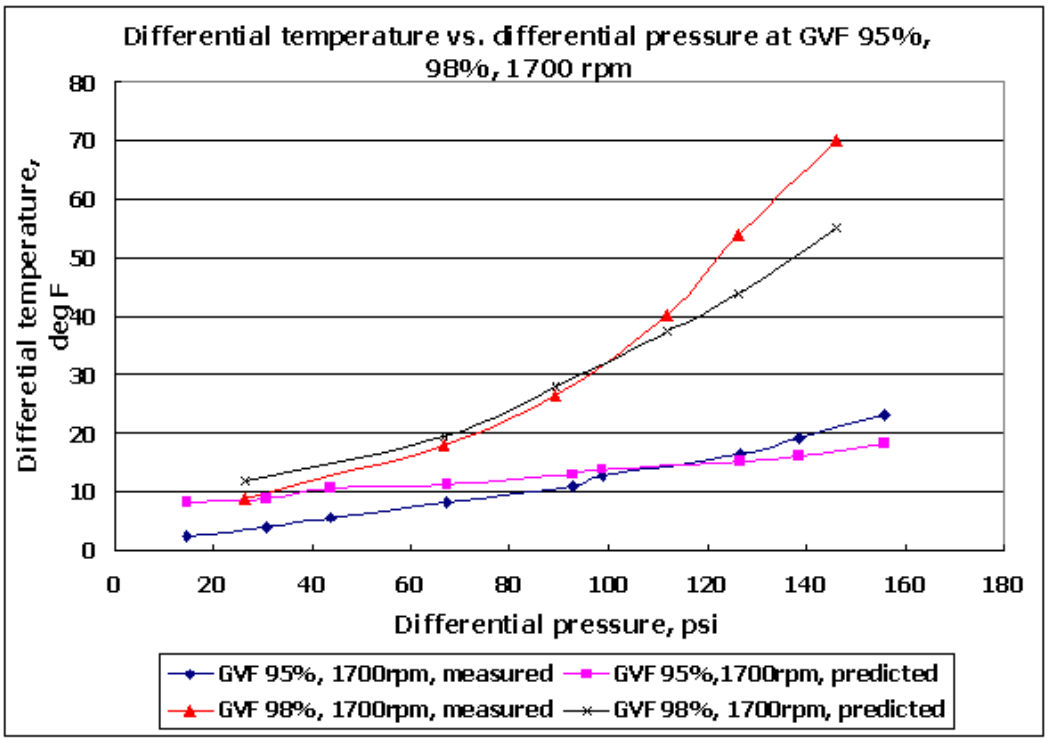

Fig. 3.17—Differential temperature vs. differential pressure with GVF 95% and 98% at 1700 rpm (water)

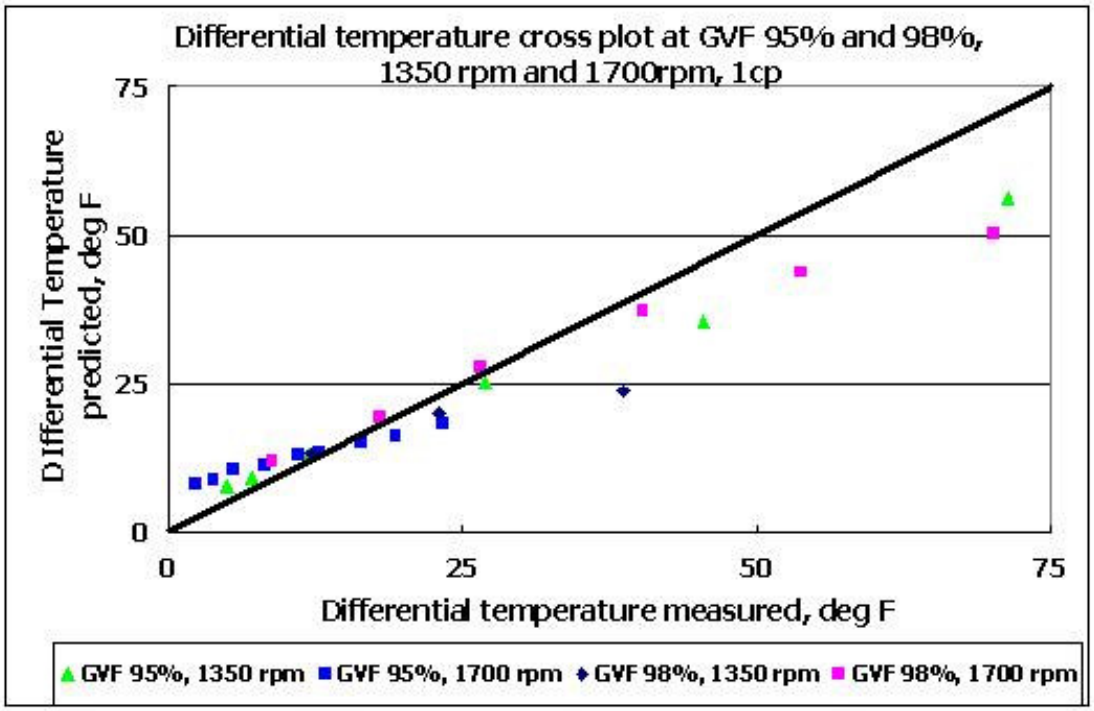

Fig. 3.18—Differential temperature cross plot with GVF 95% and 98% at 1350 rpm and 1700 rpm (water)

Fig. 3.16 and **Fig. 3.17** show the differential temperature across the Bornemann twin-screw pump with GVF 95% and 98% at 1350 rpm and 1700 rpm with water. It is clearly shown that with the same GVF, the higher is the pump speed, the higher does the temperature increase. While with the same pump speed, the higher is the GVF and the higher is the differential pressure across the pump, the higher is the differential temperature. The cross plot (**Fig. 3.18)** illustrates the error between model prediction and measured data. Though the error is increasing with higher temperature, the prediction acceptably matches the general trend of the temperature.

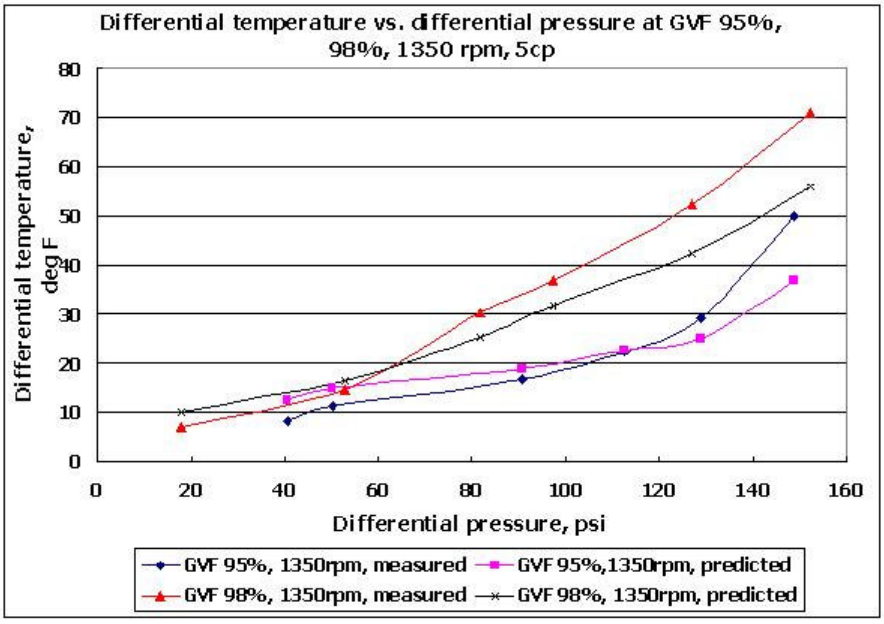

Fig. 3.19—Differential temperature vs. differential pressure with GVF 95% and 98% at 1350 rpm (5 cp glycerin solution)

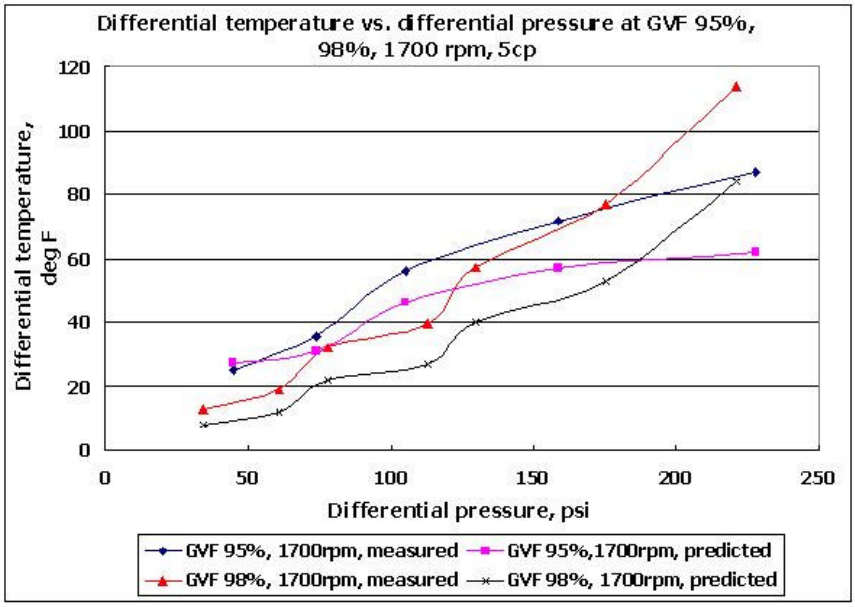

Fig. 3.20—Differential temperature vs. differential pressure with GVF 95% and 98% at 1700 rpm (5 cp glycerin solution)

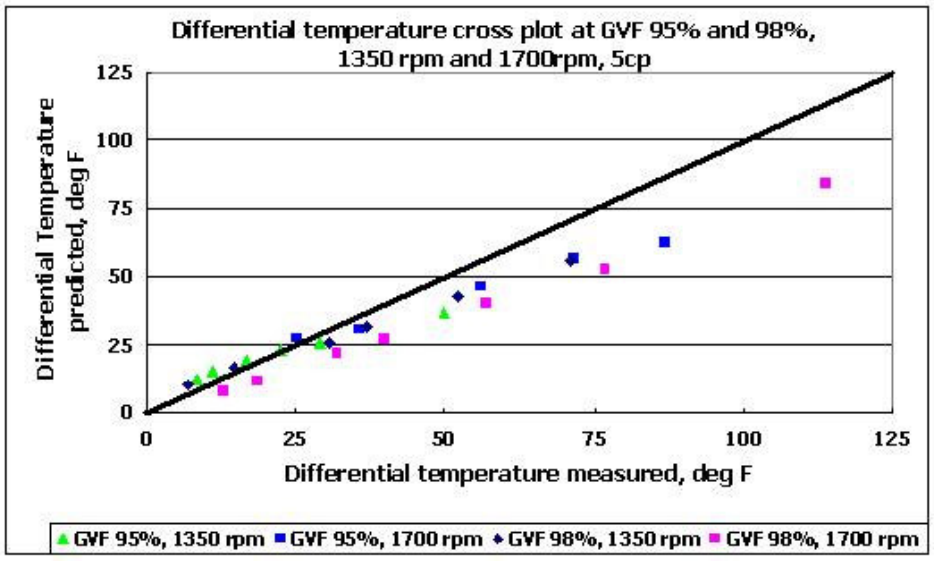

Fig. 3.21—Differential temperature cross plot with GVF 95% and 98% at 1350 rpm and 1700 rpm (5 cp glycerin solution)

The differential temperature data with 5 cp glycerin solution is shown in **Fig. 3.19** and **Fig. 3.20**. They follow the similar trend as the data with water. Since higher viscosity liquid leads to higher throughput of the pump, with same GVF, the temperature increase faster than lower viscosity liquid. This phenomenon is also shown in Fig. 3.16 and Fig. 3.17. **Fig. 3.21** illustrates good match between the measured data and the thermal model prediction except with high $50^{\circ}F$. Considering the assumption of thermal model, this deviation indicates the heat generated by gas compression can not be absorbed completely by liquid. There should be temperature difference between the gas phase and liquid phase. With high pump speed and high gas content, only a small portion of liquid is effectively removing the heat (Toma and Anderson, 2006). Future research should be focused on the heat transfer efficiency inside the twin-screw pump.

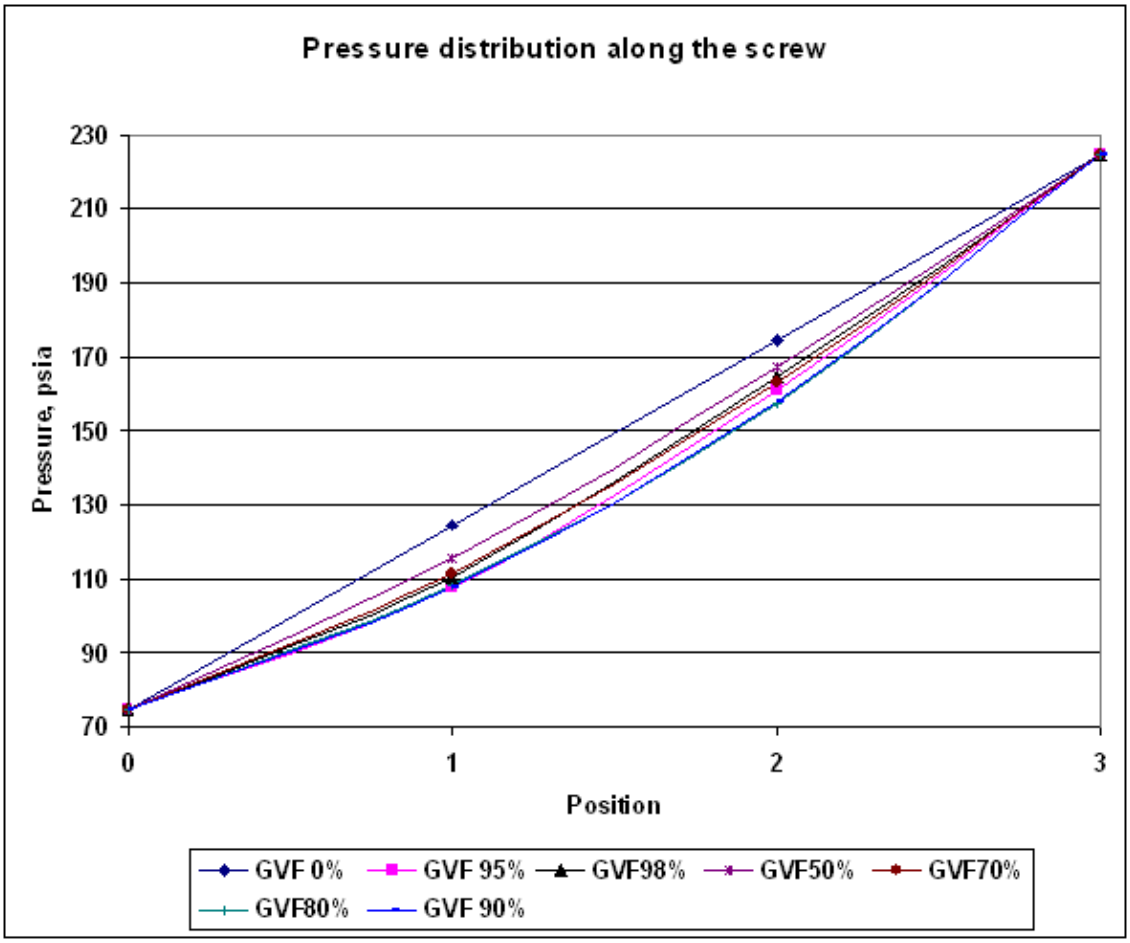

Fig. 3.22—Pressure distribution along the screw at 1700 rpm, suction pressure 60 psig and differential pressure 150 psi

Fig. 3.22 shows the predicted pressure distribution along the screw with various GVF at 1700 rpm. The suction pressure is 60 psig and the differential pressure across the pump is 150 psi. From Fig. 3.22, we find an interesting phenomenon that from GVF 50% to 70% and then 80% and 90%, the pressure profile is becoming steeper and steeper. But from 90% to 95% and then to 98%, the pressure profile is moving toward linear. This simulation results agrees with the observation of Vetter (2000).

This is due to the presence of gas slip in the clearances. Beyond certain GVF, there is not enough liquid to seal all the clearances. With increasing GVF, the liquid slip flow rate can not increase any more, instead, the gas slip flow increases. There is more gas flowing back to the previous chamber, which makes the pressure profile more linear. It is the first time that this phenomenon is explained theoretically by simulations.

Generally speaking, the comparison of experimental data and the predictions of both isothermal and non-isothermal models show a better match than “liquid slip” model with GVF 95% and 98%. The gas slip in the clearances can not be ignored with high gas content. The model agrees with the experimental data under a very wide flow rate range, different liquid viscosities and GVF. Compatible with “liquid slip” model, this model can be used to simulate the twin-screw pump performance with GVF from 0% to 99%.

4. WET GAS COMPRESSION SOLUTIONS

Efficiency and reliability are the two key issues with wet gas compression with twin-screw multiphase pump. From Fig. 3.17, we see significant increase of the differential temperature across the twin-screw pump with high GVF and high pump speed. Besides this expected temperature rise, twin-screw pump can have Loss of Prime (LOP) event, which stands for loss of pumping capacity (Nakashima et al., 2006). According to the principles of twin-screw pump, the gas is compressed by the liquid slip flow. If there is not enough liquid to seal the clearances, all the gas transported to the discharge returns back to suction in a recycling process. Then there is no gas compression and the pump loses its capacity. During LOP event, all the power is converted to internal energy and cause dramatic increase of temperature inside the pump. Finally the high temperature will lead to the thermal expansion and damage the mechanical parts. So preventing LOP event and keeping the liquid sealing in the clearances are critical to the operation of twin-screw pump under wet gas conditions.

On the other hand, because the twin-screw pump is positive displacement pump and gas is compressible, the volumetric efficiency increases with GVF increases. So there is dilemma between volumetric efficiency and reliability. To optimize the performance of twin-screw pump, specific operating condition should be considered.

The following shows two popular methods for improving the performance and reliability of twin-screw pump under wet gas condition, which are recirculation and degressive screws. Also, a novel method is proposed and investigated as an alternative to

optimize the pump performance with high gas content, which is the direct injection of high viscosity fluid into the chambers.

4.1 Liquid Recirculation

To ensure there is enough liquid inside the pump, liquid recirculation is a common feature for twin-screw multiphase pump, especially during periods of high GVF flow. Liquid recirculation is to separate the liquid phase from the gas phase at the discharge of the pump and then inject the liquid back to the suction. There are two main designs available for recirculation with twin-screw multiphase pump. One is internal recirculation patented by Bornemann as shown in **Fig. 4.1**. Both the suction and discharge are designed as upward to retain as much liquid as possible.

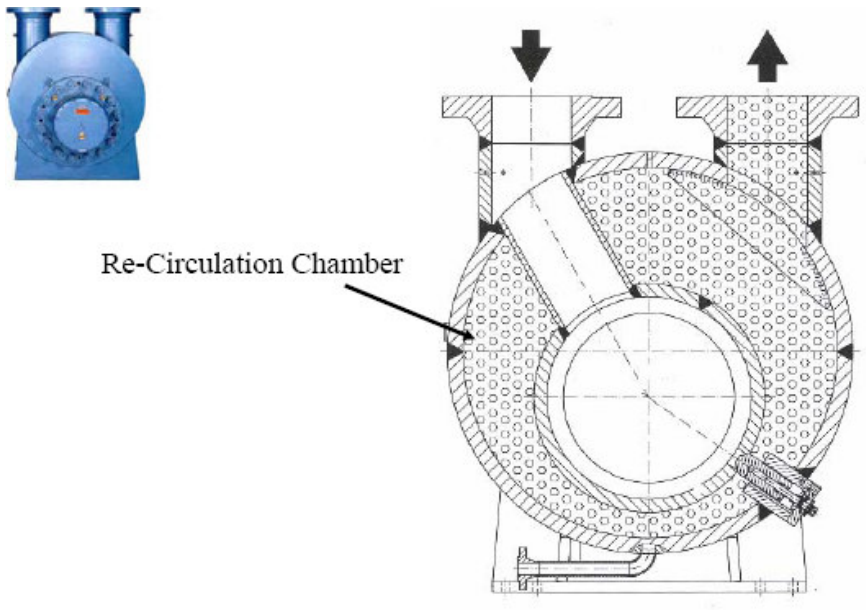

Fig. 4.1—Internal recirculation of Bornemann twin-screw pump

The other is external recirculation by Leistritz as shown in **Fig. 4.2**. In this design, a "boot" is used to accumulate liquid from discharge to circulate to the suction regulated by control valve.

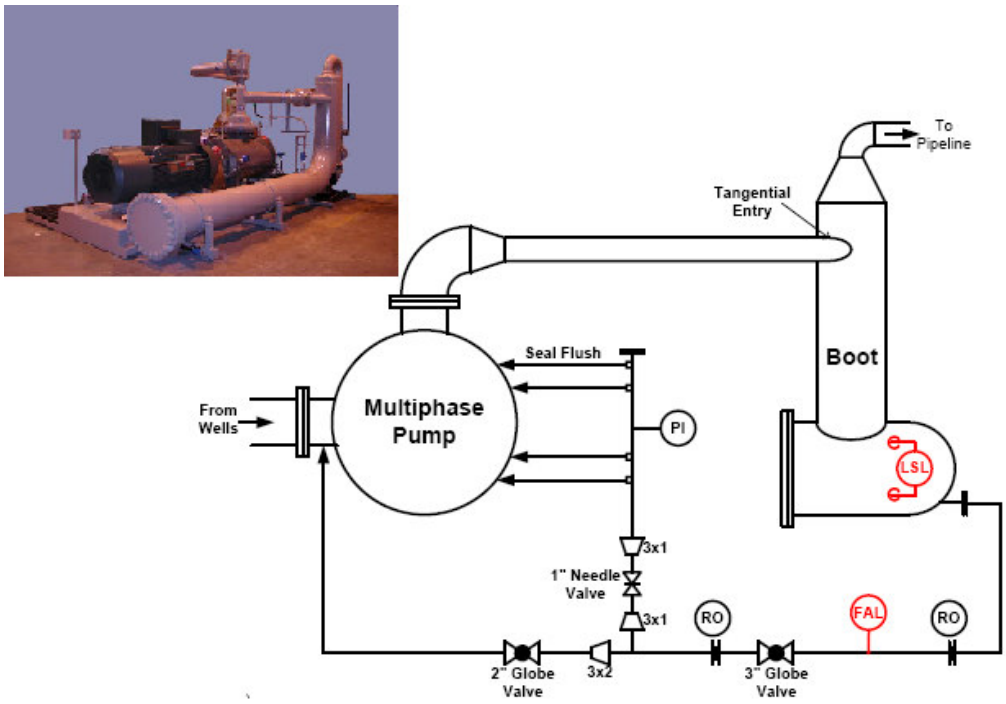

Fig. 4.2—External recirculation and seal flush of Leistritz twin-screw pump (Sinclair, 2007)

Without cooling the circulated liquid, temperature becomes the critical variable. The heat absorbed by the circulated liquid is transferred to the suction and heats the suction fluid. The gas compression is near adiabatic. To simulate the effect of circulated liquid, the effective GVF at the suction of the pump should involve the circulated liquid flow rate q_{rec}. Then effective GVF at the suction, GVF'_S is

$$GVF'_S = \frac{q_G}{q_G + q_L + q_{rec}} \tag{4.1}$$

4.2 Degressive Twin-Screw Pump

The main reason for twin-screw pump to lose efficiency and reliability is that gas is compressible and gas volume reduces from suction to discharge. Since the chamber volume is constant, there has to be additional slip flow to fill the chamber. To improve both efficiency and reliability, Bornemann developed a new generation of screws called "degressive screws" for high gas content operations. Different from traditional twin-screw pump, these degressive screws have varying pitch along the screw as shown in **Fig. 4.3**. The pitch of screw thread decreases with the spindle length. The chamber volume is reducing along the screw while moving from the suction to the discharge, which lead to a so called "build in compression"(Rausch et al., 2004). This design is very similar with the design of screw compressors, which also have decreasing chamber volume but different rotor profiles.

Fig. 4.3—Diagram of degressive screws

If the geometry of the degressive screw is provided, the theoretical volume of each chamber V_{ci} is known, Eq. (2.54) can be modified as

$$V_{ci} = V_{G(i-1)} \frac{p_{(i-1)} z_i}{p_i z_{(i-1)}} + (q_{Gi} - q_{G(i-1)}) \Delta t \frac{p_S z_i}{p_i z_S} + V_{L(i-1)} + q_{Li} \cdot \Delta t - q_{L(i-1)} \cdot \Delta t \quad (4.2)$$

The model for constant volume twin-screw multiphase developed in this research can be modified and applied to the simulation of degressive screws.

Test with degressive screws have been conducted by Bornemann (Rohlfing and Muller-Link, 2006). The results illustrate an improvement in both flow capacity and efficiency as shown in **Fig. 4.4**. Also, a slight decrease in power consumption was observed with GVF 94%.

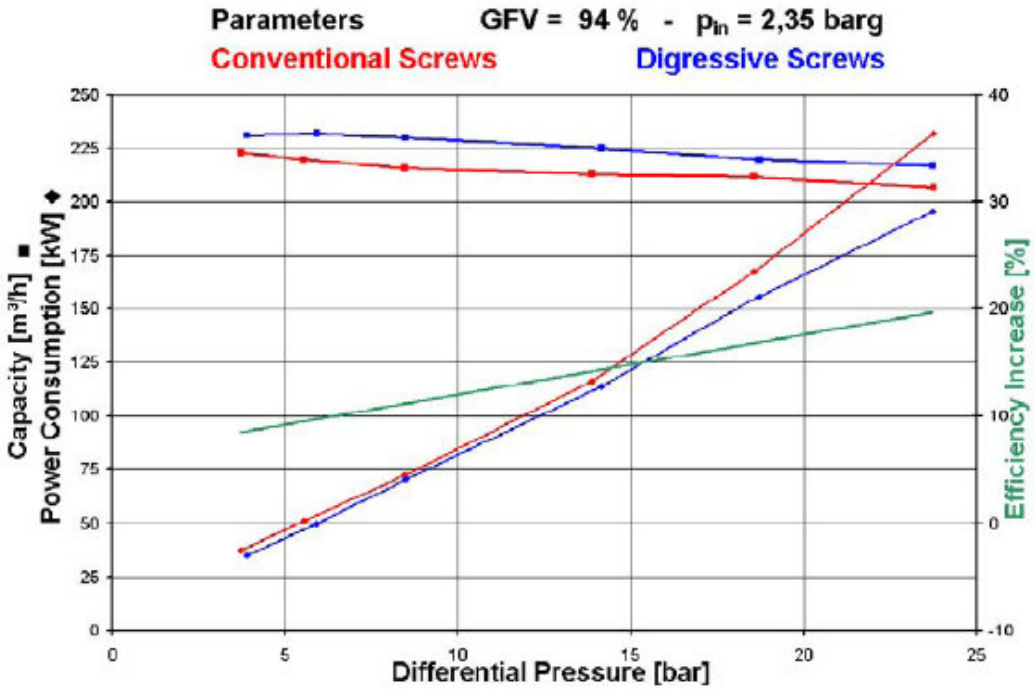

Fig. 4.4—Test results with degressive screws (Rohlfing and Muller-Link, 2006)

In fact, since the chamber volumes reduce while moving toward the discharge, less liquid slip flow is needed to compress the gas and seal the clearances. So both volumetric efficiency and reliability are improved. This new design combines the benefit of twin-screw pump and screw compressor and solve the dilemma from the basic construction. But the temperature increase is still an issue. The temperature increase can be simulated by the modified thermal model developed in this research.

Like fixed-volume-index screw compressors, the main disadvantage of the degressive screw pump is its inability to change with system's fluctuating operating conditions, resulting in periods of performance inefficiencies. With progressively smaller chambers, the pump will lose efficiency dramatically when there is liquid slug through the twin-screw pump. To handle GVF 0% to 99%, a more flexible solution is proposed, which is to inject high viscosity liquid directly into the chamber through the casing.

4.3 Effect of Liquid Viscosity

Many research (Martin, 2003; Prang and Cooper, 2004; Singh, 2003) show evidences that increasing the viscosity of the liquid phase reduces slip flow and improve the volumetric efficiency. In the simulation with her model, Martin showed a specific example where the slip flow is almost eliminated for liquid viscosity above 100cp (Martin, 2003). With increasing viscosity of liquid, with same differential pressure across the twin-screw pump, the slip flow rate is reduced and the required liquid to seal the clearances are decreasing, which allow more gas to be compressed. Then the pump

not only can compress larger volume of gas but also can handle higher GVF and higher pressure boost.

Fig. 4.5 and **Fig. 4.6** show the experimental data with water and 5 cp glycerin solutions at GVF 0%, 95% and 98% and pump speed 1350 rpm and 1700 rpm, respectively. The results clearly indicate the effect of liquid viscosity to the total flow rate and slip flow. As discussed before, at 1350 rpm, pump running with GVF 95% and glycerin mixture has the highest total flow rate due to the presence of gas slip. And the pump running with GVF 0% and water has the lowest total flow rate because of the compressibility of gas. The simulation results show the same trend as experimental results. At 1700 rpm, it is the same as 1350 rpm except the highest total flow rate is with 1 cp water and GVF 95%.

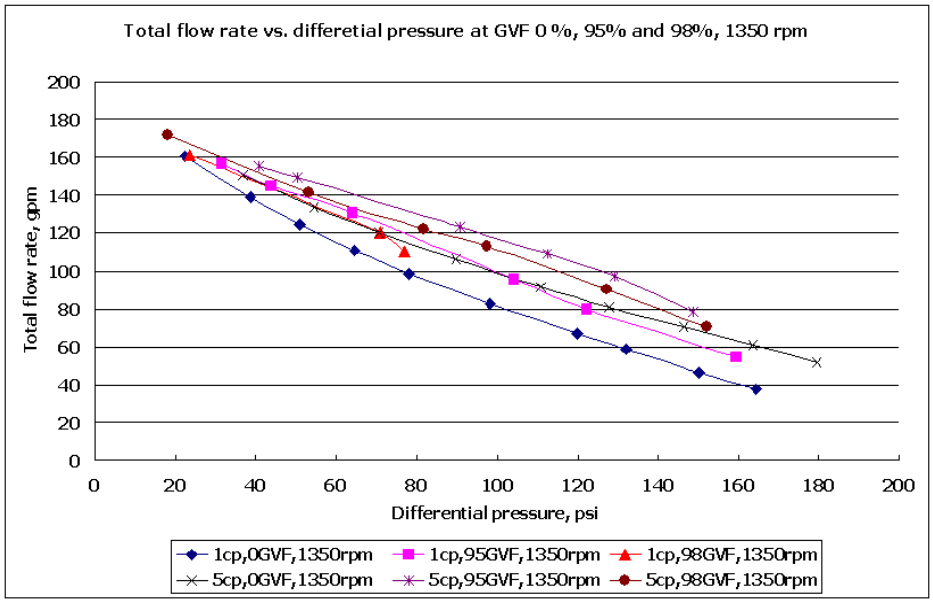

Fig. 4.5—Total flow rates vs. differential pressure with GVF 0%, 95% and 98% at 1350 rpm

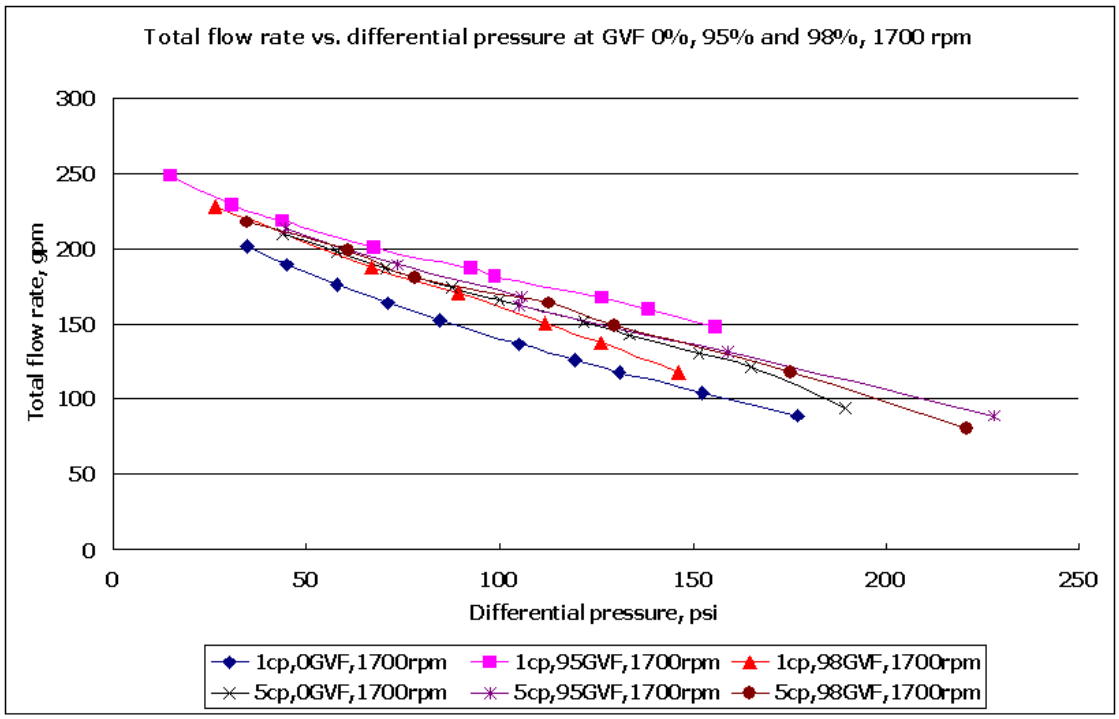

Fig. 4.6—Total flow rates vs. differential pressure with GVF 0%, 95% and 98% at 1700 rpm

4.4 Through-Casing Liquid Injection

Based on those observations, Chan proposed a concept of through-casing injection, which suggests injecting high viscosity fluid directly into the chamber (Chan, 2006). By injecting high viscosity liquid, there will be enough liquid to seal the clearances around the chambers and the total viscosity of liquid inside the pump will increase too, which will in turn limit the slip flow rate to eliminate the negative effect of additional liquid supply. As shown in **Fig. 4.7**, by increasing the amount of liquid in a specific chamber in the pump, we could increase the pressure in that chamber and allow an operator to create a more favorable linear pressure profile. This is similar to the operating

concept of the degressive screw design, but instead of decreasing the chamber volume mechanically, it will be attempted hydro dynamically. So it will be more flexible.

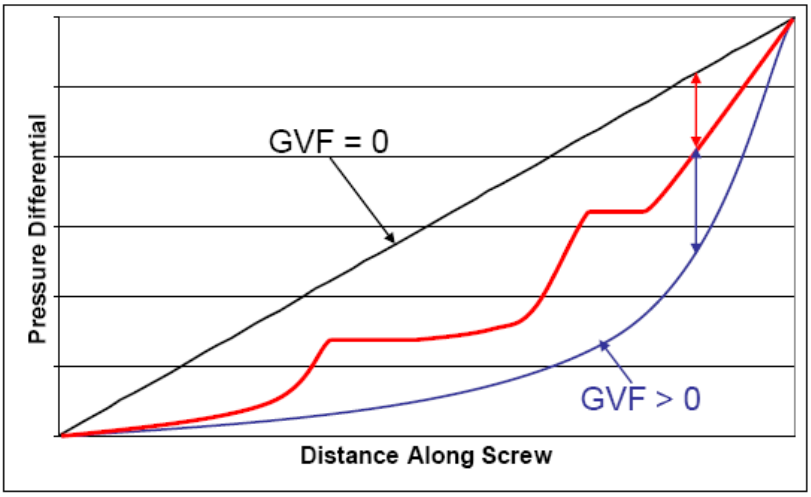

Fig. 4.7—Effect of through-casing injection on the pressure distribution along the screw

But because the injected liquid is additional to the working fluid, it is not true that the more liquid we inject into the chamber, the more effective total flow rate will we get. The injected liquid should not push the gas and liquid back. The increase of total flow rate must offset the injected liquid flow rate. So the injection rate has to be optimized. Furthermore, the injection point, which is the chamber we inject liquid into, should be evaluated. Since the through-casing high viscosity liquid injection is an alternative to improve twin-screw pump performance under wet gas condition, the developed model for twin-screw pump wet gas compression is modified to evaluate the effect of liquid viscosity, injection flow rate and injection point.

According to the concept of liquid injection, assume the liquid injection flow rate is q_{th}, and the liquid is injected in chamber i, then Eq. (2.44) to (2.46) can be modified as:

$$V_c = V_{G(i-1)} \frac{p_{(i-1)} z_i}{p_i z_{(i-1)}} + (q_{Gi} - q_{G(i-1)}) \Delta t \frac{p_S z_i}{p_i z_S} + V_{L(i-1)} + q_{inj} \cdot \Delta t + q_{Li} \cdot \Delta t - q_{L(i-1)} \cdot \Delta t \tag{4.3}$$

The total gas volume in the control volume is

$$V_{Gi} = V_{G(i-1)} \frac{p_{(i-1)} z_i}{p_i z_{(i-1)}} + (q_{Gi} - q_{G(i-1)}) \Delta t \frac{p_S z_i}{p_i z_S} \tag{4.4}$$

The total liquid volume in the control volume is

$$V_{Li} = \left(V_c - q_{L0} \cdot \Delta t - q_{G0} \cdot \Delta t\right) \cdot (1 - GVF_S) + q_{inj} \cdot \Delta t + q_{Li} \cdot \Delta t \tag{4.5}$$

And the GVF in the chamber i is

$$GVF_i = GVF_S - \frac{(q_{inj} + q_{Li}) \cdot \Delta t}{V_c} \tag{4.6}$$

By solving system of equations following the same procedure described in Section 2.3, the total flow rate vs. differential pressure, pressure distribution along the screws can be obtained.

4.5 Solutions Comparison

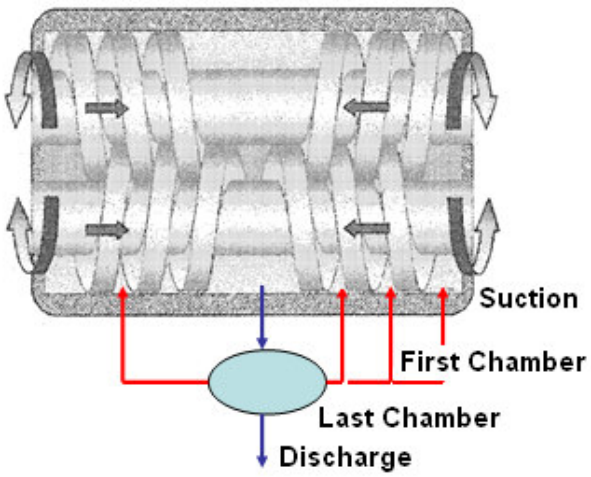

Fig. 4.8—Diagram of through- casing injection

Fig. 4.8 illustrates the diagram of thorough –casing injection. There are totally 3 inject positions in this pump: suction, first chamber and last chamber. To compare different solutions, The Bornemann MW-6.5zk-37 pump was used for simulation. The pump speed is 1700 rpm. The inlet GVF is 98%. The suction pressure is 60 psig. There are totally 12 scenarios designed to evaluate the effect of liquid viscosity, liquid injection rate and injecting position. The injection fluids are water and glycerin. The viscosity of liquid phase after glycerin injection is determined by the weight concentration of liquid mixture inside the pump and Table 3.4. The scenarios are listed in **Table 4.1**.

TABLE 4.1—LIST OF DIFFERENT LIQUID INJECTION SCENARIOS

Scenario	Injection Point	Injection Rate (of Total Flow Rate)	Liquid Viscosity (cp)
1	Suction	2%	1 (water)
2	Suction	4%	1 (water)
3	Suction	2%	5 (glycerin)
4	Suction	4%	20 (glycerin)
5	First Chamber	2%	1 (water)
6	First Chamber	4%	1 (water)
7	First Chamber	2%	5 (glycerin)
8	First Chamber	4%	20 (glycerin)
9	Last Chamber	2%	1 (water)
10	Last Chamber	4%	1 (water)
11	Last Chamber	2%	5 (glycerin)
12	Last Chamber	4%	20 (glycerin)

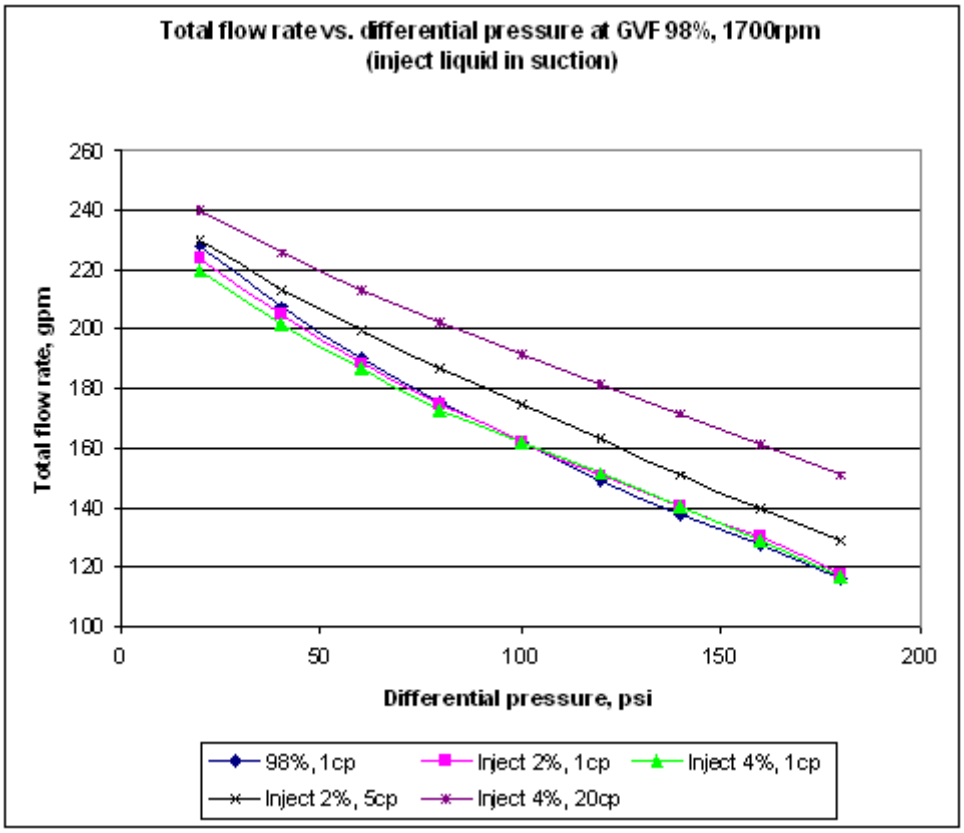

Fig. 4.9—Total flow rates vs. differential pressure with GVF 98% at 1700 rpm (inject water/glycerin in suction, scenarios 1-4)

Fig. 4.9 shows the pump performance with water/glycerin injected in suction of the twin-screw pump. The liquid injection rate is 2% or 4% of the total flow rate (scenario 1-4). According to Table 3.4, at GVF 98%, if the liquid injection rate is 2% the total flow rate, then the weight concentration of glycerin solution is about 50%. The density of the liquid mixture is 9.395 lb/gal and the viscosity is 5 cp. If the liquid injection rate is 4% of the total flow rate, then the weight concentration of the mixture is about 70%. The density of liquid phase inside the pump is 9.452 lb/gal and the viscosity is about 20 cp. The total flow rate shown in Fig. 4.8 is the effective total flow rate which

is the real total flow rate minus the liquid injection flow rate. It is clear that by increasing the liquid viscosity, the throughput of the pump increase. The effect of liquid viscosity is dominant factor to the total flow rate. But with the same liquid viscosity, the liquid injection rate is not a dominant factor in the pump performance with liquid injected in the suction.

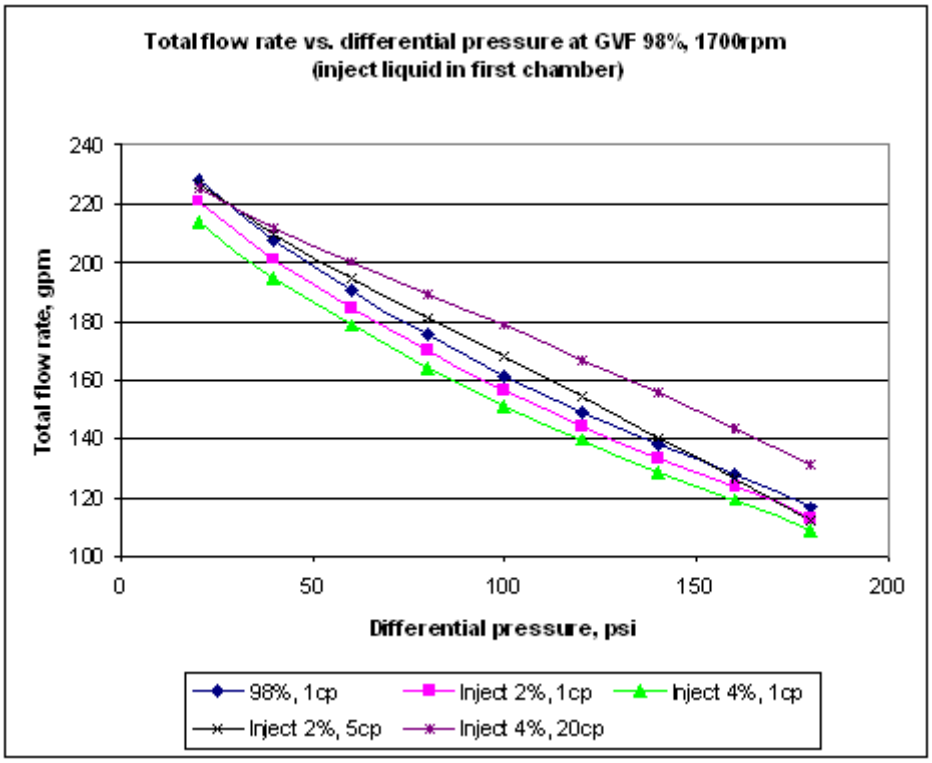

Fig. 4.10—Total flow rates vs. differential pressure with GVF 98% at 1700 rpm (inject water/glycerin in the first chamber, scenarios 5-8)

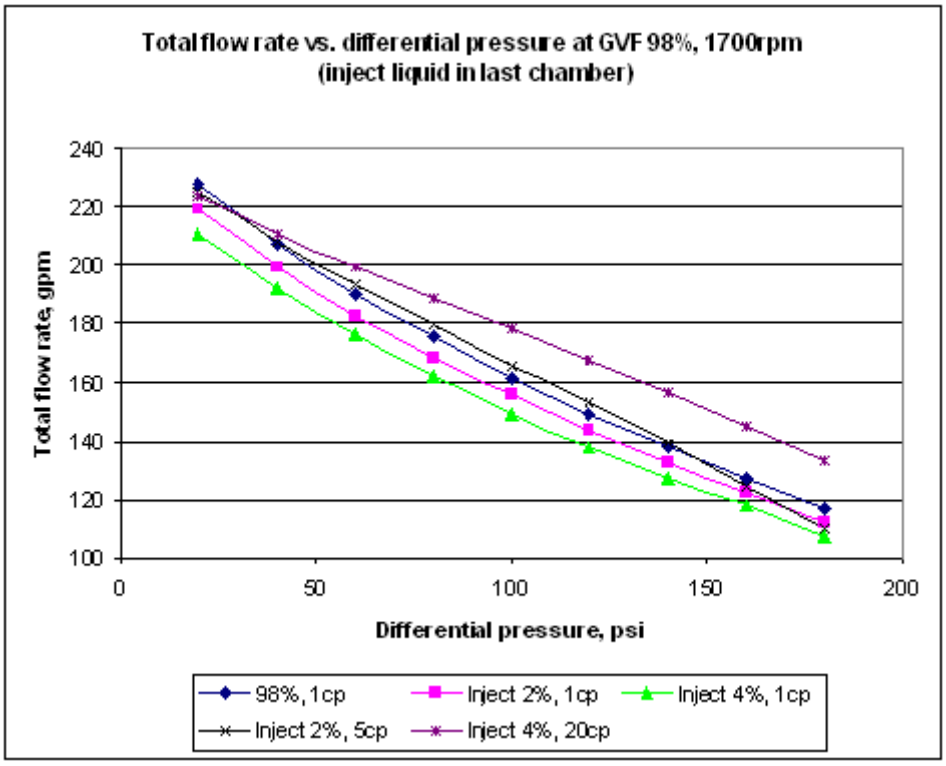

Fig. 4.11—Total flow rates vs. differential pressure with GVF 98% at 1700 rpm (inject water/glycerin in the last chamber, scenarios 8-12)

Fig. 4.10 and **Fig. 4.11** show the pump performance with water/glycerin injected in the first (scenario 5-8) and last chamber (scenario 9-12) of the twin-screw pump. The liquid injection rate is 2% or 4% of the total flow rate. Fig. 4.10 and 4.11 have the similar trend as Fig. 4.9. The injection of 4% of total flow rate of glycerin has the highest total flow rate in all three injection positions.

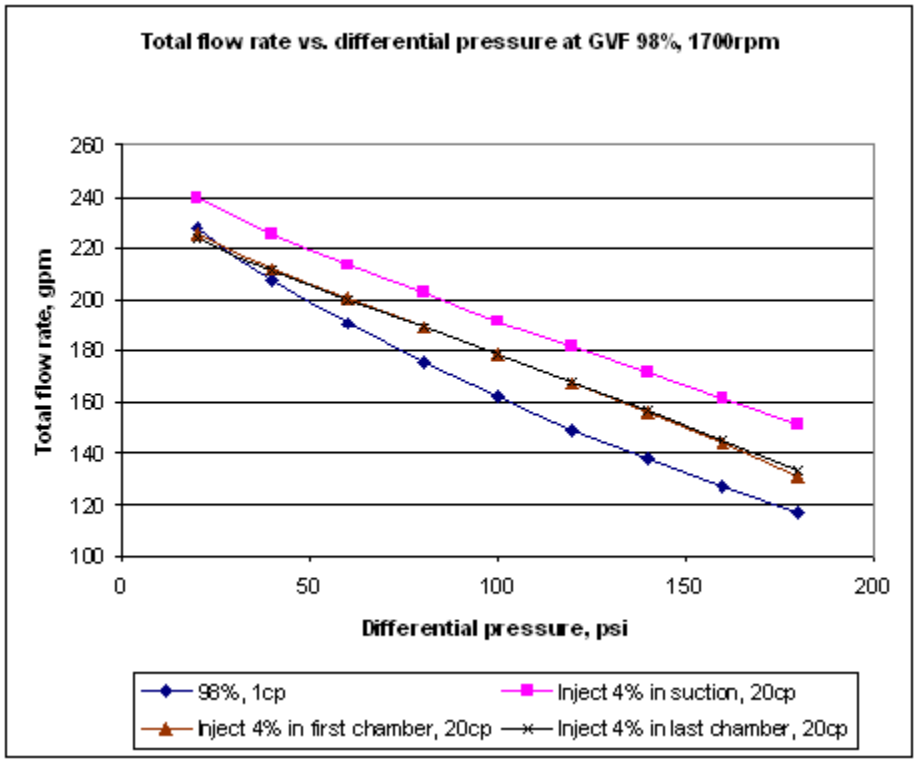

Fig. 4.12—Total flow rates vs. differential pressure with GVF 98% at 1700 rpm (inject 4% of glycerin in suction, first chamber and last chamber, scenarios 4, 8, 12)

Fig. 4.12 shows the comparison of different injection position with same injection rate, liquid viscosity. Injection in the suction has the highest total flow rate. In fact, the injection directly into the chamber increases the chamber pressure and in turn increases the differential pressure between the suction and the chamber, which encourages the slip flow as shown in Fig. **4.13**.

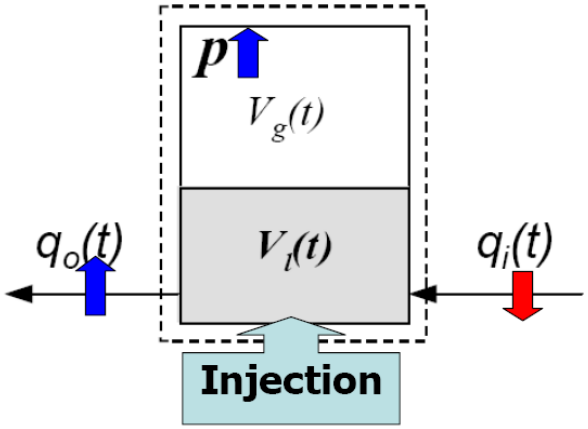

Fig. 4.13—Simplified injection model(Chan, 2006)

The volumetric efficiency increase vs. differential pressure with all three injection positions are shown in **Fig. 4.14**. With 4% of total flow rate of glycerin injected in the suction of the twin-screw pump, the volumetric efficiency can increase up to 40%.

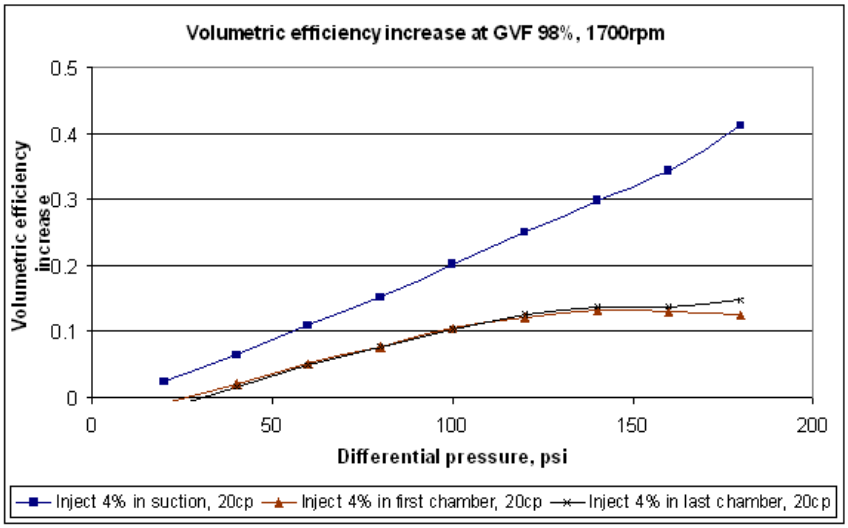

Fig. 4.14—Volumetric efficiency increase with GVF 98% at 1700 rpm (inject 4% of glycerin in suction, first chamber and last chamber, scenarios 4, 8, 12)

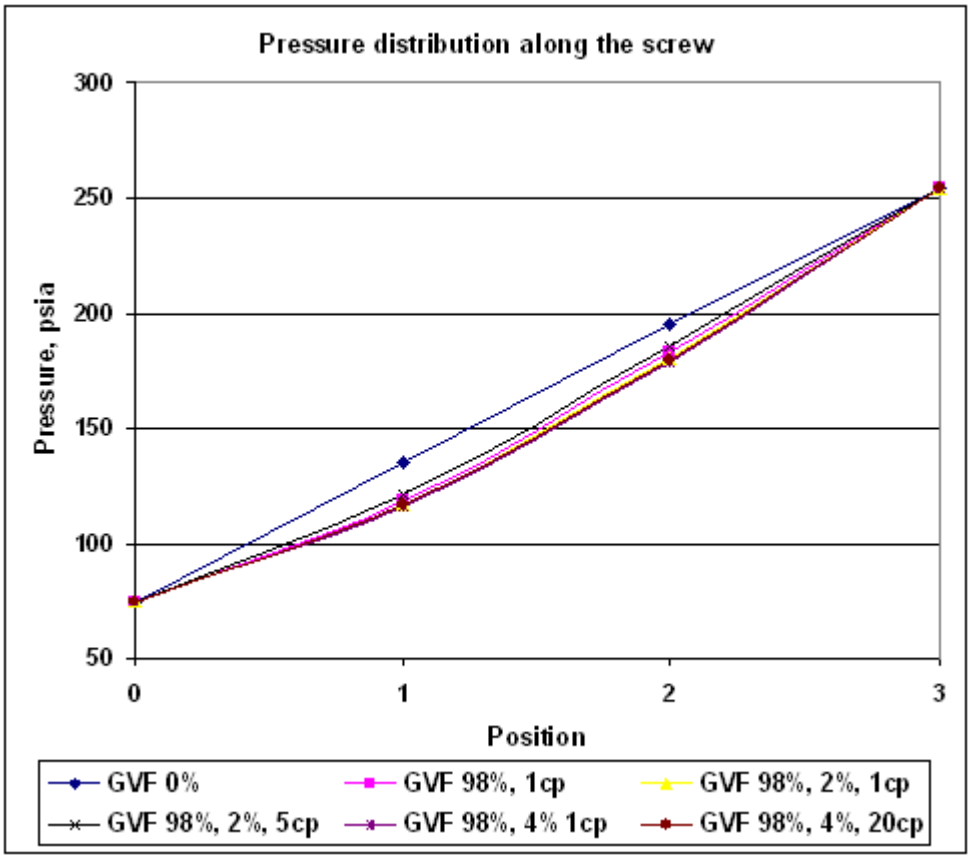

Fig. 4.15—Pressure distribution along the screw with GVF 98% at 1700 rpm (inject water/glycerin in the suction, scenarios 1-4)

Fig. 4.15 shows the pressure distribution along the screw with injection in the suction. Position 0 and 3 represent suction and discharge respectively. Position 1 and 2 represent the intermediate chambers. The differences between different scenarios are limited because the liquid injection is prone to increase the chamber pressure and the pressure profile should be less steep but the increase of liquid flow rate makes the pressure profile steeper than that of GVF 98% and the increase of liquid viscosity also makes the profile toward linear. The pressure distribution is determined on the

comprehensive effect of liquid flow rate, liquid viscosity and injection position. The comparison of pressure profiles with different injection position is shown in Fig. **4.16**. The pressure profile of injection in last chamber is the most linear and the injection in suction has the most steep pressure profile. But with high gas content, the difference is really limited.

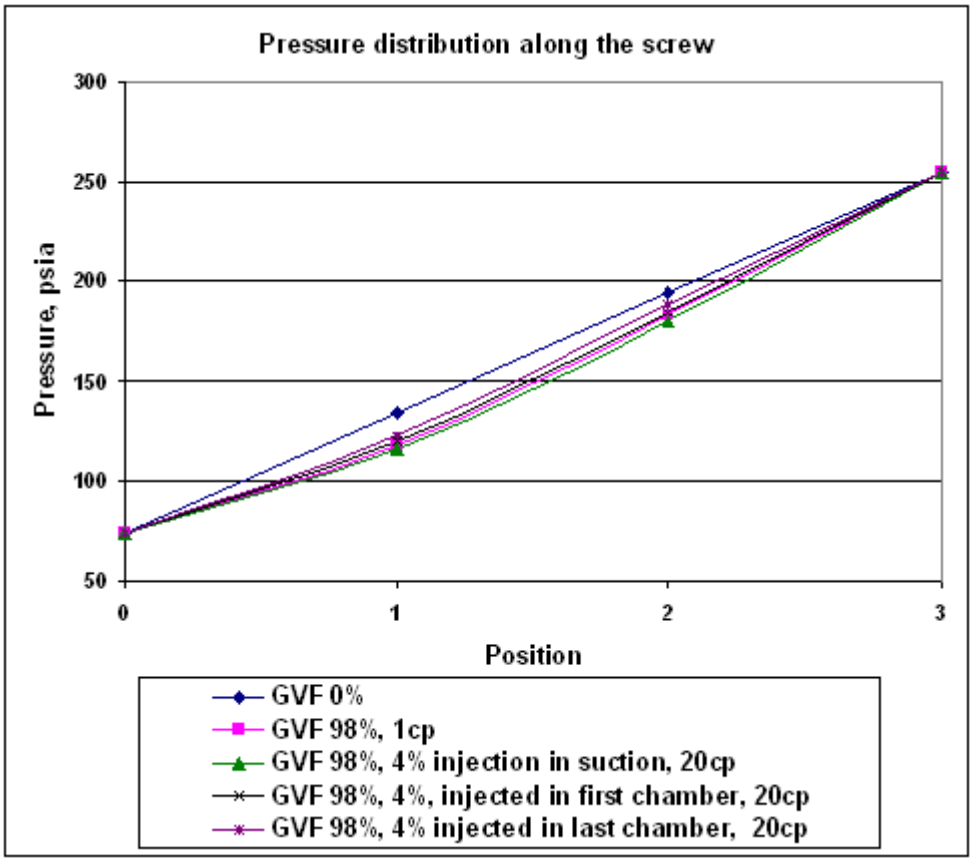

Fig. 4.16—Pressure distribution along the screw with GVF 98% at 1700 rpm (inject 4% of glycerin in suction, first chamber and last chamber, scenarios 4, 8, 12)

Generally speaking, the injection of high viscosity liquid in the suction has the highest total flow rate and volumetric efficiency. In this particular example, this method can improve the volumetric efficiency by 30%. Since this method uses liquid injection, it is more flexible than degressive screws. The simulation shows that it could be an alternative to improve twin-screw multiphase pump performance under wet gas conditions.

5. SUMMARY AND CONCLUSIONS

A new model is developed based on previous Texas A&M twin-screw pump model by Martin and Scott (2003). The idea is to utilize the pump performance curve with water provided by the pump manufacturer to generate the basic parameters of the twin-screw pump. In this model, both the gas slip and liquid slip in the pump clearances are simulated. The mechanic model is coupled with thermodynamic model to predict the pressure and temperature distribution along the screws. The comparison of experimental data and the predictions of both isothermal and non-isothermal models show a better match than previous Texas A&M twin-screw pump model with GVF 95% and 98%. The gas slip in the clearances can not be ignored with high gas content. Compatible with previous Texas A&M twin-screw pump model, this model can be used to simulate the twin-screw pump performance with GVF from 0% to 99%.

The extensive testing with field scale twin-screw pump shows a good match between the experimental data and the predicted multiphase performance. This model for the first time explains the observation of Vetter on the pressure distribution along the screws by simulation, which is that higher than certain GVF, the pressure distribution along the screw is moving toward linear with the increasing GVF due to the presence of gas slip. This really changes the traditional view of pressure profile in the twin-screw pump.

The developed model also predicted accurately the pump performance with different liquid viscosity. The effect of liquid viscosity on the total flow rate of twin-

screw pump is evaluated. Both the simulation and experimental data prove that the liquid viscosity play a key role in the twin-screw pump performance, which is the most sensitive factor.

Based on the evaluation of liquid viscosity, a novel solution is investigated with the newly developed model to improve the efficiency and reliability of twin-screw pump performance with GVF higher than 94%. The solution is to inject high viscosity liquid directly into the twin-screw pump. After the simulation of several different scenarios with various liquid injection rate and injection positions, we conclude that the volumetric efficiency increases with increasing liquid viscosity and injecting liquid in the suction is suggested.

REFERENCES

Ali, M.I., Sadatomi, M., and Kawaji, M., 1993. Adiabatic Two-Phase Flow in Narrow Channels Between Two Flat Plates. *The Canadian Journal of Chemical Engineering*, **71**: 657-666.

Brenne, L., Bjorge, T., Gilarranz, J.L., Koch, J.M., and Miller, H. 2005. *Proc.* of 34th Turbomachinery Symposium, Houston, Texas, September 12-15.

Chan, E. 2006. Wet-Gas Compression in Twin-Screw Multiphase Pumps. Thesis, Texas A&M University, College Station, Texas.

Chisholm, D., and Laird, A.D.K., 1958. Two-Phase Flow in Rough Tubes. *Transactions of the ASME*, **80**(2): 276-286.

Corless, R.J. 2000. Application of Multiphase Pump in California Heavy Oil Project. presented at the 2nd Multiphase Pump User Roundtable (MPUR) Houston, Texas, 4 May.

Corless, R.J., 2001. Multiphase Pumps Replace Conventional Heavy Oil Facilities. *Oil & Gas Journal*, **99**(39): 80-84.

Dal Porto, D.F., and Larson, L.A., 1997. Multiphase-Pump Field Trials Demonstrate Practical Applications for the Techonology. *SPE Production & Facilities*: 159-164.

Egashira, K., Shoda, S., Tochikawa, T., and Furukawa, A., 1998. Backflow in Twin-Screw-Type Multiphase Pump. *SPE Production & Facilities*: 64-69.

Giuggioli, A., Villa, M., De Ghetto, G., and Colombi, P. 1999. Multiphase Pumping for Heavy Oil: Results of a Field Test Campaign. Paper SPE 56464 presented at the 1999 SPE Annual Technical Conference and Exhibition, Houston, Texas, 3-6 October.

Gonzalez, R., and Guevara, E. 1995. Economic Field Development in Venezuela Heavy Oil Fields Using Multiphase Pumping Technology. Paper SPE 30262 presented at the 1995 SPE International Heavy Oil Symposium, Calgary, Alberta, Canada, 19-21 June.

Hirs, G.G., 1973. A Bulk-Flow Theory for Turbulence in Lubricant Films. *ASME J. of Lubrication Technology*: 137-146.

Lockhart, R.W., and Martinelli, R.C., 1949. Proposed Correlation of Data for Isothermal Two-Phase, Two-Component Flow in Pipes. *Chemical Engineering Progress*, **45**: 39-48.

Martin, A.M. 2003. Multiphase Twin-Screw Pump Modeling for the Oil and Gas Industry. Dissertation, Texas A&M University, College Station, Texas, 201 pp.

Mobbs, A. 2002. Topacio Subsea Multiphase Pumps. presented at the 4th Multiphase Pump User Roundtable, Houston, Texas, 9 May.

Muller-Link, D., Brandt, J.U., Reichwage, M., and Schroder, G. 2002. Wet Gas Compression-A Logical Step to Follow Multiphase Boosting. Paper SPE 78556 presented at the 2002 10th Abu Dhabi International Petroleum Exhibition and Conference, Abu Dhabi, 13-16 October.

Nakashima, C.Y., de Oliveira, S.J., and Caotano, E.F. 2002. *Proc.* of 2002 Engineering Technology Conference on Energy Houston, Texas, 4-5 February.

Nakashima, C.Y., De Oliveira, S.J., and Caotano, E.F., 2006. Heat Transfer in a Twin-Screw Multiphase Pump: Thermal Modeling and One Application in the Petroleum Industry. *Energy*, **31**: 3415-3425.

Pickard, B. 2003. Subsea Multiphase Pumps in the Ceiba Field - West Africa. presented at the 5th Multiphase Pump User Roundtable, Houston, Texas, 7 May.

Prang, A.J., and Cooper, P. 2004. *Proc.* of 4th North American Conference on Multiphase Technology, Banff, Canada, 3-4 June.

Prang, A.J., Hartt, R., and Cooper, P. 2002. *Proc.* of 3rd North American Conference on Multiphase Technology, Banff, Canada, 6-7 June.

Putra, E. 2001. Multiphase Pumps for Light Oil Steam Flood, from Design and Operation Perspectives. Paper SPE 72143 presented at the 2001 SPE Asia Pacific Improved Oil Recovery Conference, Kuala Lumpur, Malaysia, 8-9 October.

Putra, E., and Uphold, D.D. 1999. Multiphase Pumps for Minas Light Oil Steam Flood, Sumatra-Indonesia. Paper SPE 54294 presented at the 1999 SPE Asia Pacific Oil and Gas Conference and Exhibition, Jakarta, Indonesia, 20-22 April.

Rabiger, K., Maksoud, T.M.A., and Ward, J., 2006. Thermo- and Fluid Dynamic Model of a Multiphase Screw Pump, Operating at Very High Gas Volume Fractions. *Sonderdruck Schriftenreihe der Georg-Simon-Ohm-Fanchhochschule Nurnberg*, **35**.

Rausch, T., Th., V., Brandt, J.U., and Mewes, D. 2004. *Proc.* of 4th North American Conference on Multiphase Technology, Banff, Canada, 3-4 June.

Rohlfing, G., and Muller-Link, D. 2006. Twin-Screw Rotors-2nd Generation for Increased Efficiency. presented at the 8th Multiphase Pump User Roundtable, Calgary, Canada, 16 June.

Scott, S.L., Xu, J., and Lenz, C. 2006. Subsea Multiphase Pressure Boosting and a New Approach for Speed Control Using a Hydrodynamic Variable-Speed Drive. Paper SPE 103323 presented at the 2006 SPE Annual Technical Conference and Exhibition, San Antonio, Texas, 24-27 September.

Sinclair, G. 2007. Multiphase Pump Application at Main Pass 59 in the Gulf of Mexico. presented at the 9th Multiphase Pump User Roundtable-Europe, Amsterdam, Netherlands, 20 November.

Singh, A. 2003. Modeling Twin-Screw Multiphase Pump Performance During Periods of High Gas Volume Fraction. Thesis, Texas A&M University, College Station, Texas.

Toma, P., and Anderson, L. 2006. Gas-Liquid Heat Transfer with Multiphase Pump for Steam-Assisted Heavy Oil Recovery Fields. presented at the 8th Multiphase Pump User Roundtable, Calgary, Canada, 12 June.

Uphold, D.D. 1999. Trade-Offs of Multiphase Production: Use of Multiphase Pumps in the Hamaca Heavy Oil Project. presented at the 1st Multiphase Pump User Roundtable, Houston, Texas, 3 May.

Vena, T. 2003. Use of Multiphase Pumps at Cold Lake. presented at the Multiphase Pump User Roundtable - Canada, Calgary, Alberta, Canada, 27 October.

Vetter, G., and Wincek, M., 1993. Performance Prediction of Twin Screw Pumps for Two-Phase Gas/Liquid Flow. *Pumping Machinery,* **154**: 331-340.

Vetter, G., Wirth, W., Korner, H., and Pregler, S. 2000. *Proc.* of 17th International Pump Users Symposium, Houston, Texas.

White, J.L. 1991. *Twin screw extrusion: technology and principles*. Carl Hanser Verlag, New York, **8:** 170-181.

VITA

Name:	Jian Xu
Address:	200 Charles Haltom Ave. 3D College Station, Texas 77840
Email Address:	xujian@tamu.edu
Education:	B.S., Automation, Tianjin University, P.R. China, 2000 M.S., Electrical Engineering, Tianjin University, P.R. China, 2003